

REPUBLIQUE DU CAMEROUN

Paix – Travail – Patrie

UNIVERSITE DE YAOUNDE I

FACULTE DES SCIENCES

DEPARTEMENT DE PHYSIQUE

CENTRE DE RECHERCHE ET DE
FORMATION

DOCTORALE EN SCIENCES,

TECHNOLOGIES

ET GEOSCIENCES

Laboratoire de Mécanique, Matériaux et
Structure



REPUBLIC OF CAMEROUN

Peace – Work – Fatherland

UNIVERSITY OF YAOUNDE I

FACULTY OF SCIENCE

DEPARTMENT OF PHYSICS

POSTGRADUATE SCHOOL OF
SCIENCES,

TECHNOLOGY AND

GEOSCIENCES

Laboratory of Mechanics, Materials
and Structure

**Rotating electromechanical systems with bistable
potential, hysteretic iron-core inductor and delay**

This dissertation is submitted to the Postgraduate School of the
University of Yaoundé I in partial fulfillment of the requirements
for the degree of Philosophie Doctor (PhD) in Physics

Par : **TSAPLA FOTSA Rolande**
Master's in Physics

Sous la direction de
WOAFO Paul
Professor

Année Académique : 2018





DEDICATION

Dedication

To the Almighty Lord. In the same way that Abraham, the father of faith gave you his only son Isaac as a sacrifice, I place this work in your hands. Do what you want with it.

.

ACKNOWLEDGEMENTS

Acknowledgements

This research work carried out since the school year 2013-2014 at the Department of Physics of the University of Yaoundé 1 has been possible thanks to all those who have been able to advise, guide and encourage me throughout the project. Now my doctorate cycle is coming to the end and it is time for me to express my thanks to those who have allowed me to advance and especially to those who have accompanied me so far.

- The **Almighty Father** for all his marvellous and overabundant gifts, the always living **Lord Jesus** for his precious teachings, the **Holy Spirit** for his unspeakable power.
- The work presented in this thesis was carried out in the Laboratory of Modelling and Simulation in Engineering, Biomimetic and Prototypes (LAMSEBP) directed by **Professor WOAFO Paul**. He has cordially admitted me in his laboratory, defined the topic of this thesis and allowed me by courses and seminars that he organizes within the laboratory to familiarize myself with research subjects as interesting as varied. His scientific curiosity, his clear spirit, his very large knowledge and the perpetual follow up of this work have without any doubt be determining in this achievement. He is the one who initiated and guided my first steps on the way of research from my Master thesis, with his education and appreciated supports.
- I greatly thank **Professor KOFANE Timoléon Crépin**, whose the wide advices during courses in nonlinear physics and in the research has been very beneficial for me in my work.
- I greatly thank **Professor NDJAKA Jean-Marie Bienvenue**, the Head of the Department for his constant encouragement.
- I greatly thank **Professor TCHAWOUA Clément**, for his courses in vibration and elasticity and the large number of advices during the Licence and Master's courses.
- I greatly thank the reviewers who produced my reports.
- I wish to express my acknowledgments to all the members of the jury who have accepted to discuss and appreciate the results of this thesis in spite of their numerous duties. The President of jury **Professor KOFANE Timoléon Crépin** from the University of Yaoundé I. The members of jury namely **Professor TIEDEU Alain Bertin** from the University of Yaoundé I, **Professor TCHAWOUA Clément** from the University of

Yaoundé I, **Professor ESSIMBI ZOBO Bernard** from the University of Yaoundé I, **Professor MOUKAM KAKMENI François Marie** from the University of Buea and **Professor WOAFO Paul** the promoter of this thesis.

- I would like to thank all the **teaching staff** and personnel of the Department of Physics, Faculty of Science, University of Yaoundé I, for their teaching and help during my undergraduate courses.
- I am thankful to **Professor NANA Nbandjo Blaise**, Lecturer at the University of Yaoundé 1, Faculty of Science for his availability and his fruitful discussions.
- Special thanks also go to **Dr NANA Bonaventure**, Lecturer at the Teacher's Training College of Bambili.
- I honour through this thesis the memory of one of our teacher at University of Yaoundé 1, Faculty of Science, in the person of "**Dr MBOUSSI K. Aissatou**", who left us in February 2016 "*Peace to her soul*", she was for me a model of senior sister.
- I would like to thank all my elders who supported this work with their knowledge: **Dr ABOBDA Lejuste Theodore**, **Dr TCHEUTCHOUA FOSSI Omer**, **Dr TAKOUGANG Sifeu**, **Dr NGUETEU Serge**, **Dr TOGUE Fulbert**, **Dr SIMO Herve**, **Dr GOUNE CHENGUI Geraud Russel** and , **Dr TALLA Alain Francis**, **Mr CHAMGOUE Cheage Andre**, particularly **Mr NOTUE Kadjie Arnaud** and **Mr TCHAWOU Eder Batista** for their advice and assistance.
- My lab mates: **TOKOUE NGATCHA Dianoré**, **Dr NWAGOUM Peguy**, **METSEBO Jules**, **NDEMANOU Peguy**, **TEKAM Gabin**, **TCHAKUI Vanessa**, **ANAGUE Lionel** and **THEPI Raoul**, **KOUAMI Nadine**, **YOUMBI Daurotta**, **MAKOOU Lucienne** for their stimulating questions on this work, for the delightful atmosphere and good mood in which I all those years. Lived during all those years.
- I would like to thank all those who helped me in other ways, from the first classes of the primary school up to now. I especially think to:
 - My parents: Dad **FOTSA Martin**, Mum **FOTSA MAKOUATE Marie**, for their love, for all the advice and attendance they have about me;
 - My sister **FOTSA NGAFFO Fernande** and her husband **KENFACK JIOTSA Aurelien** for all the advice and attendance they gave me;
 - My sisters **NAUGNING FOTSA Sylvie**, **MATHO FOTSA Armelle**, **KEUBOU FOTSA Alice** and **TCHINDA FOTSA Agnes** for their encouragements;

- My brothers **TALAHFO FOTSA Jean Vincent**, **TALLA FOTSA Gervais** for their encouragements;
- My uncles **TALACFO Augustin** and **TIEBOU Joseph** who have always looked after me.
- My sincere gratitude to my parents in law **His Majesty, Me TSAMO Daniel** and **TIOFACK Jacqueline** for their encouragements;
- I particularly thank my husband, **TSAMO Duplex** whose love, presence, advice and encouragements during all my PhD thesis gave me the courage for the accomplishment of this work. May God the Almighty bless you for all that.
- I particularly thank my children **TSAMO FOTSA Yanice Mayeul**, **TSAMO KEMVOU Merveille Chanelle** and **TSAMO TIOACK Rolex Wise** for their infinite love.
- I am also thankful all my nephew and niece, whose love always gave me the courage for the accomplishment of this work.
- I would like to thank my friends **NGOUFFO NIMPA Germaine**, **KOUAMI MBEUNGA Nadine**, and **ZOUDA Albertine**.

All those whose names have not been mentioned here, but who have contributed in one or other way to the success of this work should hereby receive my sincere gratitude.



CONTENTS

Contents

Dedication	i
Acknowledgements.....	iii
Contents.....	ii
Abstract.....	v
Résumé	vii
List of abbreviations.....	ix
List of tables.....	xi
List of Figures.....	xiii
0- General introduction	2
1- Literature review	7
1.1. Introduction	7
1.2. Types of electromechanical systems.....	7
1.2.1. Microelectromechanical Systems (MEMS).....	8
1.2.2. Nano electromechanical systems (NEMS).....	9
1.2.3. Macro electromechanical systems (MaEMS).....	10
1.3. Nonlinear dynamics.....	11
1.3.1. Chaos: control and anti-control	12
1.3.2. Route to chaotic dynamics on MaEMS	13
1.4. Some interesting MaEMS	16
1.4.1. MaEMS as motor.....	16
1.4.2. MaEMS as generator	21
1.5. Derivation of the magnetic potential energy	26
1.6. Some essential works carried out on MaEMS in our research group	28
1.7. Motivation and challenges	29
1.8. Conclusion.....	30
2- Methodology	32
2.1. Introduction	32
2.2. Mathematical formalisms and numerical methods	32
2.2.1. Mathematical formalisms	32
2.2.2. Numerical methods.....	35
2.3. Computational tools for the characterization of the dynamical states of non-linear systems.....	38
2.3.1. Time histories diagram and phase portraits	39

2.3.2.	Bifurcation diagrams	39
2.3.3.	Lyapunov exponents	40
2.4.	Conclusion	40
3-	Results and discussions	43
3.1.	Introduction	43
3.2.	Dynamical behaviour of a bistable rotating electromechanical system	44
3.2.1.	System and equations	44
3.2.2.	Oscillatory states in the absence of three magnets	47
3.2.3.	Dynamics in the presence of the magnets	49
3.2.4.	The Hamiltonian chaos	57
3.3.	Dynamical behaviour of a bistable rotating electromechanical system with spring, hysteretic iron-core inductor and delay	59
3.3.1.	System and equations	59
3.3.2.	Dynamic in absence of permanent magnets	64
3.3.3.	Inducing chaos using three magnets.	68
3.3.4.	Chaotic dynamics generated from delay	73
3.4.	Analysis of an electromechanical system with translational and pendulum motion	77
3.4.1.	Electromechanical system and equations	77
3.4.2.	Effects of the bistable potential energy	83
3.4.3.	Electromechanical device with hysteretic iron-core inductor	88
3.4.4.	Effect of the delay on electromechanical system	93
3.5.	Conclusion	96
	General conclusion	98
	Annex- Derivation of the magnetic potential energy	101
	Bibliography	105
	List of publications	115



ABSTRACT

Abstract

This thesis analyses the behaviour of rotating and pendulum rod like electromechanical arms. The goal ultimate is to design chaotic sieves and mixers. After the schematic representation and description of each prototype, the mathematical models are established and the appropriate theoretical methods are used to study their dynamical behaviours. The main results obtained are expressed in terms of design, modelling and dynamic characterization of new electromechanical devices.

- The first device designed is an electromechanical system which rotates on an arc of a circle a rigid arm acting as a particle in a bistable potential due to three appropriately placed magnets. This first device is modelled, the analysis of the dynamics subjected to the action of a source of sinusoidal voltage and of a voltage source of square form is made. This analysis highlights the chaotic behaviour used in the mixing and sieving processes;
- The second device designed differs from the first by the fact that its movement is framed by the symmetrically fixed springs and by the fact that the hysteresis of the inductance is taken into account through an inductance-intensity characteristic of the strongly nonlinear. Here again the reinforcement of the complexity of the dynamic behaviours is ensured on the one hand by the introduction of a bistability created by symmetrically arranged magnets and on the other hand by the introduction of a delay generated by feedback from a mechatronic device;
- The third device designed has a pendula behaviour presenting both a translational movement through a horizontal rod and a pendulum movement through a second rod. This double movement gives the device several different functions in terms of applications. As in the case of the first two devices, complexification is ensured by the creation of bistability by magnets, the non-linear characteristic of the inductance and the use of a delayed feedback force.

Keywords: Electromechanical systems, rotating arm, electric motors, bistable potential, hysteretic iron core inductor, delay, chaos.

RÉSUMÉ

Résumé

Cette thèse analyse le comportement des bras électromécaniques rotatifs et pendulaires. Le but ultime est de concevoir des tamis et des mélangeurs chaotiques. Après la représentation schématique et la description de chaque prototype, les modèles mathématiques sont établis et les méthodes théoriques appropriées sont utilisées pour étudier leurs comportements dynamiques. Les principaux résultats obtenus s'expriment en termes de conception, modélisation et caractérisation dynamique de nouveaux dispositifs électromécaniques.

- Le premier dispositif conçu est un système électromécanique faisant tourner sur un arc de cercle un bras rigide se comportant comme une particule dans un potentiel bistable à cause de trois aimants placés de manière appropriée. Ce premier dispositif est modélisé, l'analyse de la dynamique soumise à l'action d'une source de tension sinusoïdale et d'une source de tension de forme carré est faite. Cette analyse fait ressortir des comportements chaotiques utilisés pour les processus de mixage et de tamisage.
- Le deuxième dispositif conçu diffère du premier par le fait que le bras est assujéti à deux ressorts fixés symétriquement et que l'hystérésis de l'inductance est prise en compte à travers une caractéristique inductance-intensité du courant de forme fortement non linéaire. Ici aussi, le renforcement de la complexité des comportements dynamiques est assuré d'une part par l'introduction d'une bistabilité créée par des aimants symétriquement disposés et d'autre part par l'introduction d'un retard généré par rétroaction à partir d'un dispositif mécatronique ;
- Le troisième dispositif conçu a un comportement pendulaire présentant à la fois un mouvement de translation à travers une tige horizontale et un mouvement pendulaire à travers une seconde tige. Ce double mouvement confère au dispositif plusieurs fonctions différentes en termes d'applications. Comme pour les deux premiers dispositifs, la complexification est assurée par la création de la bistabilité par des aimants, la caractéristique non linéaire de l'inductance et l'usage d'une force de rétroaction avec retard.

Mots clés : Systèmes électromécaniques, bras rotatifs, moteurs électriques, potentielle bistable, Inducteur de noyau de fer hystérétique délais, chaos.

LIST OF ABBREVIATIONS

List of abbreviations

EMS: Electro Mechanical System
BLDC: Brushless Direct Current
MaEMS: Macro-Electro Mechanical System
NEMS: Nano-Electro Mechanical System
MEMS: Micro-Electro Mechanical System
VLST: Very Large-Scale Integration
ITRS: International Technical Roadmap for Semiconductor
MD: Molecular Dynamic
KCL: Kirchhoff's Current Law
KVL: Kirchhoff's Voltage Law
DC: Direct Current
AC: Alternating Current
SEDC: Separately-Excited Direct Current
PMDC: Permanent Magnet Direct Current
CCDC: Compound-Connected Direct Current
SCDC: Series-Connected Direct Current
ShCDC: Shunt-Connected Direct Current
TDFC: Time Delay Feedback Control
RK4: Fourth-order Runge-Kutta
EMF: ElectroMotive Force
BEF: Back Electromotive Force
NODE: Nonlinear Ordinary Differential Equation
DDE: Delay Differential Equations
ODE: Ordinary Differential Equation



LIST OF TABLES

List of tables

Table 1 - Parameters of the electromechanical system (some of these parameters are indicated in Figure 5).	45
Table 2 - Parameters of the electromechanical system.....	61
Table 3 - New parameters of the electromechanical system (some of these parameters are indicated in Figure 16).....	63
Table 4 - Parameters of the electromechanical system.....	78
Table 5 - Parameters of the electromechanical system.....	89



LIST OF FIGURES

List of Figures


Figure 1 - Schematic representation of SEDC motor [13].	18
Figure 2 - Schematic diagram of an energy harvester model [98].	22
Figure 3 - Schematic representation of the rotational wheel system harvester that consist of permanent magnets attached to a wheel.	24
Figure 4 - Schematic structure for the derivation of the magnetic potential energy.	26
Figure 5 - Schematic representation of the electromechanical system.	44
Figure 6 - Frequency-responses of the maximal angular displacement (a) and maximal electrical current (b) and the magnitude of the external excitations (the results from the analytical expression (3.10)). With the parameters of Table 1.	49
Figure 7 - Potential energy due to springs (a), potential energy due to magnets (b) and total potential energy (c) as function of the angular displacement for some parameters of table 1.	50
Figure 8 - Bifurcation diagram depicting the global maxima of the angular rotating arm displacement (a) and the largest Lyapunov exponent (b) versus the amplitude E with the parameters of Table 1 and for $\varpi=6.0$.	51
Figure 9 - Time histories(a), (b) and phase portraits (c), (d) obtained with the parameters of Figure 8 and E=2 (a), (c); E=8 (b), (d).	52
Figure 10 - Bifurcation diagram depicting global maxima of the angular rotating arm displacement (a) and the largest Lyapunov exponent (b) versus the parameter ϖ for E=17. With the parameters of Table 1.	53
Figure 11 - Time histories and phase portraits in the (y, \dot{y}) plane: period-1T oscillations Figure 11 (a) and 11 (c) with $\varpi=2$. Chaotic oscillations Figure 11 (b) and 11 (d) with $\varpi=6$. Using the parameters of Figure 10.	54
Figure 12 - Bifurcation diagram depicting global maxima of the angular rotating arm displacement (a) and the largest Lyapunov exponent (b) versus the parameter E.	55
Figure 13 - Bifurcation diagram depicting global maxima ϖ of the angular rotating arm displacement (a) and the largest Lyapunov exponent (b) versus the parameter ϖ with the parameters of Figure 12.	56
Figure 14 - Variation of the fractal structure of the basin of attraction for $\Omega=2.5$ and (a) $\gamma_4=10$, (b) $\gamma_4=5$, (c) $\gamma_4=1$, (d) $\gamma_4=0.02$. Other parameters of Table 1.	59
Figure 15 - Electromechanical system with rotating arm.	60
Figure 16 - Electromechanical rotating arm with three permanents magnets.	63
Figure 17 - Frequency-responses of the (a) angular displacement (b) electrical current with the parameters values of Table 3, for the magnitude of the external excitation E=0.5. (the point (·) for the numerical simulation of the differential equation. (3.26) and the lines (-) for the analytical expression (3.27).	66
Figure 18 - Bifurcation diagram depicting global maxima of the angular rotating arm displacement (a) and the largest Lyapunov exponent (b) versus the parameter ϖ for E=6. With the parameters of Table 2.	67
Figure 19 - Bifurcation diagram depicting global maxima of the angular rotating arm displacement (a) and the largest Lyapunov exponent (b) versus the parameter of Figure 18 and for $\varpi=0.6$.	68
Figure 20 - Elastic potential energy (a), magnetic potential energy (b) and magneto elastic potential energy (c) as function of the angular displacement.	69

Figure 21 - Bifurcation diagram depicting global maxima of the angular rotating arm displacement (a) and the largest Lyapunov exponent (b) versus the parameter E obtained for $\varpi=0.6$. With the parameters of Table 2.	70
Figure 22 - Time histories(a), (b) and phase portraits (c), (d) obtained with the parameters of Figure 21 and for $E=4.0$ (a), (c); $E=9.0$ (b), (d).	71
Figure 23 - Bifurcation diagram depicting global maxima of the angular rotating arm displacement (a) and the largest Lyapunov exponent (b) versus the parameter ϖ obtained with $E=6$. With the parameters of Table 2.	72
Figure 24 - Time histories (a), (b) and phase portraits (c), (d) obtained for $\varpi=0.69$ (a), (c); $\varpi=0.57$ (b), (d).....	73
Figure 25 - Bifurcation diagram depicting global maxima of the angular rotating arm displacement (a) and the largest Lyapunov exponent (b) versus the parameter E obtained with the parameters of Figure 24 and for $\varpi=0.57$; $v=0.085$; $\tau_i=20$	75
Figure 26 - Bifurcation diagram depicting global maxima of the angular rotating arm displacement (a) and the largest Lyapunov exponent (b) versus the parameter ϖ obtained with the parameters of Figure 25 and for $E=4$	76
Figure 27 - Electromechanical device	77
Figure 28 - phase portraits obtained with the parameters of Table 4. $E_0 = 0.1$ (a), $E_0 = 0.5$ (b), $E_0 = 5.0$ (c), $E_0 = 10$ (d) and $\varpi = 0.8$	80
Figure 29 - phase portraits obtained with the parameters of Table 4. $\varpi = 0.2$ (a), $\varpi = 0.8$ (b), $\varpi = 1.0$ (c), $\varpi = 5.0$ (d) and $E_0 = 0.5$	81
Figure 30 – Frequency-responses of the (a) angular displacement (b) electrical current: curves from the harmonic balance approximations (-) and curves from the direct numerical simulations (o) with the parameters of Table 4 and $E_0=0.1$	83
Figure 31 - Electromechanical device with bistable potential	84
Figure 32 - Bifurcation diagram depicting the global maxima of the angular pendulum arm displacement (a) and the largest Lyapunov exponent (b) versus the amplitude with the parameters of table 4, for $m=0.07$ and $\varpi=0.35$	86
Figure 33 : Time histories (a), (b) and phase portraits (c), (d) obtained with the parameters of Figure 4 and (a), (c); (b), (d)	87
Figure 34 - The Poincarré map of a chaotic state with the parameters of Figure 5 and for $\varpi=0.35$, $E_0=9.0$	87
Figure 35 - Bifurcation diagram depicting global maxima of the angular pendulum arm displacement (a) and the largest Lyapunov exponent (b) versus the parameter ϖ with the parameters of Figure 32 and for $E_0=9.0$	88
Figure 36 - Electromechanical pendulum arm with hysteretic iron core inductor	89
Figure 37 - Phase portraits obtained with the parameters of Table 5. $E_0=0.1$ (a), $E_0=0.5$ (b), $E_0=5.0$ (c), $E_0=10.0$ (d) and $\varpi=0.8$	91
Figure 38 - Phase portraits obtained with the parameters of Table 4, Table 5. $\varpi=0.2$ (a), $\varpi=0.8$ (b), $\varpi=1.0$ (c), $\varpi=5.0$ (d) and $E_0=5.0$	91
Figure 39 - Electromechanical pendulum arm with hysteretic iron core inductor and bistable potential energy.	92
Figure 40 - Bifurcation diagram depicting global maxima of the angular pendulum arm displacement (a) and the largest Lyapunov exponent (b) versus the parameter N obtained with the parameters of Table 4, Table 5 and for $\varpi=0.35$, $E_0 =9.0$	93

Figure 41 - Bifurcation diagram depicting global maxima of the angular pendulum arm displacement (a) and the largest Lyapunov exponent (b) versus the parameter τ obtained with the parameters of Table 4 and for $\varpi=0.8$, $E_0=0.5$ 94

Figure 42 - Phase portraits (a), (b) and Time histories (c), (d) obtained with the parameters of Figure 41 and $\tau_0=13$ (a), (c); $\tau_0=14.5$ (b), (d)..... 95

Figure 43 - Bifurcation diagram depicting global maxima of the angular pendulum arm displacement (a) and the largest Lyapunov exponent (b) versus the delay obtained with the parameters of Table 4, Table 5 and for $N=780$, $\varpi=0.35$, $E_0=7.7$, $\nu=0.25$ 96



GENERAL INTRODUCTION

0- General introduction

Electromechanical systems (EMS) are made of two main parts (electrical and mechanical), which are coupled together via magnetic, piezoresistive, piezoelectric and capacitive couplings [1-10]. If micro-electromechanical systems (MEMS) are now more attractive worldwide, macro-electromechanical systems (MaEMS) still have interest since they are present in various engineering and domestic equipments [3]. Moreover, their modeling equations present some complexities which are interesting and stimulating challenges, both mathematically and numerically. In the majority of these EMS, the mathematical modeling is done and, among the state solutions that may appear, chaos and mechanisms of routes to chaos have received the greatest attention. In the field of nonlinear dynamics, control problems for complex oscillatory EMS have attracted significant interest and a considerable effort has been devoted to the study of oscillatory, chaotic states and the route of chaos of some MaEMS [3,10,13–20]. For instance, in **Ref.13**, the authors proposed a feedback control method to generate complex behavior in a linear EMS device. They showed that, for appropriate range of control parameters, the device exhibits period- nT and chaos oscillations. Kitio Kwuimy and Wofo [21], studied experimentally and numerically a self-sustained macro-electromechanical system. They showed that, by tuning some physical parameters, the device exhibits periodic oscillations and complex dynamics by using low DC power.

Amongst the EMS, electromechanical pendulum arms constitute a physical object, fascinating physicists and therefore becoming one of the paradigms in the study of physics and natural phenomena. It finds uses in varied structural applications. From the technological point of view, it is the fundamental elements of an engineering structure and one of the objects that have deserved more attention in the modelling of several kinds of phenomena related to oscillations. In the framework of manufacturing industries, electromechanical pendulum arm is the essential component for the automation of processes [17]. Recently, many investigations dealing with the rotating electromechanical arms have been carried out [17,22,23]. For example, the study of an electromechanical system consisting of rigid pendulum arms, magnetically coupled with electrical circuits by means of electromechanical transducers has been considered with the analysis of bifurcation structure and chaos control [17]. Depending on the form of the external excitation and the set of the chosen parameters, EMS lead to various interesting

phenomena such as frequency entrainment, harmonic, subharmonic, super harmonic oscillations, and chaotic behavior [13-19].

The automation of some hard mechanical work has gathered an increasing interest during this last decade [24]. As far as sieve process is concerned, chaotic dynamics is expected to ensure a good performance of the device [18,20,25]. Consequently, intense research activities are presently conducted for the chaotic dynamics of pendulum arms which are currently the standard approach to automatize sieve or mixing processes [22]. To achieve the automation of the sieve or mixing processes, some researchers convert the translational movement into rotational movement and vice versa via the slider crank mechanism. Another method is to fix one arm to a rotary motor and analyze the possibility to have very small amplitude of vibration [13,19,22].

Many methods are used to characterize the chaos behavior in an EMS. Along these lines, numerical indicators such as the Lyapunov exponents and bifurcation diagrams are usually used to determine the appropriate range of parameters for which the device exhibits period- nT and chaos oscillations [26-31]. Kitio Kwuimy et al [3] used the Lyapunov exponent and bifurcation diagram to predict chaos in an electromechanical device constituted by a self-sustained MaEMS made up of a Rayleigh–Duffing oscillator actuating a mechanical arm through a magnetic coupling. To bring chaos in the EMS dynamic one can use the time delay feedback control (TDFC) [30] or the electronic and/or mechanical components which have nonlinear characteristics [31]. The limitation is the difficulty in having mechanical components with clearly identified nonlinear characteristics. These studies have been guided by the fact that chaos is useful and beneficial in some applications such as vibrating sieves [17,22,23], industrial mixers [24], industrial shakers [18] and monitoring compaction [20]. In that spirit, enhancing the complexity of the rotating electromechanical arm behavior has also attracted the attention of various scientists. Zheng-Ming Ge *et al.* [25], studied a brushless dc motor (BLDCM) system and found a very rich dynamics, that was rendered more complex using an anti-control scheme.

Among the EMS, a particular class is that containing asynchronous motor, which is encountered in various industrial modern processes. In most of these EMS powered by sinusoidal input voltage, chaotic behavior appears for appropriate range of parameters when the device consists of electronic and/or mechanical components which have nonlinear characteristics [3, 29, 32] such as capacitors with nonlinear charge-voltage characteristics [33,34], inductance with nonlinear term in the flux-voltage characteristics [35], and so on. In practice, electronic components deliver low power and it is difficult to have mechanical

components with clearly identified nonlinear characteristics. Consequently, the chaotification technique which consists to introduce nonlinear components in the EMS is limited to low power devices (e.g., microelectromechanical systems). In the absence of nonlinear components, one sometimes uses anticontrol of chaos methods [29,35-38], and Time Delay Feedback Control (TDFC) [25]. These studies have been extended to hydro-turbine system showing nonlinear dynamics [40-43]. Research is still in progress to find other ways to induce chaos in EMS, particularly in EMS using electric components that can be used to provide high power actuation force. Such a problem is considered in this work.

In this work, we provide another way to generate chaos in the dynamics of electromechanical systems consisted of rotating and pendulum arm. This is based on the generation of a bistable potential in the electromechanical system and by inducing a hysteretic iron-core inductor and delay in the electromechanical systems. The EMS proposed in this thesis are inspired by some previous works such as in [13], where Tcheutchoua Fossi *et al.* used feedback control to generate complex phenomenon in a simple electromechanical system. By using the power supply feedback control, the authors observed that the system exhibits complex dynamical behaviors such as jump phenomenon, Sommerfeld effect, period- nT and chaotic oscillations. In [17], Mogo and Wofo studied a nonlinear electromechanical device with a pendulum arm. The authors observed that the system exhibits complex dynamical behaviors such as multi-periodic, quasi-periodic, and chaotic responses. In this thesis, we provide new designs to chaotify the same device.

The first device studied in this thesis is an electromechanical system, which consists of a mechanical rotating arm activated by a rotary electric motor. Its shaft is fixed mechanically at its two ends by two spiral torsion springs put up in anti-parallel manner. The coupling between the electrical and mechanical parts is realized through the electromagnetic force due to a permanent magnet. One permanent magnet is fixed at the free end of the mechanical arm. In the right and in the left of the mechanical arm at equal distances to the equilibrium position, there are two other permanent magnets placed on top of a non-ferromagnetic bearer.

The second device studied in this thesis is an electromechanical system with rotating arm. It is made of an electrical circuit driving a mechanical part. The rotating arm is a thin rod on which electrical windings are applied. In order to make the electromechanical rotating arm oscillations chaotic, one permanent magnet is fixed at the free end of the mechanical arm. In the right and in the left sides of the mechanical arm, at equal distances to the equilibrium

position, there are two other permanent magnets also fixed somewhere in the whole system. to enhance the complexity of the device a mechatronic delay generator is introduced. Purposely mechatronic generator is a velocity sensor, such as a tachometer where the measured angular velocity is proportional to the output voltage of the meter.

The third device is an electrodynamic transducer. The mechanical part consists of a translational rod activating a pendulum arm. The pendulum arm returns to its equilibrium position by a spring of stiffness. To make the electromechanical pendulum arm oscillations chaotic, one permanent magnet is fixed at the free end of the pendulum arm (the mass of the pendulum arm will therefore increase). In the right and in the left sides of the pendulum arm, at equal distances to the equilibrium position, there are two other permanent magnets. Then we assume that the ferromagnetic core inductance is a function of the current in the electrical circuit.

The present work is therefore divided in three chapters. In chapter one, we focus on different types and some utilities of EMS. Brief generalities and definition of nonlinear dynamics are given. The attention is particularly focused on the chaotic dynamics and the route to chaotic dynamics on MaEMS. We briefly expose few literature reviews on some interesting electromechanical systems and some works from our research group; then the derivation of the magnetic potential energy. Next, the motivations and challenges are given. In chapter two, we focus on the mathematical formalism and numerical methods used to characterize the dynamical states of the physical systems studied. The third chapter presents the results and discussions of the devices studied in this thesis. Concerning the a bistable rotating electromechanical system, we present the system and equation, oscillatory states in the absence of three magnets next, dynamics in presence of the magnets are investigated. The Hamiltonian chaos is also analysed. According to a bistable rotating electromechanical system with springs, hysteretic iron-core inductor and delay, the system and equation are given, dynamics in absence of permanent magnets next, dynamics in presence of the magnets are investigated. For the electromechanical system with translational and pendulum motion, we present the system and equations, next the effect of the bistable potential energy is analysed, the effect of the hysteretic iron-core induction on electromechanical device is investigated. Then the effect of delay on electromechanical system with bistable potential and hysteretic iron core inductor is also analysed. We end with a general conclusion where the main results of the work are summarized and perspectives related to our present achievements are sketched.



CHAPTER 1

Literature review

CHAPTER 1

1- Literature review

1.1. Introduction

This chapter deals with the literature review on research on electromechanical systems with emphasis on those delivering rotating motion. In section 1.2, general information are given on electromechanical systems. Section 1.3 concentrates on nonlinear dynamics in some electromechanical systems with focus on control and anticontrol of chaos. Recent physical models of rotating electromechanical systems are presented in section 1.4. section 1.5 is concerned with the derivation of the potential due to the interaction of magnets. In section 1.6, we present some results obtained in our research group. This leads to the problems studied in this thesis in section 1.7. Section 1.8 concludes the chapter.

1.2. Types of electromechanical systems

In newtonian physics, there is a universal law of conservation of energy, which says that: energy (usually defined as the ability to perform work) can be neither created nor be destroyed however, it can change from one form to another. There are many different forms of energy around us such as: electrical, mechanical, electromagnetic, chemical, and thermal to name a few. For energy conversion between electrical and mechanical forms, electromechanical devices are developed. Depending on their dimensions, they are called Nano (dimension less than one cubic micrometer), micro (dimension less than one cubic millimeter), and Macro-Electromechanical Systems, denoted as NEMS, MEMS and MaEMS respectively. The potential of very small machines was appreciated before the technology existed that could make them (see, for example, Richard Feynman's famous 1959 lecture: There's Plenty of Room at the Bottom).

1.2.1. Microelectromechanical Systems (MEMS)

Microelectromechanical systems (MEMS), also written as Micro-Electro-Mechanical System, is the technology of microscopic devices. It merges at the Nano-scale into nanoelectromechanical systems (NEMS) and nanotechnology. MEMS are separate and distinct from the hypothetical vision of molecular nanotechnology or molecular electronics. MEMS are usually consisted of a central unit that processes data (the microprocessor) and several components that interact with the surroundings such as micro-sensors [45]. At these size scales, the standard constructs of classical physics are not always sufficient. Because of the large surface area to volume ratio of MEMS, surface effects such as electrostatics and wetting dominate over volume effects such as inertia or thermal mass. The fabrication of MEMS evolved from the process technology in semiconductor fabrication device, i.e. the basic techniques are deposition of material layers, patterning by photolithography and etching to produce the required shapes [46].

Some common commercial applications of MEMS include: Inkjet printers, which use piezoelectric or thermal bubble ejection to deposit ink on paper. Accelerometers in modern cars for a large number of purposes including airbag deployment and electronic stability control. Accelerometers and MEMS gyroscopes in remote controlled, or autonomous, helicopters, planes and multirotor (also known as drones), used for automatically sensing and balancing flying characteristics of roll, pitch and yaw. Accelerometers in consumer electronics devices such as game controllers (Nintendo Wii), personal media players / cell phones (Apple iPhone, various Nokia mobile phone models, various HTC PDA models) [47] and a number of Digital Cameras (various Canon Digital IXUS models). MEMS are also used in PCs to park the hard disk head when free-fall is detected, to prevent damage and data loss. MEMS gyroscopes used in modern cars and other applications to detect yaw; e.g., to deploy a roll over bar or trigger electronic stability control [48] MEMS microphones in portable devices, e.g., mobile phones, head sets and laptops. The market for smart microphones includes smartphones, wearable devices, smart home and automotive applications [49]. Silicon pressure sensors e.g., car tire pressure sensors, and disposable blood pressure sensors. Displays e.g., the digital micro mirror device (DMD) chip in a projector based on DLP technology, which has a surface with several hundred thousand micro mirrors or single micro-scanning-mirrors also called micro scanners. Optical switching technology, which is used for switching technology and alignment for data communications. Bio-MEMS applications in medical and health related technologies from Lab-

On-Chip to Micro Total Analysis (biosensor, chemosensory), or embedded in medical devices e.g. stents [50]. Interferometric modulator display (IMOD) applications in consumer electronics (primarily displays for mobile devices), used to create interferometric modulation reflective display technology as found in Mirasole displays. Fluid acceleration such as for micro cooling. Micro-scale energy harvesting including piezoelectric [51] electrostatic and electromagnetic micro harvesters. Micro machined ultrasound transducers [52, 53].

1.2.2. Nano electromechanical systems (NEMS)

Nano electromechanical systems (NEMS) are a class of devices integrating electrical and mechanical functionality on the nanoscale. NEMS form the logical next miniaturization step from so-called microelectromechanical systems (MEMS) devices. There are many potential applications of machines at smallest sizes. We have atomic force microscope tips, efficient sensors to detect stresses, vibrations, forces at the atomic level, and chemical signals [54], the accelerometers, or detectors of chemical substances in the air [55]. Among the expected benefits, include greater efficiencies and reduced size, decreased power consumption and lower costs of production in electromechanical systems [54]. In 2000, the first very-large-scale integration (VLSI), NEMS device was demonstrated by researchers at IBM [56]. Stefan Haan [57] has described further devices. In 2007, the International Technical Roadmap for Semiconductors (ITRS) [58] contains the NEMS in Memory as a new entry for the Emerging Research Devices section.

Computer simulations have long been important counterparts to experimental studies of NEMS devices. Through continuum mechanics and Molecular Dynamics (MD), important behaviours of NEMS devices can be predicted via computational modelling before engaging in experiments [59-62]. Additionally, combining continuum and MD techniques enables engineers to efficiently analyse the stability of NEMS devices without resorting to ultra-fine meshes and time-intensive simulations [59].

Key hurdles currently preventing the commercial application of many NEMS devices include low-yields and high device quality variability. The focus is currently shifting from experimental work towards practical applications and device structures that will implement and profit from such novel devices [63]. The next challenge to overcome involves understanding all of the properties of these NEMS. In the case where one does not have access to these

miniaturized components and to the devices indispensable for their studies, it will be practically impossible to pass to the experimental phase, hence the interest of the study of the MaEMS.

1.2.3. Macro electromechanical systems (MaEMS)

If MEMS and NEMS are now more attractive worldwide, MaEMS still have interest since they are present in various engineering and domestic equipment's [64]. MaEMS can also be found in areas like: manufacturing, communication, or energy production. Mechanical motion is typically converted into electrical energy and vice versa through various transducers mechanisms such as piezoelectricity, electromagnetic induction, electrostatic, magnetostrictive and biological processes [65].

Though energy conversion can have place via many converters, the magnetic field is practically use as is most suited for practical devices. In these devices, electromechanical systems thus consist of an electrical subsystem (electric circuit such as windings), a magnetic subsystem (magnetic field), and a mechanical subsystem (mechanically movable parts such as a rotor in a rotating electrical machine). Voltages and currents are used to describe the state of the electrical subsystem and the basic circuit laws govern it are Ohm's law, Kirchhoff's current law (KCL) and Kirchhoff's voltage law (KVL). The state of the mechanical subsystem can be described in terms of positions, velocities, accelerations, and is governed by Newton's laws. The magnetic subsystem fits between the electrical and mechanical subsystems and acting in the energy conversion. When coupled with an electric circuit, the magnetic flux interacting with the current in the circuit would produce a force or torque on a mechanically movable part. On the other hand, the movement of the moving part will make some variation of the magnetic flux linking the electric circuit and induce an electromotive force (EMF) in the circuit. Two categories of MaEMS where mechanical and electrical components are coupled via electromagnetic induction are considered in this report.

The first category treats on energy conversion device, which allows electrical energy to be transformed into mechanical energy. Such devices are studied in the literature for instance, in [13], the authors use feedback control to induce chaos motion in a rotary motor when its shaft is fixed mechanically at its both ends by two spiral torsion springs. J. B. Mogo et al [17] have designed a system consists of two permanent magnets which produces a uniform magnetic flux normal to the gap, and a coil which is free to move axially within the gap. Such a system can

be an electromechanical pendulum whose study has been well analysed in the literature. In reference [66], the authors have considered the stiffness of the spring and a self-sustained electromechanical transducer. The effects of discontinuity of elasticity and damping of the electromechanical transducer have been studied. The analysis when the capacitor is added on the electrical part [66-68] has been studied.

The second category concerned the MaEMS which allows mechanical energy to be transformed into electrical energy. The energy shortage is increasingly noticeable due to the impressive number of application in the daily live. At home, early man relied on fire for the luxuries of light, heat and cooking. Today, at the flick of a switch, a push of a button, we can have instant power. The alarm, electric razor, the light in our bedroom, microwaves, toasters, sandwich makers, electric jugs, food processors, freezers, televisions, computers, lamps, DVD players, play Stations, washing machines, dishwashers and clothes dryers need electricity to function. Electricity not only plays a big part in our lives at home, but it is extremely important for everything in the world around us.

1.3. Nonlinear dynamics

Nonlinear dynamics has its origins in the famous "three body problem" and the attempts, at the turn of the century, by the great French mathematician and physicist, Henri Poincaré, to calculate the motion of a planet around the sun when under the perturbing influence of a second nearby planet or moon. In many cases, as expected, the presence of the third body acted to modify the original orbit. However, there were also situations in which the planet moved in a highly erratic way, even to the extent of behaving chaotically. To have discovered chaos at the heart of an apparently stable solar system came as a considerable surprise. However, further exploration of these ideas had to await the development of new mathematical techniques (major contributions coming from mathematicians and theoretical physicists in the Soviet Union) and the development of high-speed computers capable of displaying their complex solutions visually, on a screen, or graphically.

Today, nonlinear dynamic, of which chaos theory forms an important part, is currently an active and fashionable discipline that is having a profound effect on a wide variety of topics in the hard sciences. Its combination of novel mathematics and high speed computing, has produced new insights into the behaviour of complex systems and reveals surprising results

even in the simplest nonlinear models. Recently the chaos theory has found applications in economics, ecology, populations dynamics, the health sciences, sociology, financial market, optics, power electronics, telecommunications, engineering and so on [70-73]. It was also demonstrated that chaotic behaviour appears in all systems presenting some nonlinearities; e.g. epidemiology [74-80].

Nonlinear problems are of interest to engineers, physicists and mathematicians and many other scientists because most systems are inherently nonlinear in nature. In physical sciences, a nonlinear system is a system in which the output is not directly proportional to the input [81]. Nonlinear systems may appear chaotic or unpredictable. Typically, the behaviour of a nonlinear system is described in mathematics by a nonlinear system of equations. It is a set of simultaneous equations in which the unknowns (or the unknown functions in the case of differential equations) appear as variables of a polynomial of degree higher than one or in the argument of a function which is not a polynomial of degree one. In other words, in a nonlinear system of equations, the equation(s) to be solved cannot be written as a linear combination of the unknown variables or functions that appear in them [82]. It does not matter if nonlinear known functions appear in the equations. In particular, a differential equation is linear if it is linear in terms of the unknown function and its derivatives, even if nonlinear in terms of the other variables appearing in it [83].

1.3.1. Chaos: control and anti-control

Chaos control refers to the situation where chaotic dynamics is weakened or eliminated by appropriate controls, while Anti-control of chaos (or chaotification) means, to make an originally non-chaotic dynamical system chaotic, maintained, or enhance the existing chaos of a chaotic system when it is healthy and useful. Chaos control and anti-control technologies have a major impact on many novel, time and energy-critical applications. Among them, we have high-performance circuits and devices (e.g., delta-sigma modulators and power converters), liquid mixing, chemical reactions, biological systems (e.g., in the human brain, heart, and perceptual processes). We also have secure information processing [84], electro domestic and industrial products like shakers, mixers, vibration hammers and various machines for milling, impact printing, sewing, washing and soil compacting tamping. This new and challenging research and development area has become interdisciplinary, involving systems and control engineers, theoretical and experimental physicists, applied mathematicians, physiologists, and

above all, circuits and devices specialists. Both control and anti-control of chaos can be analysed using chaos and bifurcation theories, and can be implemented by suitable design of control and switching circuitries. Chaos refers to one type of complex dynamical behaviours that possess some very special features such as being extremely sensitive to tiny variations of initial conditions [85], having bounded trajectories in the phase space but with a positive maximum Lyapunov exponent. Chaos oftentimes coexists with some other complex dynamical phenomena like bifurcations, fractals, and strange attractors.

Due to its intrinsic dynamical complexity, chaos was once believed to be neither controllable nor predictable and therefore, useless. However, recent research advances have demonstrated that chaos not only is (long-term) controllable and (short-term) predictable, but can also be beneficial to many real-world applications. In fact, control and anti-control of chaos have become a rallying point for an important segment overlapping engineering, physics, mathematics, and biomedical science. Chaos control refers to the situation where chaotic dynamics is weakened or eliminated by appropriate controls, while anti-control of chaos means that chaos is created, maintained, or enhanced when it is healthy and useful. Both control and anti-control of chaos can be accomplished via some conventional and non-conventional methods such as microscopic parameter perturbation, bifurcation monitoring, entropy reduction, state pinning, phase delay, and various feedback and adaptive controls [86].

1.3.2. Route to chaotic dynamics on MaEMS

To have chaotic dynamics in the MaEMS dynamics, we can use: feedback control method to generate complex behaviour in a linear EMS device [13], the Time Delay Feedback Control (TDFC) [87]. One can also use electronic and/or mechanical components with a nonlinear characteristics [88] such as:

-Spring with nonlinear stiffness:

$$k(x) = k_0 + k_1 x^2, \quad (1.1)$$

k_0 is the stiffness for small stretching, x the elongation and k_1 a coefficient of nonlinearity. Electromechanical devices with a nonlinear spring have been studied by Chedjou et al [48, 60], Chembo et al [79], and Yamapi et al [77, 80].

-Capacitors with nonlinear charge-voltage: A circuit element whose charge $q(t)$ and voltage $v(t)$ falls on some fixed (characteristic) curve in the $q-v$ plane represented by the equation $f(q, v) = 0$ at any time t is called a time-invariant capacitor. If the measure $q-v$ characteristic curve is a straight line passing through the origin, then the capacitor is said to be linear and it satisfies the voltage-current relation

$$i = C \frac{dv}{dt}. \quad (1.2)$$

Examples are Electrolytic capacitors, polarized and are connected in the circuit observing the correct polarity, ceramic capacitors generally used where small capacitances are required in an electrical circuit, their capacitances are given in picofarads, tubular capacitors generally marked in microfarads. Other capacitors as varactors diode and junction diodes, have the nonlinear character [3, 88, 89]. Mogo et al in [90] use a nonlinear capacitor constituted by an ideal operational amplifier of reference LF356, four diodes of reference 1N4001, two linear condensers c_1 and c_2 , one linear resistance R_1 where the nonlinear characteristic of the capacitor is a constitutive relation of the form:

$$v(q) = \frac{q}{c_1} + 2v_0 \sinh^{-1}\left(\frac{-q}{2I_0 R_1 c_2}\right), \quad (1.3)$$

where I_0 the leakage current, and v_0 the characteristic voltage.

-Inductance with nonlinear term in the flux-voltage: The formulas for the calculation of the self-inductance are given bellow [91]:

Single layer coil:

$$L = \frac{(rN)^2}{9r + 10l}, \quad (1.4)$$

multilayer coil:

$$L = \frac{0.8(rN)^2}{6r + 9r + 10l}, \quad (1.5)$$

single layer spiral coil:

$$L = \frac{(rN)^2}{8r + 11l}, \quad (1.6)$$

where L is the self-inductance, N the total numbers of turns, r the mean radius, and l the length and the depth of the coil respectively. The magnetic circuit is saturated when the current i flowing into the inductor is greater than the nominal current i_0 , (γ is the saturated parameter) and the flux-current Ψ characteristics can be approximated by a mathematical relation of the form [92]:

$$\Psi = Li_0 \left[\left(\frac{i}{i_0} \right) + \gamma \tanh \left(\frac{i}{i_0} \right) \right]. \quad (1.7)$$

Electronic components deliver low power, this is a very great difficulty when we carry out experimentation. It is also difficult to identify nonlinear characteristics in electronic and/or mechanical components. As consequence, the chaotification technique which consists to introduce electronic components in the EMS, is limited to low power devices (e.g., microelectromechanical systems).

Research is still in progress to find other ways to induce chaos in EMS, particularly in EMS using linear electric and/or mechanic components that can be used to provide high power actuation force, this problem is considered in this research work. A very large field of research is still in progress, when chaos is generated in EMS. In this work, the generation of the chaotic behaviour in EMS is achieved by the introduction of a bistable potential in a device dynamic using three permanent magnets in one hand. On the other hand, we also use the nonlinear hysteretic iron-core inductor express as [74]:

$$L = \left[\frac{\mu_0 N^2 A}{l} + \frac{B_s N^2 \alpha A}{2l} \cdot \frac{2}{1 + \cosh\left(\frac{\alpha Ni}{l} - \sigma_1\right)} \right], \quad (1.8)$$

where $\sigma_1 = \beta \text{sign}\left(\frac{di}{dt}\right)$, and $\mu_0 = 4\pi \cdot 10^{-7}$ H/m is the air permeability, α and β are two parameters which can be determined from the relation between the magnetic induction and the magnetic field. The ferromagnetic core inductance L in equation (1.8) is a function of the current i in the electrical circuit.

However, the investigation of chaos in motors drive attracted just a few authors in literature. Recently, the investigation of chaos in motor drives has been accelerated. Moreover, recent research has shown that chaos dynamics in motor drive can actually be useful under certain conditions, and there is interest in utilizing the very nature of chaos. For example, chaos is thought to be important in fluid mixing and vibrating sieves. Thus, a controllable chaotic motor drive, namely chaotifying a motor drive, is highly desired for some practical engineering system.

1.4. Some interesting MaEMS

The devices that we will present below have been studied in our research group. We describe their mode of operation, and present the equations that govern their dynamics while specifying the methods used to obtain these equations.

1.4.1. MaEMS as motor

Motors is an electromechanical system that refers to a mechanical element coupled to electrical circuits via electromechanical transducers. The input transducer takes electrical signals from the input circuit and provides mechanical stimuli to the mechanical system. One can thus define electric motors as rotating EMS that convert electrical energy into mechanical one and are among the most efficient means of producing mechanical vibrations. Electric motors are used in various branches of engineering, they are very durable devices and they can be found in a huge array of applications. Electric motors are so ubiquitous that it's hard to gather few appliances without finding one that has not an electric motor somewhere. From toys to the fans on air-conditioning, heating systems and beyond, electric motors are among the most common electrical components in use today.

Electric motors modelling equations present some complexities which are interesting and stimulating challenges both mathematically and numerically. Considerable efforts have been devoted to the study of oscillatory and chaotic states of some vibrational EMS [3,13-19,94]. Many methods are used to characterize the chaos behaviour in an EMS. Along these lines, numerical indicators such as the Lyapunov exponents and bifurcation diagrams are usually used to determine the appropriate range of parameters for which the device exhibits nT period-oscillations and chaos oscillations [3].

Nonlinear dynamics of MaEMS have been studied recently [17]. Depending on the form of the external excitation and the set of the chosen parameters, electric motors lead to various interesting phenomena such as frequency entrainment, harmonic, subharmonic, super harmonic oscillations, and chaos [13, 14-19]. These contributions have also shown that nonlinear phenomena can have negative interest or useful effects in science and engineering. The negative effects are due to the fact that nonlinear phenomena can conduct to a malfunction of systems and cut short their live cycle, or drive the systems to a reversal and catastrophe phenomena. The complexity of the Electric motors behaviour has attracted the attention of various scientists [94]. In fact, its useful interests are their many applications in engineering fields. For instance, chaos has been used in the building of better digital filters. To model the structural dynamics in such structures as buckling columns and the secure communication [87, 95]. Industrial mixing processes [47, 96], chaotic industrial shaking processes [8] and monitoring compaction [47]. There are several electromechanical devices that operate in motor mode, we will present only a few here.

1.4.1.1. Rotary motor

The electric motors also called electric actuators consist of a fixed part called a stator and a mobile part called a rotor. The stator core is made up of many thin metal sheets, called laminations. Laminations are used to reduce energy losses that would result if a solid core were used. The rotor usually has conductors laid into it which carry currents that interact with the magnetic field of the stator to generate the forces that turn the shaft. However, some rotors carry permanent magnets, and the stator holds the conductors.

According to whether the excitation current is continuous or alternating, there are two main families of electric motors, namely: AC motors and DC motors. Each family is made up of a wide variety of actuators depending on their use. Here we will focus only on DC motor.

1.4.1.2. Direct Current (DC) motors

By the manner to connect the stator with rotor, one distinguishes: Separately Excited Direct Current (SEDC) motor (as for instance Permanent Magnet Direct Current (PMDC) motor), Compound-Connected Direct Current (CCDC) motor, Series Connected Direct Current (SCDC) motor and Shunt Connected Direct Current (ShCDC) motor.

1.4.1.3. Separately Excited Direct Current (SEDC) motor

The choice of separately excited DC motor is because in addition to its industrial applications we can obtain the other from it changing simply the manner to connect the rotor with stator. Often used as actuators, SEDC motor is used in trains and for automatic traction purposes. The schematic representation of SEDC motor is shown below:

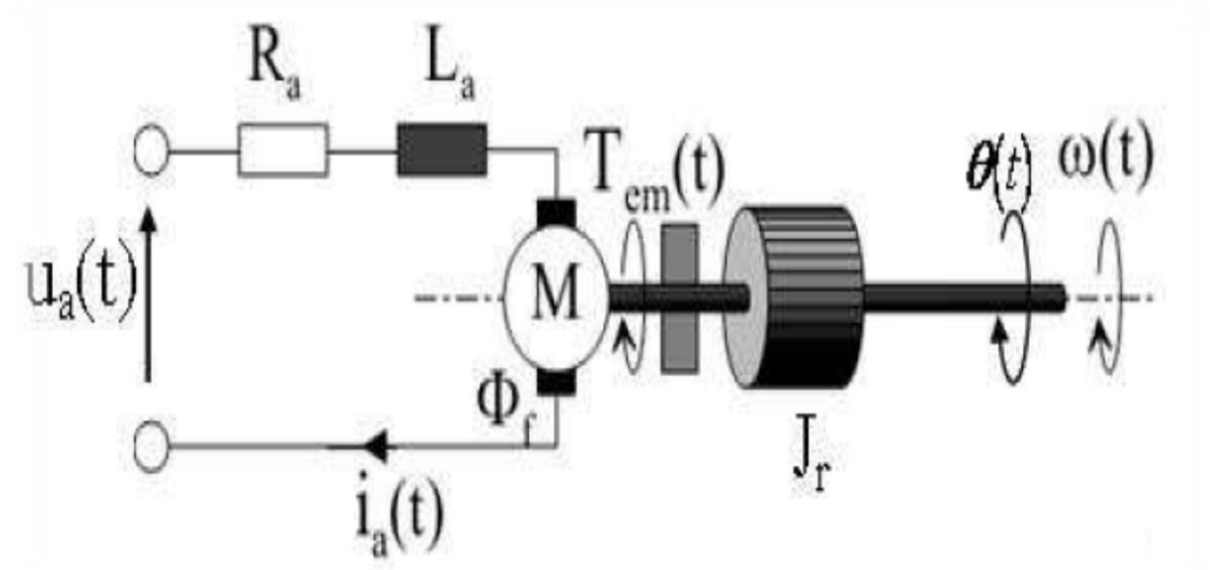


Figure 1 - Schematic representation of SEDC motor [13].

L_a and R_a are respectively the self-inductance and resistance of the rotor, $U_a(t)$ is the external voltage and $i_a(t)$ the current across the rotor. $\omega(t)$ is the angular velocity of the rotor motion and $\Phi_f = k_f i_f(t)$ the magnetic inductor flux.

Using the Kirchhoff's voltage law, the equation of the electrical part is given by the following equation [19]:

$$L_a \frac{di_a}{dt} + R_a i_a + e_m(t) = u_a(t), \quad (1.9)$$

where, at the left side, the first term is the voltage across the inductor, the second term is the ohmic voltage and the third term $e_m(t) = k_E \Phi_f \omega(t)$ is the back electromotive force (BEMF)

which represents the coupling term between the electrical part and mechanical part of the device and k_E the BEMF constant.

Using the Newton second law of dynamics for rotating motions and taking into account Laplace force, the equation of the mechanical part is obtained as:

$$\left\{ \begin{array}{l} \frac{d\theta}{dt} = \omega(t) \\ J_r \frac{d\omega}{dt} + C_v \omega(t) + T_f \text{sign}(\omega(t)) = T_{em}(t) - T_L \end{array} \right. \quad (1.10)$$

where:

$J_r : [kg.m^2]$ is the rotor inertia coefficient, $C_v : [N.m.s]$ the viscous friction coefficient, $T_f : [N.m]$ the dry friction torque, $T_{em}(t) = k_T i_a(t)$ the electromagnetic torque due to the Laplace force, $T_L : [N.m]$ the resistive torque due to external load and k_T the torque constant. $T_{em}(t)$ represents the coupling term between the mechanical part and the electrical part of the device. Then, the electromechanical equations of SEDC motor are written as:

$$\left\{ \begin{array}{l} \frac{d\theta(t)}{dt} = \omega(t) \\ L_a \frac{di_a}{dt} + R_a i_a + K_E \Phi_f(t) \omega(t) = u_a(t) \\ J_r \frac{d\omega(t)}{dt} + C_v \omega(t) + T_f \text{sign}(\omega(t)) = K_T \Phi_f(t) i_a - T_L \end{array} \right. \quad (1.11)$$

Replacing the winding stator by a pair of permanent magnets (see Figure 1), the magnetic flux stator $\Phi_f = cst$ and therefore, the system of equation (1.11) can be expressed as [97]:

$$\left\{ \begin{array}{l} \frac{d\theta(t)}{dt} = \omega(t) \\ L_a \frac{di_a}{dt} + R_a i_a + K_E \omega(t) = u_a(t) \\ J_r \frac{d\omega(t)}{dt} + C_v \omega(t) + T_f \text{sign}(\omega(t)) = K_T i_a - T_L \end{array} \right. \quad (1.12)$$

This set of equations represent the mathematical modelling of PMDC motors that is the case of constant magnetic flux.

1.4.1.4. Electromechanical pendulum as motor

The electromechanical pendulum is moved under the action of an external voltage source. In this case, we consider that the pendulum is in horizontal position so, the weight of the mechanical part will no longer be considered. The electric circuit used to drive the rotating arm consists of a resistor R , an inductor L and the external excitation is a voltage $u(t)$ all connected in series. The rotating arm is a thin rod of mass m and length ℓ . The rod has a plate of length $\sigma\ell$ (with $\sigma = \frac{1}{2}$), on which n electrical windings are applied. The coupling term between the electrical and mechanical part (that is the induced electromotive force taking into account the flux of linkage between the rotational displacement θ and the magnetic field B) is [17]:

$$e(t) = -nB\sigma^2 \frac{\ell^2}{2} \frac{d\theta}{dt}. \quad (1.13)$$

The Laplace force ($nB\sigma\ell i$) assumed applied at the centre ($\frac{\sigma\ell}{2}$) of the plate gives rise to the moment $\frac{nB\sigma^2\ell^2}{2} i$. The displacement applied on the springs during the rotating arm oscillations expressed as $\frac{\ell}{2} \sin(\theta)$ and the displacement between the springs force and the rotational axis ($\frac{\ell}{2} \cos(\theta)$) give the moment of the force due to the action of the linear springs as

$$F = k \frac{\ell^2}{4} \sin(\theta) \cos(\theta). \quad (1.14)$$

We assume that the total mass of the conducting wire and the plate bathing in the magnetic field can be neglected compared to the rotating arm mass. The rotating arm moves in a viscous medium with frictional coefficient β_1 . The resulting electromechanical equations that govern the system are:

$$\begin{cases} L \frac{di}{d\tau} + Ri + nB\sigma^2 \frac{\ell^2}{2} \frac{d\theta}{dt} & = u(t) \\ J \frac{d^2\theta}{dt^2} + \frac{\beta_1 \ell}{2} \frac{d\theta}{d\tau} + k \frac{\ell^2}{4} \sin(\theta) \cos(\theta) - \frac{niB\sigma^2 \ell^2}{2} & = 0 \end{cases} \quad (1.15)$$

Where i is the electric current flowing in the electrical circuit.

1.4.2. MaEMS as generator

Generators are devices that collect energy from the natural and artificial sources and convert them into electrical one. Generators require specific environmental conditions; for instance, solar cells and piezoelectric generators require sunlight and mechanical vibration respectively. An electromechanical generator is a device that converts mechanical energy (environmental vibrations) into electrical energy. There are several types of electromechanical generator, we will present some.

1.4.2.1. Electromechanical pendulum as generator

The device shown in Figure 2 is an electromechanical pendulum in which the stator is constituted of two permanent magnets and produce a constant magnetic field. One linear spring is fixed on the rod bearing the proof mass. While the unidirectional and horizontal external excitation which can be a wind or the motion of a given fluid is applied, the pendulum oscillates from left to right side around the vertical position with an angle θ . The motion of the pendulum due to the external excitation is converted into electrical energy which can be used to power a resistor load, the case where the fixed spring is nonlinear have been well studied in the literature [98].

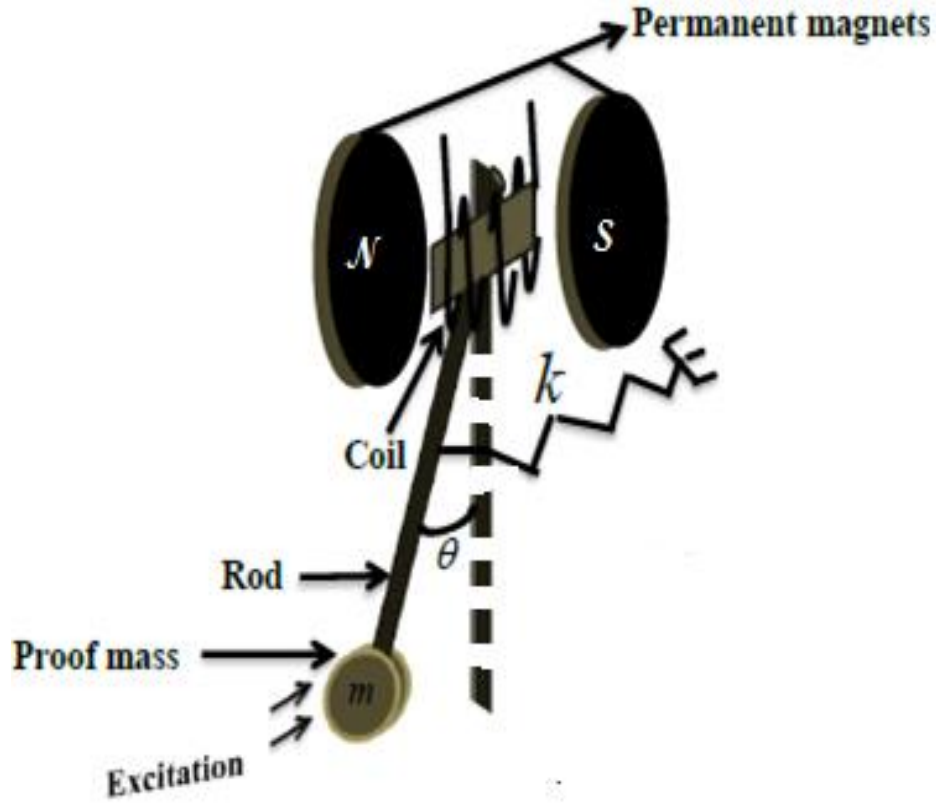


Figure 2 - Schematic diagram of an energy harvester model [98].

The inductance of the coil is linear and is given as:

$$L_0 = \frac{\mu_0 \mu_r n^2 \sqrt{a^2 + b^2}}{\pi} . \quad (1.16)$$

The expression of the coil resistance:

$$R_i = 2\rho \frac{(a+b)}{S_c} n . \quad (1.17)$$

Using Kirchhoff's laws, the equation of the electrical part is given by the following relation:

$$L \frac{di}{dt} + (R_i + R_L) i = e(t) , \quad (1.18)$$

where $i(t)$ is the current across the electrical coil. In equation (1.15), the first term is the voltage across the inductor, the second term is the ohmic voltage and the third term express as.

$$e(t) = 0.5nBb^2 \frac{d\theta}{dt} . \quad (1.19)$$

Equation (1.19) represents the coupling term between the electrical and mechanical part, R_L is the load resistance. For the mechanical part, the horizontal displacement applied on the spring during the rod oscillations is expressed as:

$$z = 0.5l \sin \theta. \quad (1.20)$$

Using Newton's second law of dynamics for rotational motion, and taking into account the Laplace force, the equation of the mechanical part is given by equation (1.21):

$$J \frac{d^2\theta}{dt^2} + \frac{l}{2} m_{\Delta} g \sin \theta + \frac{\beta l}{2} \frac{d\theta}{dt} + k \frac{l^2}{4} \sin(\theta) \cos(\theta) + \frac{nBb^2}{2} i = l(F_0 + F_1 \cos(\Omega t) \cos \theta), \quad (1.21)$$

where J is the total moment of inertia and m_{Δ} the total mass of the mechanical structure, Ω is the frequency of the environmental vibrations. The resulting electromechanical equations that govern the system are:

$$\begin{cases} L \frac{di}{d\tau} + (R_i + R_L) i & = 0.5nBb^2 \frac{d\theta}{dt} \\ J \frac{d^2\theta}{dt^2} + \frac{l}{2} m_{\Delta} g \sin \theta + \frac{\beta l}{2} \frac{d\theta}{dt} + k \frac{l^2}{4} \sin(\theta) \cos(\theta) + \frac{nBb^2}{2} i & = l(F_0 + F_1 \cos(\Omega t) \cos \theta \end{cases}. \quad (1.22)$$

The next paragraph investigates the design of an energy harvesting device that uses the rotating magnetic field to produce the electrical energy from electromagnetic induction.

1.4.2.2. Rotary wheel

Figure 3 shows the schematic representation of the rotational wheel system harvester that consists of permanent magnets attached to the wheel whose motion is activated by the external torque. The energy harvesting system from a rotational wheel require constant or time dependent torques. The movement is studied with one dimension in polar axis, noted θ which is the angle swept by a given radius of the wheel

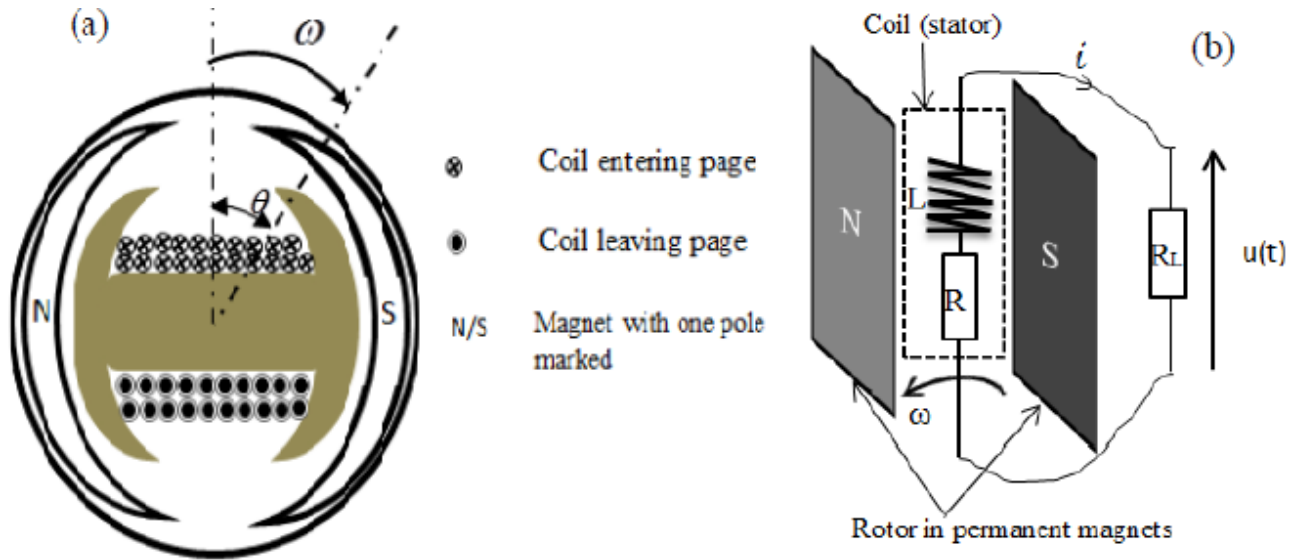


Figure 3 - Schematic representation of the rotational wheel system harvester that consist of permanent magnets attached to a wheel.

Electrical circuit consists of two permanent magnets attached to a wheel. A fixed coil with iron core is placed between the permanent magnets of the wheel. The rotational motion of the wheel around the coil converts the external stresses into electrical energy which powers a resistor load (Figure 3(b)). In fact, a magnetic flux variation induces a voltage at the coil terminals and this energy is delivered to the resistive load. The power delivered to the resistive load R_L , can then be obtained from:

$$P = UI = R_L I^2, \quad (1.23)$$

with R_L the load resistance and I the induced current trough the generator. Using Newton's second law for rotational movement to the wheel, it is found that the mechanical system is described by the following differential equation:

$$J \frac{d^2\theta}{dt} + C \frac{d\theta}{dt} + F_l = T(t), \quad (1.24)$$

where, the wheel inertia is defined as: $J = MR^2$, R is the radius of the wheel, and C is the viscous damping. The torque of Laplace's force is:

$$F_l = BIl_c, \quad (1.25)$$

l_c is the length of the coil and $T(t)$ the external torque due to the ambient force. The magnetic flux density B within the windings is:

$$B = B_0 \cos \theta . \quad (1.26)$$

B_0 is the maximum of the magnetic field delivered by permanent magnets. It is assumed that the magnetic circuit can be subjected to the magnetic flux more than its ability. In that case, its inductance follows a nonlinear behaviour, and its expression is [95]:

$$L=L_0 \left[1 + \gamma - \gamma \tanh^2 \left(\frac{i}{i_0} \right) \right], \quad (1.27)$$

with the linear inductance

$$L_0 = \mu_r \mu_0 S \frac{n^2}{l_c}, \quad (1.28)$$

γ the saturation parameter [68,95], S the coil section and l the total length of the winding. i_0 is the normalized current, n is the number of coil turns. According to Kirchhoff's law for the electrical circuit, it is found that the electrical system is described by the follow differential equation:

$$L_0 \left[1 + \gamma - \gamma \tanh^2 \left(\frac{i}{i_0} \right) \right] \frac{di}{dt} + Ri + R_L i - e(t) = 0. \quad (1.29)$$

According to the faraday's law, the induced voltage across the coil is:

$$e(t) = B_0 S n \frac{d\theta}{dt} \sin \theta , \quad (1.30)$$

and the internal resistance of the coil is:

$$R_{in} = \rho \frac{l}{s_f} . \quad (1.31)$$

s_f is the copper section. The governing equations of the mechanical and electrical parts are derived are:

$$\left\{ \begin{array}{l} L_0 \left[1 + \gamma - \gamma \tanh^2 \left(\frac{i}{i_0} \right) \right] \frac{di}{dt} + (R + R_L) i + B_0 S n \frac{d\theta}{dt} \sin \theta = 0 \\ J \frac{d^2 \theta}{dt} + C \frac{d\theta}{dt} + B_0 I l l_c \cos \theta = T(t) \end{array} \right. \quad (1.32)$$

1.5. Derivation of the magnetic potential energy

Let's considered E_{mag} as the magnetic potential energy. To derive this magnetic potential energy, let us consider Figure 4.

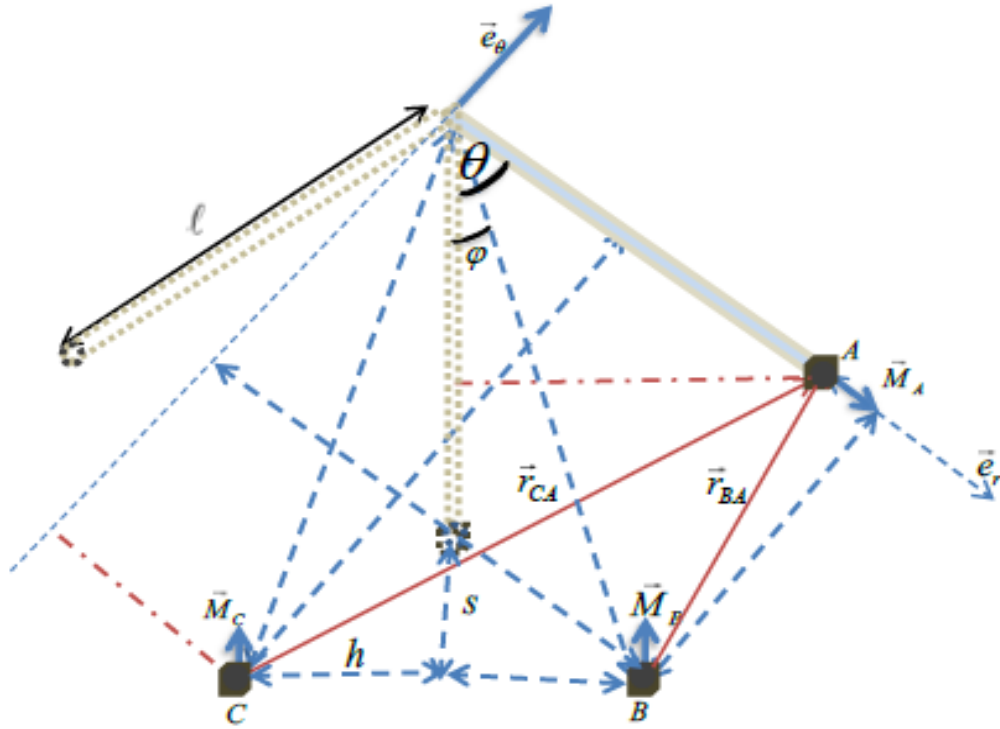


Figure 4 - Schematic structure for the derivation of the magnetic potential energy.

The magnets A, B, C are identical. The potential energy of the magnet A in the field generated by the magnets B and C is [99]:

$$E_{mag} = -(\vec{B}_{BA} + \vec{B}_{CA}) \cdot \vec{M}_A = \frac{\mu_0 M_A^2 \cos \theta}{2\pi} \left(\frac{1}{r_{BA}^3} + \frac{1}{r_{CA}^3} \right), \quad (1.33)$$

where \vec{B}_{BA} and \vec{B}_{CA} are respectively the magnetic field creates on magnet A by magnet B and magnet C . The distance between B and A is given in annex. Taking into account these distance, one obtains the potential energy:

$$E_{mag} = \frac{\mu_0 M_A^2 \cos \theta}{2\pi} \left[\frac{1}{\left[q_1 - p_1 \sin\left(\frac{\pi}{2} - \theta - \varphi\right) \right]^{\frac{3}{2}}} + \frac{1}{\left[q_1 - p_1 \sin\left(\frac{\pi}{2} - \theta + \varphi\right) \right]^{\frac{3}{2}}} \right] \quad (1.34)$$

where:

$$q_1 = \ell^2 + h^2 + (s + \ell)^2; \quad p_1 = 2\ell\sqrt{h^2 + (s + \ell)^2}; \quad \varphi = \arctan\left(\frac{h}{s + \ell}\right) \quad (1.35)$$

The interaction force between the magnets can be obtained by taking the gradient of equation (1.34)

$$\vec{f}_{mag} = -\overrightarrow{grad}(E_{mag}) = -\frac{1}{\ell} \frac{d}{d\theta} (E_{mag}) \vec{e}_\theta$$

$$= \frac{\mu_0 M_A^2}{2\pi\ell} \left[\left[\frac{1}{\left[q_1 + p_1 \sin\left(\theta - \frac{\pi}{2} + \varphi\right) \right]^{\frac{3}{2}}} + \frac{1}{\left[q_1 + p_1 \sin\left(\theta - \frac{\pi}{2} - \varphi\right) \right]^{\frac{3}{2}}} \right] \sin \theta \right. \\ \left. + \frac{3}{2} \left[\frac{p_1 \sin\left(\theta - \frac{\pi}{2} + \varphi\right)}{\left[q_1 + p_1 \sin\left(\theta - \frac{\pi}{2} + \varphi\right) \right]^{\frac{5}{2}}} + \frac{p_1 \sin\left(\theta - \frac{\pi}{2} - \varphi\right)}{\left[q_1 + p_1 \sin\left(\theta - \frac{\pi}{2} - \varphi\right) \right]^{\frac{5}{2}}} \right] \cos \theta \right] \vec{e}_\theta .$$

(1.36)

By taking into account the fact that magnets are at the end (distance ℓ) of the rotating arm, the displacement between the magnetic force and the rotational axis (ℓ) give the moment of the magnetic force as:

$$\vec{F}_{mag} = \frac{\mu_0 M_A^2}{2\pi} \left[\begin{array}{c} \left(\frac{1}{\left[q_1 + p_1 \sin\left(\theta - \frac{\pi}{2} + \varphi\right)\right]^2} + \frac{1}{\left[q_1 + p_1 \sin\left(\theta - \frac{\pi}{2} - \varphi\right)\right]^2} \right) \sin \theta \\ + \frac{3}{2} \left(\frac{p_1 \sin\left(\theta - \frac{\pi}{2} + \varphi\right)}{\left[q_1 + p_1 \sin\left(\theta - \frac{\pi}{2} + \varphi\right)\right]^2} + \frac{p_1 \sin\left(\theta - \frac{\pi}{2} - \varphi\right)}{\left[q_1 + p_1 \sin\left(\theta - \frac{\pi}{2} - \varphi\right)\right]^2} \right) \cos \theta \end{array} \right] \vec{k}.$$

(1.37)

As summary, the interaction force between the magnets is well a unidirectional force and directed by \vec{e}_θ , otherwise, it might present at a pitch phenomenon.

1.6. Some essential works carried out on MaEMS in our research group

Nonlinear dynamics of MaEMS have been studied recently [17]. Depending on the form of the external excitation and the set of the chosen parameters, electric motors lead to various interesting phenomena such as frequency entrainment, harmonic, subharmonic, super harmonic oscillations, and chaos [13, 14-19]. The automation of some hard mechanical work using electric motors has gadered and increasing interest during this last decade [30]. As far as sieve process is concerned, chaotic dynamic is expected to ensure a good performance of the device [87-96]. Consequently, intense research activities are actually conducted for the chaos dynamic of pendulum arms which are currently the standard approach to automatize sieve or mixing process [18]. In order to design a home sieving device and an industrial sieving device, the nonlinear dynamics in electromechanical systems with rotating electric motors has been studied recently [97]. Their dynamical behaviors show common nonlinear phenomena such as jump, period- nT oscillations, quasi-periodic and chaotic motions. Depending of their parameters values, the device can operate either in the regular states or in the chaotic states during its functioning. The authors used Intermittent Power Supply Feedback Control (IPSFC) and Field Oriented Control (FOC) associate to Time Delay Feedback Control (TDFC) to generate desired complex phenomena such as period- nT oscillations and chaotic motions in the home sieving

device and industrial sieving device respectively. These studies are interesting because the disorder involve the dispersion of the particles. In [90] the modeling and dynamics of systems consisting of rigid and flexible pendulum arms, magnetically coupled with electrical circuits by means of electromechanical transducers are considered. The control law is designed following an energy-based approach. The forced response of pendula is very rich and complex. Bifurcation diagrams show various states of the model: uniperiodicity, period-doubling, quasiperiodic, multiperiodicity, as well as chaotic behavior.

These contributions have also shown that nonlinear phenomena can have negative interest or useful effects in science and engineering. The negative effects are due to the fact that nonlinear phenomena can conduct to a malfunction of systems and cut short their live cycle, or drive the systems to a reversal and catastrophe phenomena. The complexity of the Electric motors behaviour has attracted the attention of various scientists [30]. In fact, its useful interests are their many applications in engineering fields. For instance, chaos has been used in the building of better digital filters. To model the structural dynamics in such structures as buckling columns and the secure communication [87, 95]. Industrial mixing processes [20,96], chaotic industrial shaking processes [8] and monitoring compaction [29].

1.7. Motivation and challenges

The investigation of chaotic motors drive both on feedback, and time-delay feedback are highly presented in the literature. The EMS constituted by asynchronous motors when they are supplied with sinusoidal voltage, exhibit chaotic behaviour for some parameter's values. Those EMS have nonlinear electronic and/or mechanical components such as capacitors with nonlinear charge-voltage characteristics and inductance with nonlinear term in the flux-voltage characteristics just to name a few. **The limitation is that** practically, electronics components deliver low power and it is difficult to have mechanical components with nonlinear characteristics. Since the disorder involve the dispersion of the particles, chaotic motors, are highly desired for some practical engineering system. Research is still in progress to find other ways to induce chaos in motor drive.

The purpose of this thesis, is to induce the chaotic dynamics to rotating arm of electromechanical robots by inducing a bistable potential in the electromechanical system. This is done by considering one permanent magnet fixed at the free end of a mechanical rotating arm. In the right and in the left of the equilibrium state of the mechanical rotating arm, there

are two other permanent magnets. On the other hand, as the ferromagnetic circuit is made of steel or iron sheet, the flux through the iron core is not always constant, but can vary with the current, the effects of such behavior on the dynamical behaviors of the device allows us to delineate the domains of regular periodic dynamics and that of chaotic dynamics when the device parameters change. **This is the induction of a hysteretic iron-core inductor within the device. The third method is the use of delay in the electromechanical system** in fact, the time delay here can be due to an embedded control system that serves as the communication system taking a message at the source (tachogenerator) and sending it to the receiver (electrical part of the electromechanical rotating arm).

1.8. Conclusion

In this chapter, we have presented some important notions and definitions of topics of this thesis. We have presented some MaEMS, some applications in electricity are presented. Some brief generalities and definition of nonlinear dynamic are given and a particular attention on chaotic phenomenon and the route to chaotic dynamic of MaEMS are discussed. We also presented some MaEMS coming from the literature and in our research group. It follows that, key part of this thesis is: **the generation of complex dynamical behaviour using bistable potential, hysteretic iron-core inductor and delay in an electromechanical rotating arm activated by a rotary motor.** We ended the chapter by presenting the motivations and challenges. The next chapter presents the methods used in this thesis.



CHAPTER 2

Methodology



CHAPTER 2

2- Methodology

2.1. Introduction

This chapter deals with the presentation of the analytical and numerical simulations methods that will be used to solve the problems of the thesis. Section 2.2 presents the mathematical formalisms and the numerical methods used to solve the differential equations as well as the hardware and software used. In section 2.3, the computational tools for the characterization of the dynamical is given. The conclusion of the chapter appears in section 2.4.

2.2. Mathematical formalisms and numerical methods

To solve the Nonlinear Ordinary Differential Equations (NODEs) describing the mathematical models of our devices. One uses some mathematical formalisms and numerical methods which are presented here.

2.2.1. Mathematical formalisms

Three analytical formalisms are presented. The first is the linear stability analysis which is used to analyse the stability of the electromechanical system around its equilibrium points. The second shows the principle of harmonic balance used to obtain the analytical solutions of the systems (NODEs) that describe the mathematical models of our devices. The third presents the Melnikov method for chaos, guarantees that the electromechanical system has a smale horseshoe type chaos.

2.2.1.1. Linear stability analysis of ordinary differential equations

An important issue in any dynamical system is the investigation of the stability of their steady-state solutions or fixed points. To this end let us consider a given set of autonomous ODEs of first order, written in the vector form:

$$\frac{dX(t)}{dt} = F(X(t), \beta) \quad (2.1)$$

Where $X(t) = (x_1(t), x_2(t), \dots, x_n(t))$ is the vector of the n dynamical variables of the system, a set of parameters β and $F = (F_1, F_2 \dots, F_n)$ is a differentiable vector function. Suppose that X_0 is a steady state. The linear stability analysis is based on analysing the time-dependent trajectory of a system slightly perturbed from a steady state X_0 . Therefore, the solution $X(t)$ can be represented as a sum of the steady state X_0 and a small perturbation $\delta X(t)$:

$$X(t) = X_0 + \delta X(t) \quad (2.2)$$

Inserting (2.2) in (2.1) and linearizing around the steady state X_0 leads to the variational equation for the variable $\delta X(t)$.

$$\frac{d\delta X(t)}{dt} = J\delta X(t), \quad (2.3)$$

Where J , the matrix of the partial derivatives is called the Jacobian matrix. The eigenvalues of the linear system of the equations (2.3) can be found from the characteristic equation of the system:

$$\det(\lambda I - J) = 0 \quad (2.4)$$

Where, I is the unit matrix and, λ are the eigenvalues of the system (2.4) and roots of the characteristic equation. The stability of the steady state X_0 . Is determined by the eigenvalues of the system (2.4), as follows:

- If the eigenvalues of the Jacobian matrix all have real parts less than zero, then the steady state is stable;
- If at least one of the eigenvalues of the Jacobian matrix has real part greater than zero, then the steady state is unstable.

This mathematical formalism is the basic principle of linear stability analysis for ODEs. It will be used in the following chapter to analyze the stability of the equilibrium points of electromechanical rotating arms.

2.2.1.2. Principle of harmonic balance

This method is widely used to determine an approximate periodic solution of NODE(s) submitted to sinusoidal excitations [100,101]. Consider the following differential equation:

$$\ddot{x} + x = \mu f(x, \dot{x}, t), \quad (2.5)$$

where the function $f(x, \dot{x}, t)$ contains explicitly the time t and we assume that $f(x, \dot{x}, t+T) = f(x, \dot{x}, t)$ the harmonic solution of this equation is expressed in the form:

$$x(t) = A_0 \sin(\omega t) + B_0 \cos(\omega t), \quad (2.6)$$

where $x_{\max} = \sqrt{A_0^2 + B_0^2}$ is the maximal amplitude of oscillations. Replacing equation (2.6) into equation (2.5) and equating separately the coefficient of sine and cosine terms, which have the same harmonics, one obtains (neglecting harmonics order greater than one) a system of algebraic equations which are the amplitude equations. This procedure is the basic principle of harmonic balance. It will be used in chapter 3 to obtain the amplitude and frequency response curves of the electromechanical devices with rotating arm.

2.2.1.3. Melnikov criteria for chaos

A key point with unstable and chaotic engineering system is to derive a mathematical condition overlapping the parameters of the system and leading to such phenomenon. Melnikov method is one of the best approach for this task. It is an analytic technique, which can be used to deduce the presence of chaos in a dynamical system. It helps to define the conditions for the existence of the so-called transverse intersection points between unstable separatrix or the appearance of the fractality on the basin of attraction. This approach was first used by Holmes (1979) to study the chaotic attractor of a periodically driven Duffing oscillator with linear stiffness. Frey and Simiu (1993) presented a generalized random Melnikov technique to study the effect of noise on near integrable second order dynamical system. We consider the following class of systems:

$$\begin{cases} \dot{x} = \frac{\partial H}{\partial y}(x, y) + \varepsilon g_1(x, y, t, \varepsilon) \\ \dot{y} = -\frac{\partial H}{\partial x}(x, y) + \varepsilon g_2(x, y, t, \varepsilon) \end{cases} \quad (x, y) \in \mathbb{R}^2, \quad (2.7)$$

Or, in vector form,

$$\dot{q} = JDH(q) + \varepsilon g(q, t, \varepsilon), \quad (2.8)$$

Where, $q = (x, y)$, $DH = \left(\frac{\partial H}{\partial x}, \frac{\partial H}{\partial y} \right)$, $g = (g_1, g_2)$, $J = \begin{pmatrix} 0 & 1 \\ -1 & 0 \end{pmatrix}$

H is the Hamiltonian and g is the is a periodic perturbation function. The unperturbed system possesses a hyperbolic fixed point, p_0 connected to itself by a homoclinic orbit $q_0(t) \equiv (x_0(t), y_0(t))$. The unperturbed system is obtained from (2.8) by setting $\varepsilon = 0$

$$\dot{q} = JDH(q) \quad (2.9)$$

In the presence of the perturbation, $g(q, t, \varepsilon)$, the orbit is perturbed. When the perturbed and the unperturbed manifolds intersect transversally, the geometry of the basin of attraction may become fractal, indicating the high sensitivity to initial conditions, thus chaos. Let the Melnikov function, which gives a measure of the leading order distance between the stable and unstable manifold, can be used to tell when the stable and unstable manifolds intersect transversally be defined as :

$$M_e(t_0) = \int_{-\infty}^{+\infty} JDH(\bar{q}(t) \wedge g(\bar{q}(t), t + t_0)) \quad -\infty < t < +\infty \quad (2.10)$$

If $M_e(t_0)$ has simple zeros so that for a given $t_0 \neq 0$, one has $M_e(t_0) = 0$ with $\frac{dM_e(t_0)}{dt_0} \neq 0$ at $t_0 = 0$ (condition for transversal intersection), then the system (2.10) can present fractal basin boundaries for motions around the stable equilibrium point. The Melnikov's formalism will be use in chapter 3 to find the condition for the appearance of horseshoe chaos characterized by the fractality of the basin of attraction.

2.2.2. Numerical methods

It is known that ODEs (Ordinary Differential Equations) do not have exact analytical solutions. Therefore, analytical methods used permit only to obtain approximate solutions. One interesting technique used to study the systems of ODEs is the computer simulation. Many different methods have been proposed and used in an attempt to solve accurately various types of ODEs However, there are a handful of methods known and used universally (i.e., Runge-Kutta, Adams-Bashforth-Moulton and Backward Differentiation Formulae methods). All these discretize the differential system to produce a difference equation or map. The methods obtain different maps from the same differential equation, but they have the same aim; that the dynamics of the map should correspond closely to the dynamics of the differential equation. From the Runge-Kutta family of algorithms come arguably the most well-known and used methods for numerical integrations [104, 105]. Thus, we will review briefly two numerical

integration methods namely fourth order Runge-Kutta (RK4) for ODEs and DDEs (Delay Differential Equations).

2.2.2.1. Fourth-order Runge-Kutta method for ordinary differential equations

That methods have been elaborated for the first time in 1894 by Runge and have been improved by W. Kutta in 1901. the Runge-Kutta methods are an important family of implicit and explicit iterative methods for the approximation of solutions of ODEs. The basics of those methods are presented in the course of Numerical Methods courses delivered to Master students in physics at University of Yaoundé 1 [106]. They use both the trapezium numerical integration and Simpson methods. Those methods are widely used since they are most stables. Consider the ordinary first order differential equation:

$$\frac{dy}{dx} = f(x, y), \quad (2.11)$$

with $y(x_0) = y_0$ is a vectorial variable. The aim is to find the solutions of equation (2.48) using RK4 method, knowing $y(x_0)$. This method stipulates that:

$$y(x+h) = y(x) + \frac{1}{6}(L_1 + 2L_2 + 2L_3 + L_4), \quad (2.12)$$

h is the time step of x . L_1 , L_2 , L_3 and L_4 are express as follows:

$$L_1 = hf(x, y(x)); \quad L_2 = hf\left(x + \frac{1}{2}h, y(x) + \frac{L_1}{2}\right); \quad L_3 = hf\left(x + \frac{1}{2}h, y(x) + \frac{L_2}{2}\right); \quad \text{and}$$

$$L_4 = hf(x+h, y(x) + L_3)$$

This iteration procedure needs the initial value of y , that is when $x = x_0$ and the other values of y can be calculated using the relation (2.49). When the differential equation is of second order, one put it on the form of a system of first order differential equations written as follows,

$$\begin{cases} \frac{dy}{dx} = z = g(z) \\ \frac{dz}{dx} = f(x, y, z) \end{cases}, \quad (2.13)$$

and the Fourth Order Runge Kutta (RK4) iterations are given by the following relations:

$$\begin{cases} y(x+h) = y(x) + \frac{1}{6}(K_1 + 2K_2 + 2K_3 + K_4) \\ z(x+h) = z(x) + \frac{1}{6}(L_1 + 2L_2 + 2L_3 + L_4) \end{cases} \quad (2.14)$$

where

$$\begin{aligned} L_1 &= hf(x, y, z); & L_2 &= hf\left(x + \frac{1}{2}h, y + \frac{K_1}{2}, z + \frac{L_1}{2}\right); & L_3 &= hf\left(x + \frac{1}{2}h, y + \frac{K_2}{2}, z + \frac{L_2}{2}\right); \\ K_1 &= hg(z); & K_2 &= hg\left(z + \frac{L_1}{2}\right); & K_3 &= hg\left(z + \frac{L_2}{2}\right); & K_4 &= hg(z + L_3); \\ L_4 &= hf(x+h, y + K_3, z + L_3) \end{aligned} \quad (2.15)$$

Are intermediate coefficients and x runs for time incrementation.

We will use this method in chapter 3 to solve numerically the differential equations which govern the dynamical behavior of the studied devices.

2.2.2.2. Fourth-order Runge-Kutta method for delay differential equations (DDEs)

In DDEs, the dynamics at each instant x depends on the value of the vector y at the same instant t , but also on the value of y at a previous instant $t - \tau$, with $\tau > 0$ [107]. If we introduce the delayed variable $y(x - \tau)$ and the n -dimensional vectorial flow:

$G = (G_1, G_2, \dots, G_n)$, a DDE should formally read:

$$\frac{dy(x)}{dx} = G(x, y(t), y(x - \tau)) \quad \text{with } y(x) = g(x) \text{ for } x \in [-X, 0], \quad (2.16)$$

Where g is an n -dimensional vectorial function of time $y(x) = (y_1(x), y_2(x), \dots, y_n(x))$ and $y(x - \tau) = (y_1(x - \tau), y_2(x - \tau), \dots, y_n(x - \tau))$ vectorial variables. At the difference, of ODE where the initial conditions were given by a discrete and finite set of values, initial conditions in DDEs should be indicated (by the mean of a function) for all the values contained into the continuous interval $[-X, 0]$, so that an infinity of values should be known to characterize the system.

The RK4 scheme for DDE is given by [83]

$$y(x+h) = y(x) + \frac{h(L_1 + 2L_2 + 2L_3 + L_4)}{6}, \quad (2.17)$$

$$x = x+h. \quad (2.18)$$

Where,

$$\left\{ \begin{array}{l} L_1 = G(x, y(\tau, x), y(x)), \\ L_2 = G(x + \frac{h}{2}, y(\tau, x), y(x) + \frac{hL_1}{2}) \\ L_3 = G(x + \frac{h}{2}, y(\tau, x), y(x) + \frac{hL_2}{2}) \\ L_4 = G(x+h, y(\tau, x), y(x) + hL_3) \end{array} \right., \quad (2.19)$$

where x runs for time incrementation.

Differential equations with delay will be solve numerically in chapter 3 using the fourth order Runge-Kutta algorithm for delay

2.2.2.3. Hardware and software

During the postgraduate training, we used a Laptop computer running Windows 7 operating System and three major softwares: FORTRAN, MATLAB and MAPLE trial version.

2.3. Computational tools for the characterization of the dynamical states of non-linear systems

The dynamical states of physical systems studied in this work are governed by the systems of NODE. According to their parameters values, these physical systems can present various dynamical behaviours such as periodic, quasi-periodic and chaotic motions. Dynamical states of the nonlinear systems are usually investigated with a number of numerical tools such as the time histories diagram, phase portraits diagrams, bifurcation diagrams and Lyapunov exponent.

In this section, we give a brief account of the computational techniques which are used for characterizing different dynamical states of physical systems studied in this work.

2.3.1. Time histories diagram and phase portraits

The first approach of the detection of different dynamics states is visual and it is based to the computer simulation of NODE. Varying the parameter values of NODE, one observes carefully the time histories and phase portraits. The chaotic behaviour is distinguished from others by its extreme irregularity.

A phase portrait of a dynamical system is a mathematical space having orthogonal coordinate directions which represent each of the variables needed to specify the instantaneous state of the system. The state of a particle moving in one dimension is specified by its position and velocity. The state of a dynamical system is represented by a point in the phase space. As the system evolves in time, it constitutes a trajectory in the phase space. Phase portraits are an invaluable tool in studying dynamical systems. They consist of a plot of typical trajectories in the state space. This reveals information such as whether an attractor, a limit cycle is present for the chosen parameter value. However, the drawback of this computational tool is that it can be hard to distinguish the quasi-periodicity and chaos phenomena by using the phase portrait diagram. The dynamical behaviors of the devices mathematically represented by ordinary differential equations in chapter 3 are illustrated using numerical simulation to present Time histories and phase portraits.

2.3.2. Bifurcation diagrams

Another approach of the detection of dynamical states is the bifurcation diagram. Bifurcation diagram is helpful to understand how the long-term behaviour of a model changes as parameter values change. A bifurcation can also be defined as the event in which one of the properties of a dynamical system changes qualitatively when a control parameter of the system is varied. Points on the diagram that represent change in the behaviour are called bifurcation points [94,108]. This diagram is very important for the study of the route to chaos. But the Achilles heel of this method is the confusion between the quasi-periodicity and chaos phenomena. We can identify various routes to chaos taken by dynamical systems. The most common are: the

period doubling route, the quasi-periodic route and intermittency route. The most reliable indicator of chaos phenomenon is the maximum one-dimensional Lyapunov exponent.

2.3.3. Lyapunov exponents

Named after Lyapunov, a Russian mathematician, Lyapunov exponents are the widely accepted tools for characterizing chaotic and periodic states of a dynamical system. Lyapunov exponents describe the rate of divergence or convergence of nearby trajectories on to the attractor in different directions in phase space. It gives a measure of the sensitive dependence upon initial conditions which is a characteristic of chaotic system. The Lyapunov exponent expresses the convergence (when negative) or divergence (when positive) of nearby trajectories. Therefore, a state of the system is said to be chaotic if the Lyapunov exponent is positive (which corresponds, in the bifurcation diagram, to a cloud of points). The state of the system is said to be periodic if the exponent is negative (this corresponds, to a curve lines in the bifurcation diagram). The case $\lambda_{\max} = 0$ corresponds to the quasi-periodic state of the system. The maximum one-dimensional Lyapunov exponent is defined as:

$$\lambda_{\max} = \lim_{t \rightarrow +\infty} \left\{ \frac{1}{t} \ln [D(t)] \right\}, \quad (2.20)$$

with

$$D(t) = \sqrt{\delta_1^2 + \delta_2^2 + \delta_3^2}, \quad (2.21)$$

where $D(t)$ is the distance between neighbouring trajectories. It is computed from the variationally equations obtained by perturbing the solutions of equations (2.13) as follows

$$x \rightarrow x + \delta_1; \quad y \rightarrow y + \delta_2; \quad \dot{y} \rightarrow \dot{y} + \delta_3.$$

2.4. Conclusion

The objective of this chapter has been to present the mathematical formalisms and numerical simulation methods used to study the dynamics of the physical systems proposed in this thesis. We started by the presentation of the mathematical formalisms and the numerical methods used to solve the differential equations as well as the hardware and software used.

Then, an overview on the tools that will be used for characterization of the dynamical states of dynamical systems under consideration in the thesis has been given. The next chapter focuses on the dynamics of the electromechanical systems with rotating arm considered in this thesis.



CHAPTER 3

Results and discussions



CHAPTER 3

3- Results and discussions

3.1. Introduction

In this chapter, we present and discuss the results of the work done in this thesis. The effects of the bistable potential energy, hysteretic iron-core inductor and tachogenerator on the behaviours of electromechanical rotating and pendulum arms are studied. In section 3.2 a device consisting of an induction motor activating a rotating rigid arm is designed and comprises a bistable potential due to the presence of three permanent magnets. Its mathematical equations are established and the numerical results both in the absence and in the presence of magnets are compared. The generation of chaotic behavior is achieved using two different external excitations: sinewave and square wave. In the presence of magnets, the system presents periodic and dissipative chaotic dynamics. Approximating the global potential energy to a bistable quartic potential, the Melnikov method is used to derive the conditions for the appearance of Hamiltonian chaos. Section 3.3 present a new model of electromechanical system with rotating arm having nonlinear hysteretic iron-core inductor. Its mathematical equations are established and studied numerically. The generation of the chaotic behavior is achieved using two methods: introduction of a bistable potential by adding three permanent magnets in front of the rigid arm and the use of a delay generator. In section 3.4 a model of electromechanical system with pendulum arm constituted by linear components is analyzed. Its mathematical equations are established and studied numerically. The device firstly exhibits periodic dynamical behavior. The generation of the chaotic behavior is achieved using three methods. The first method is the introduction of a bistable potential by adding three permanent magnets in front of the rigid arm. The second method is the use of hysteretic iron-core inductor within the system and the third method is the use of a delay generator. In section 3.5, we end this chapter by a conclusion.

3.2. Dynamical behaviour of a bistable rotating electromechanical system

3.2.1. System and equations

The device shown in Figure 5 is an electromechanical system which consists of a mechanical rotating arm activated by a rotor. Its shaft is fixed mechanically at its two ends by two spiral torsion springs put up in anti-parallel manner. The coupling between the electrical and mechanical parts is realized through the electromagnetic force due to a permanent magnet. It creates a Laplace force in the mechanical part and the Lenz electromotive voltage in the electrical part. The electrical part of the system consists of a resistor R , an inductor L and a voltage source $u(t)$, all connected in series. One permanent magnet is fixed at the free end of the mechanical arm. In the right and in the left of the mechanical arm at equal distances to the equilibrium position, there are two other permanent magnets placed on top of a non-ferromagnetic bearer.

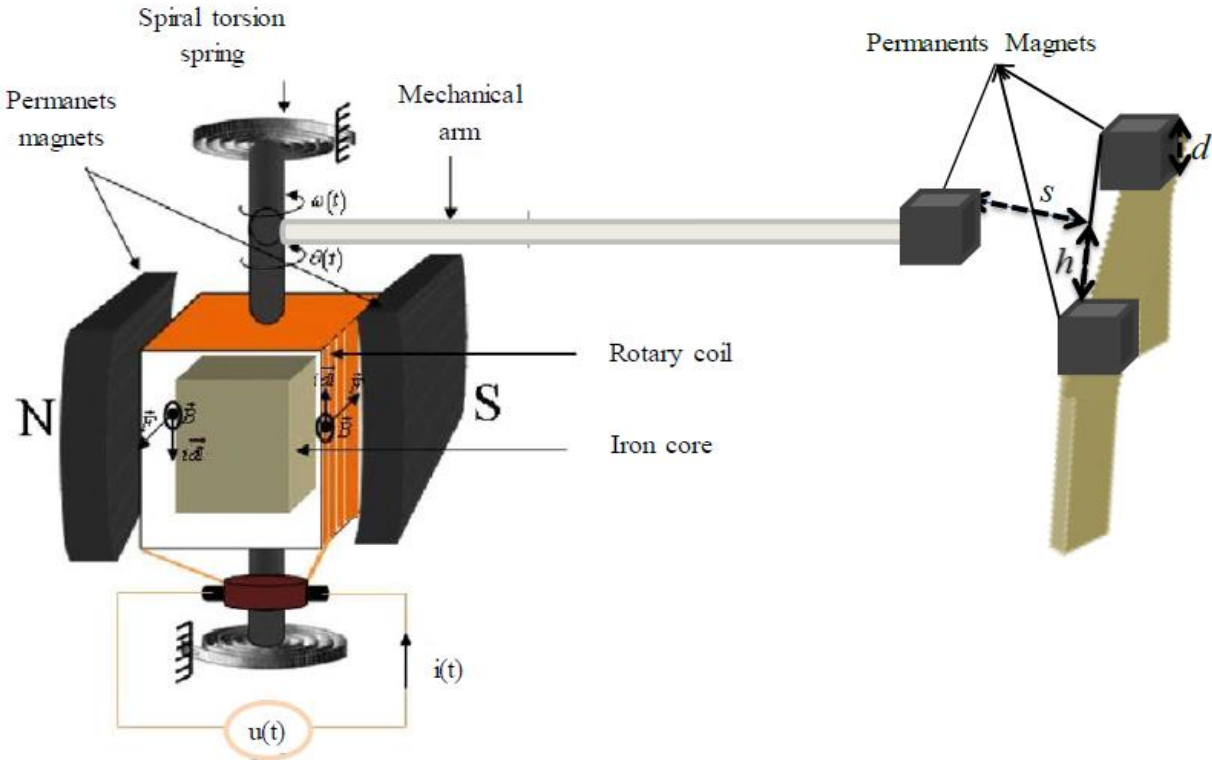


Figure 5 - Schematic representation of the electromechanical system.

Values and dimensions of the parameters of the device are given as follow.

Parameters	Values	Dimensions
Inductance: L	0.2	H
Resistance: R	2	Ω
Rotor inertia moment: J_r	4.1×10^{-2}	$kg.m^2$
Viscous damping coefficient: c_v	0.13×10^{-3}	$N.m.s / rad$
Back electromotive force constant: K_E	0.75×10^{-2}	$V.s / rad$
Stiffness coefficient: c_r	4×10^{-3}	$N.m / rad$
Torque constant: K_T	0.75×10^{-1}	$N.m / A$
Lenght of the mechanical arm ℓ	0.5	m
Magnetic moment M_A of the magnet	1.2	$A.m^2$
Magnets position h (see Fig.5)	0.02	m
Distance s of the free end of the arm and middle of the distance between the magnets	0.05	m

Table 1 - Parameters of the electromechanical system (some of these parameters are indicated in Figure 5).

These values are selected in order to provide to the device the appropriate dynamical states that can be beneficial for applications. By adding equation (1.37) to equation (1.12) where f_{mag} is the interaction force between the magnets, it is found that the system is described by the following set of differential equations:

$$\begin{cases} L \frac{di(t)}{dt} + Ri(t) + K_E \frac{d\theta}{dt} = u(t) \\ J_r \frac{d^2\theta}{dt^2} + c_v \frac{d\theta}{dt} + c_r \theta + \ell f_{mag} = K_T i(t) \end{cases} \quad (3.1)$$

Assuming that the potential U is the sum of the elastic potential energy and magnetic potential energy, one obtains:

$$U = \frac{c_r}{2} \theta^2 + \frac{\mu_0 M_A^2 \cos \theta}{2\pi} \left[\left[q_1 - p_1 \sin\left(\frac{\pi}{2} - \theta - \varphi\right) \right]^{-\frac{3}{2}} + \left[q_1 - p_1 \sin\left(\frac{\pi}{2} - \theta + \varphi\right) \right]^{-\frac{3}{2}} \right]. \quad (3.2)$$

The first term is the elastic potential energy due to the linear springs and the second term is the mechanical potential energy due to the magnets (see section 1.5, chapter 1) [109].

using the dimensionless variables:

$$\bullet = \frac{d}{d\tau}, \quad y = \frac{\theta}{\theta_0}, \quad x = \frac{i}{i_0}, \quad \tau = \omega_e t, \quad (3.3)$$

where i_0 and θ_0 are the normalized current and angular displacement. Replacing equations (3.3) into (3.1), one obtains the following dimensionless form

$$\begin{cases} \dot{x} = -\lambda_2 x - \lambda \dot{y} + E \sin(\varpi \tau) \\ \ddot{y} = \lambda_3 x - \lambda_1 \dot{y} - y - \beta g(y\theta_0) \end{cases}, \quad (3.4)$$

where

$$g(y\theta_0) = \left[\begin{aligned} & \left(\left[q_1 + p_1 \sin(y\theta_0 - \frac{\pi}{2} + \varphi) \right]^{\frac{3}{2}} + \left[q_1 + p_1 \sin(y\theta_0 - \frac{\pi}{2} - \varphi) \right]^{\frac{3}{2}} \right) \sin y\theta_0 \\ & + \frac{3}{2} \left(\begin{aligned} & p_1 \left[q_1 + p_1 \sin(y\theta_0 - \frac{\pi}{2} + \varphi) \right]^{\frac{5}{2}} \cos(y\theta_0 - \frac{\pi}{2} + \varphi) + \\ & p_1 \left[q_1 + p_1 \sin(y\theta_0 - \frac{\pi}{2} - \varphi) \right]^{\frac{5}{2}} \cos(y\theta_0 - \frac{\pi}{2} - \varphi) \end{aligned} \right) \cos y\theta_0 \end{aligned} \right],$$

and with the following rescaling:

$$\lambda_3 = \frac{K_T i_0}{J_r \omega_e^2 \theta_0}; \quad \lambda_1 = \frac{c_v}{J_r \omega_e}; \quad \lambda_2 = \frac{R}{L \omega_e}; \quad \omega_e^2 = \frac{c_r}{J_r}; \quad \beta = \frac{\mu_0 M_A^2}{2\pi \theta_0 J_r \omega_e^2}; \quad \varpi = \frac{\omega}{\omega_e}; \quad \lambda = \frac{K_E \theta_0}{L i_0}; \quad (3.5)$$

$$E = \frac{u_0}{L i_0 \omega_e}$$

3.2.2. Oscillatory states in the absence of three magnets

In the absence of three magnets, the dimensionless equations of the electromechanical system are given by equations (3.6).

$$\begin{cases} \dot{x} = -\lambda_2 x - \lambda \dot{y} + E \sin(\varpi \tau) \\ \ddot{y} = \lambda_3 x - \lambda_1 \dot{y} - y \end{cases} . \quad (3.6)$$

Considering external excitation as a constant source ($u(t) = E$), the equilibria of the new system are the solutions of the following algebraic equations

$$\begin{cases} \dot{x} = -x - \lambda v + E \\ \dot{y} = v \\ \dot{v} = \lambda_3 x - \lambda_1 v - \lambda_2 y \end{cases} . \quad (3.7)$$

By solving $\dot{x} = 0$; $\dot{y} = 0$; $\dot{v} = 0$, one finds that equation (3.7) has a unique equilibrium point $E_1(E, \frac{\lambda_3 E}{\lambda_2}, 0)$ with $\lambda_2 \neq 0$. The characteristic equation of the Jacobian matrix at E_1 is:

$$\sigma^3 + (1 + \lambda)\sigma^2 + (\lambda_1 + \lambda\lambda_3 + \lambda_2)\sigma + \lambda_2 = 0, \quad (3.8)$$

where σ is the eigenvalue of the system at E_1 . Using Routh-Hurwitz criteria, this equation has all roots with negative real parts (meaning that E_1 is stable) if and only if the following analytic relations are satisfied:

$$\begin{cases} 1 + \lambda > 0 \\ (1 + \lambda)(\lambda_1 + \lambda\lambda_3 + \lambda_2) - \lambda_2 > 0. \\ \lambda_2 > 0 \end{cases} . \quad (3.9)$$

Since $\lambda > 0$; $\lambda_1 > 0$; $\lambda_2 > 0$; and $\lambda_3 > 0$, the equilibrium point E_1 is a stable point for the system (3.7).

To derive the amplitude of the harmonic oscillatory states ($E \neq 0$) delivered by equation equations (3.6), let us express its solution as:

$$\begin{cases} x(\tau) = A_0 \sin(\varpi\tau) + B_0 \cos(\varpi\tau) \\ y(\tau) = A_1 \sin(\varpi\tau) + B_1 \cos(\varpi\tau) \end{cases}, \quad (3.10)$$

where A_0, A_1, B_0, B_1 are unknown parameters to be determined. $y_{\max} = \sqrt{A_1^2 + B_1^2}$ represents the maximal amplitude of y and $x_{\max} = \sqrt{A_0^2 + B_0^2}$ represents the maximal amplitude of x . Inserting equation (3.10) into equation (3.6), and equating the sine ($\sin(\varpi\tau)$) and cosine ($\cos(\varpi\tau)$) terms separately, it comes that the unknown parameters satisfying the following expressions:

$$\begin{aligned} A_0 &= \frac{(\varpi^4 + \lambda_2^2 + (\lambda_3 \lambda_1 \lambda + \lambda_1^2 - 2\lambda_2)\varpi^2)E}{\varpi^6 + (\lambda_1^2 - 2\lambda_3\lambda - 2\lambda_2 + 1)\varpi^4 + (\lambda_2^2 + 2\lambda_3\lambda_2\lambda + \lambda_1^2 + 2\lambda_3\lambda_1\lambda + \lambda_3^2\lambda^2 - 2\lambda_2^2)\varpi^2 + \lambda_2^2} \\ B_0 &= \frac{(-\varpi^4 - \lambda_2\lambda_3\lambda - \lambda^2 + (\lambda_3\lambda - \lambda_1^2 + 2\lambda_2)\varpi^2)E\varpi}{\varpi^6 + (\lambda_1^2 - 2\lambda_3\lambda - 2\lambda_2 + 1)\varpi^4 + (\lambda_2^2 + 2\lambda_3\lambda_2\lambda + \lambda_1^2 + 2\lambda_3\lambda_1\lambda + \lambda_3^2\lambda^2 - 2\lambda_2^2)\varpi^2 + \lambda_2^2} \\ A_1 &= \frac{-((1 + \lambda_1)\varpi^2 - \lambda_2)\lambda E}{\varpi^6 + (\lambda_1^2 - 2\lambda_3\lambda - 2\lambda_2 + 1)\varpi^4 + (\lambda_2^2 + 2\lambda_3\lambda_2\lambda + \lambda_1^2 + 2\lambda_3\lambda_1\lambda + \lambda_3^2\lambda^2 - 2\lambda_2^2)\varpi^2 + \lambda_2^2} \\ B_1 &= \frac{-(-\varpi^2 + \lambda_1 + \lambda_3\lambda + \lambda_2)\lambda_3 E\varpi}{\varpi^6 + (\lambda_1^2 - 2\lambda_3\lambda - 2\lambda_2 + 1)\varpi^4 + (\lambda_2^2 + 2\lambda_3\lambda_2\lambda + \lambda_1^2 + 2\lambda_3\lambda_1\lambda + \lambda_3^2\lambda^2 - 2\lambda_2^2)\varpi^2 + \lambda_2^2} \end{aligned} \quad (3.11)$$

Considering equation (3.11), we analyse the behaviour of the device given in Figure 5, in absence of the three permanent magnets. When the normalized frequency of the external excitation ϖ is varied, the results are presented in Figure 6. When ϖ increases from 0 to 2, the response amplitude y_{\max} increases from a minimal value to the higher value 2.3 corresponding to 33° ($\theta = y \times \theta_0$) then decreases thereafter to the lower value. The response amplitude x_{\max} decreases, then increases from a minimal value 2.03×10^{-4} which corresponds to 1.015×10^{-4} A ($i = x \times i_0$) to a higher value 1.871×10^{-3} which corresponds to 0.9355×10^{-3} A. These behaviours are usually called resonance phenomenon for the mechanical part and anti-resonance for the electrical part. Thus, when the high amplitude is achieved in the mechanical part, for a frequency close to 1, the amplitude of the electric signal is the lowest. Due to the linear form of equation (3.6), one also observes that the maximal dimensionless

value of the angular displacement and the electrical current increases linearly with the magnitude of the external excitation (Figure not presented here).

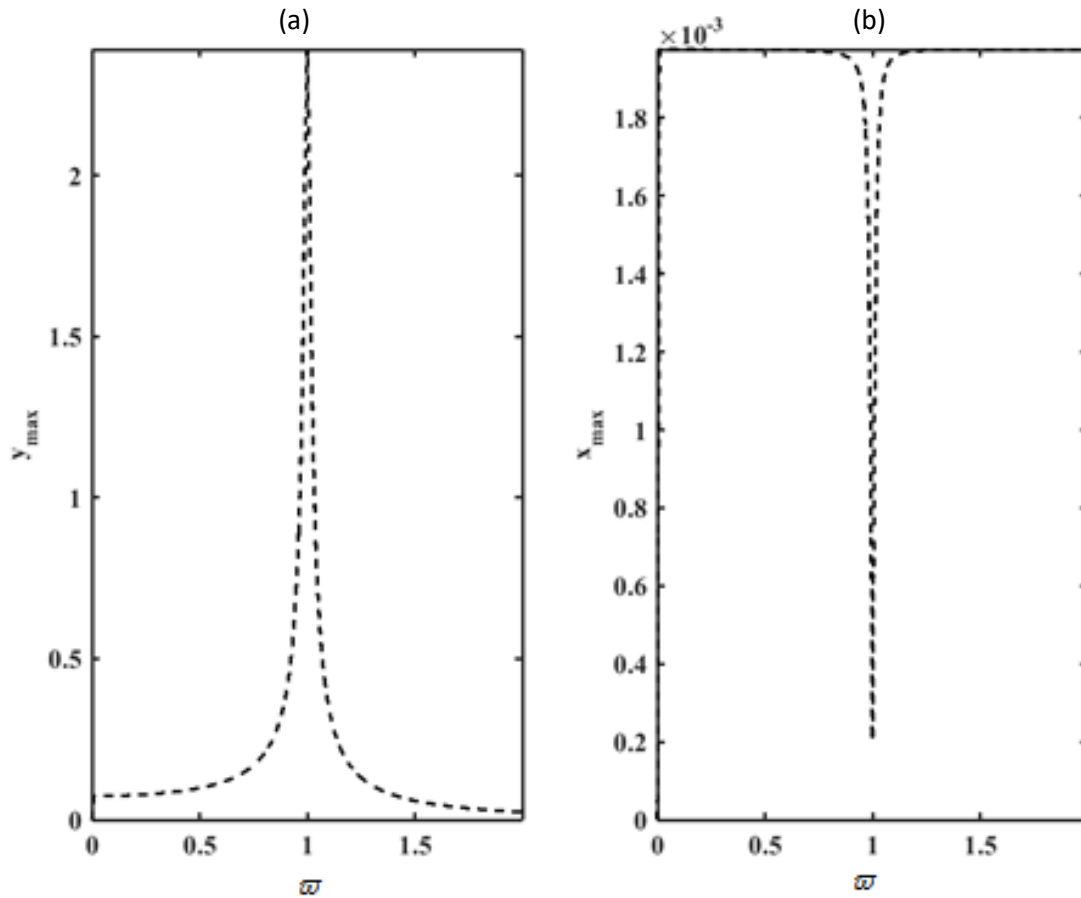


Figure 6 - Frequency-responses of the maximal angular displacement (a) and maximal electrical current (b) and the magnitude of the external excitations (the results from the analytical expression (3.10)). With the parameters of Table 1.

3.2.3. Dynamics in the presence of the magnets

In order to induce a new way to yield the system in chaotic state, we will add three permanent magnets. One permanent magnet is fixed at the free end of the mechanical arm. In the right and in the left of the mechanical arm at equal distance to the equilibrium position, there are two other permanent magnets placed on top of a non-ferromagnetic bearer. For a certain distance between the permanent magnets, this configuration makes possible to create a bistable potential allowing to induce chaotic behaviour in a rotating electromechanical arm.

The numerical analysis of the total potential energy describes in equation (3.2) is analysed here. The first term of equation (3.2) is the elastic potential energy due to the linear springs and the second term of the same equation is the magnetic potential energy due to the magnets. These potential energies as well as the total potential energy are respectively represented in Figures 7 (a), 7 (b) and 7 (c). As it can be seen, the association of the elastic potential energy and magnetic potential gives a bistable total potential energy for appropriate value of the distance between the magnets.

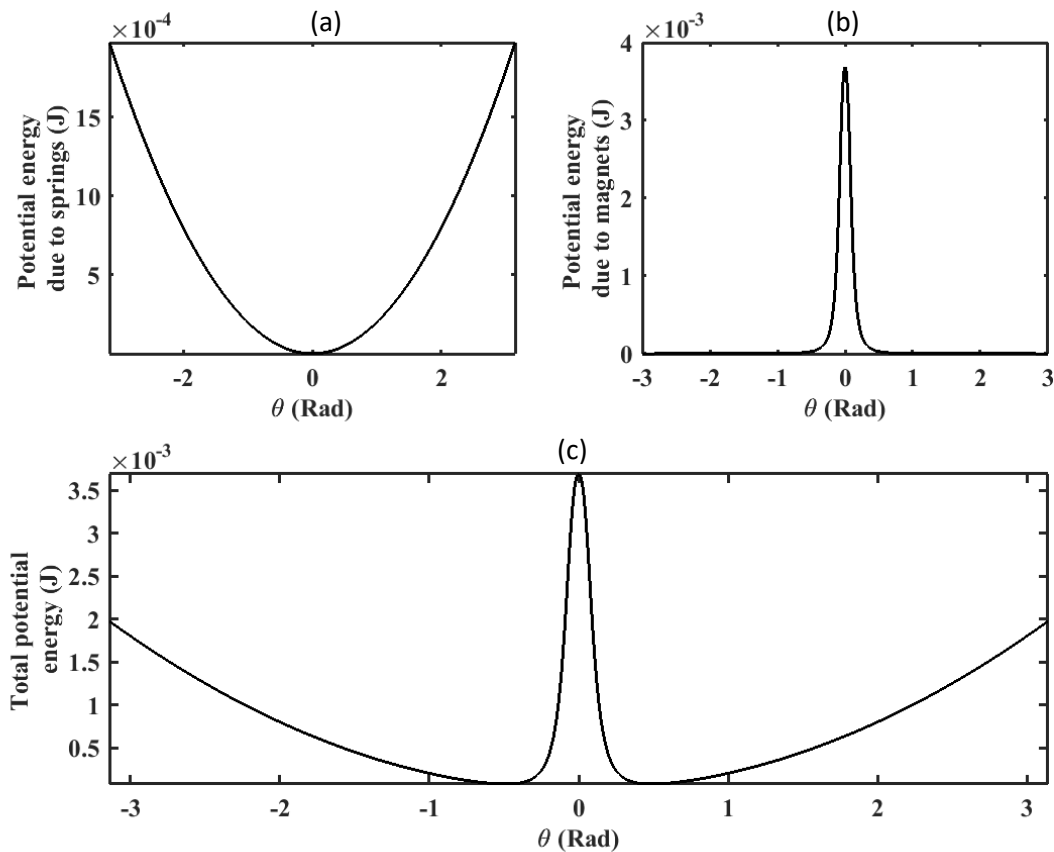


Figure 7 - Potential energy due to springs (a), potential energy due to magnets (b) and total potential energy (c) as function of the angular displacement for some parameters of table 1.

The rotating arm presents two stable points located on both sides of an unstable point

In this subsection, the magnitude of the external source and the normalized frequency are used as control parameters. The external excitation is a sinusoidal voltage. In order to find the range of the amplitude E of the external excitation, for which the device exhibits chaos

dynamics, we have plotted the bifurcation diagram in Figure 8 (a) and its Lyapunov exponent in Figure 8 (b) as the function of E .

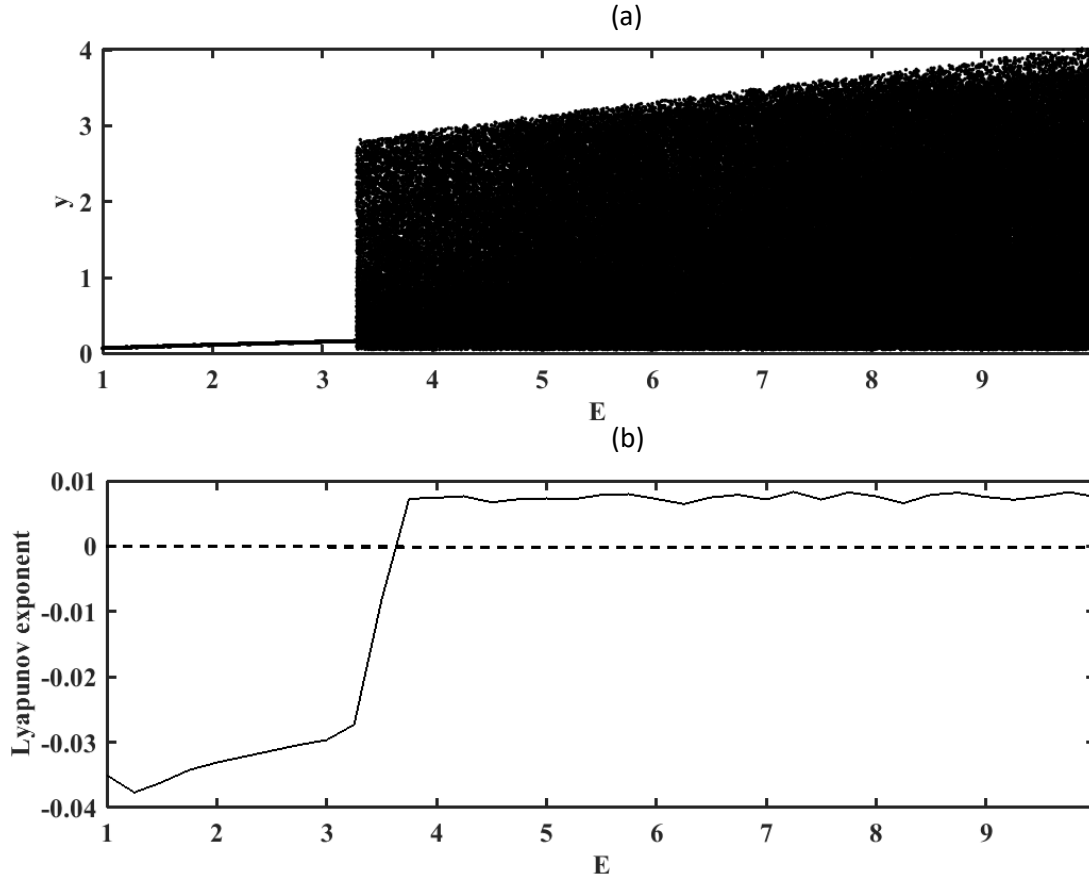


Figure 8 - Bifurcation diagram depicting the global maxima of the angular rotating arm displacement (a) and the largest Lyapunov exponent (b) versus the amplitude E with the parameters of Table 1 and for $\varpi=6.0$.

Figure 8 indicates that the behaviour of the device exhibits non-chaotic oscillations for $E \in [1;3.5]$ and chaotic oscillations for $E \in [3.75;10]$. It can be observed that the corresponding Lyapunov exponent plotted in Figure 8(b) converges to a positive value only when $E \in [3.75;10]$. This confirms that our device (see Figure 5) can oscillate with a chaotic dynamic under certain conditions in presence of the magnets.

To complement the results presented in Figure 8, time histories and corresponding phase portraits are displayed in Figure 9. They are indicating chaotic states and periodic oscillations.

Figure 9 (a) and 9 (c) show 1T-periodic oscillations while Figure 9 (b) and 9 (d) demonstrate chaotic oscillations.

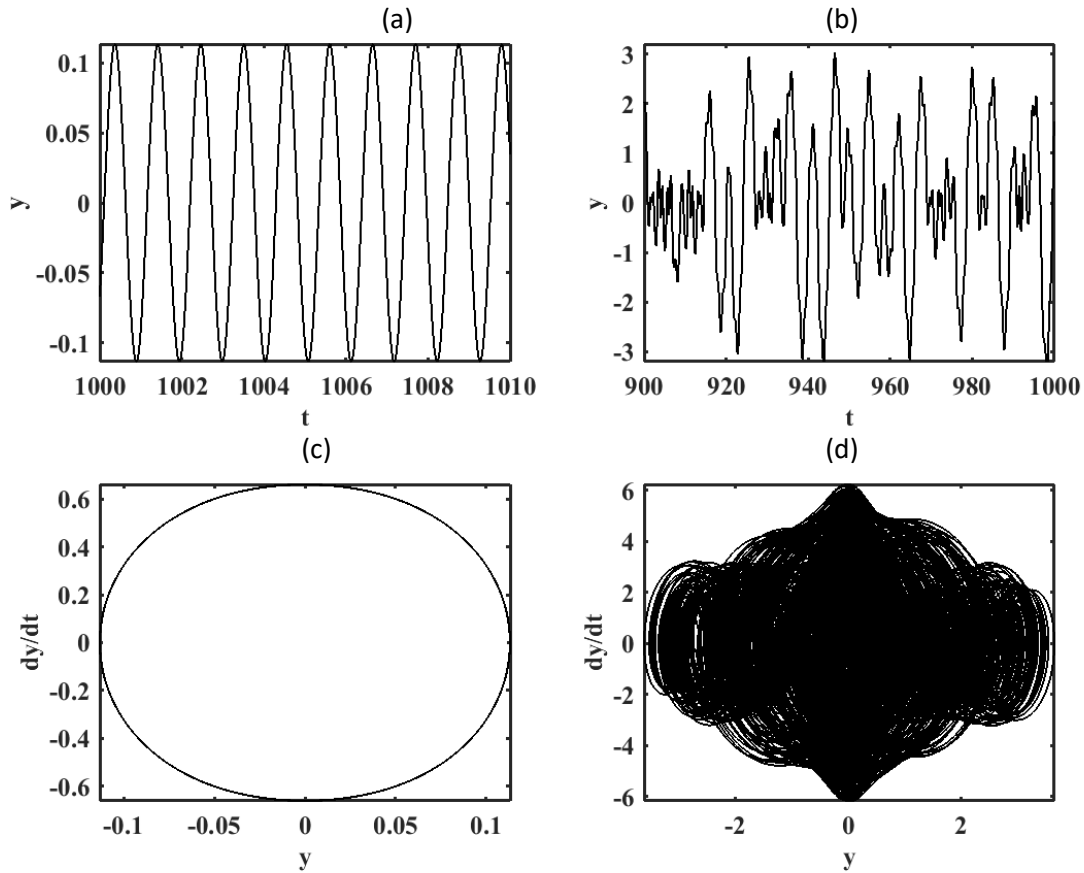


Figure 9 - Time histories(a), (b) and phase portraits (c), (d) obtained with the parameters of Figure 8 and $E=2$ (a), (c); $E=8$ (b), (d).

Similarly, Figure 10 presents the bifurcation diagram and the corresponding variation of the Lyapunov exponent when the normalized frequency ϖ is vary. When the normalized frequency of the external excitation ϖ increases from the value $\varpi = 1.0$, the electromechanical device moves from a periodic state to a chaotic state at $\varpi = 5.6$ with some scenarios of quasiperiodic and chaotic behaviours. This persists until $\varpi = 7.9$ where only periodic oscillations continue to be displayed. The periodic orbit exists until $\varpi = 12.0$

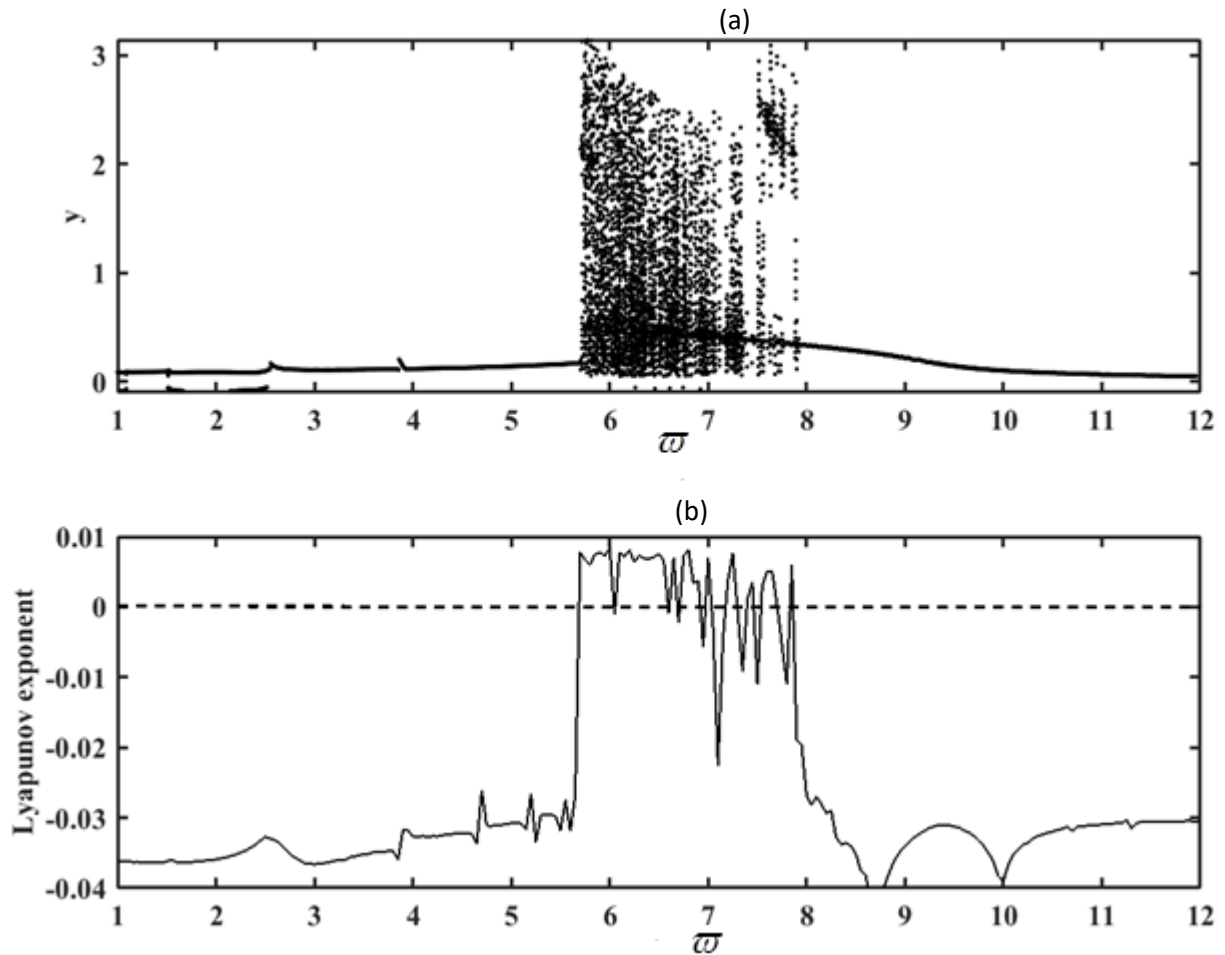


Figure 10 - Bifurcation diagram depicting global maxima of the angular rotating arm displacement (a) and the largest Lyapunov exponent (b) versus the parameter ω for $E=17$. With the parameters of Table 1.

Figure 11 shows some typical time histories and phase portraits of the rotating arm motion for different values of ω . Figure 11 (a) and 11 (c) show periodic 1T oscillations while Figure 11 (b) and 11 (d) depict chaotic oscillations.

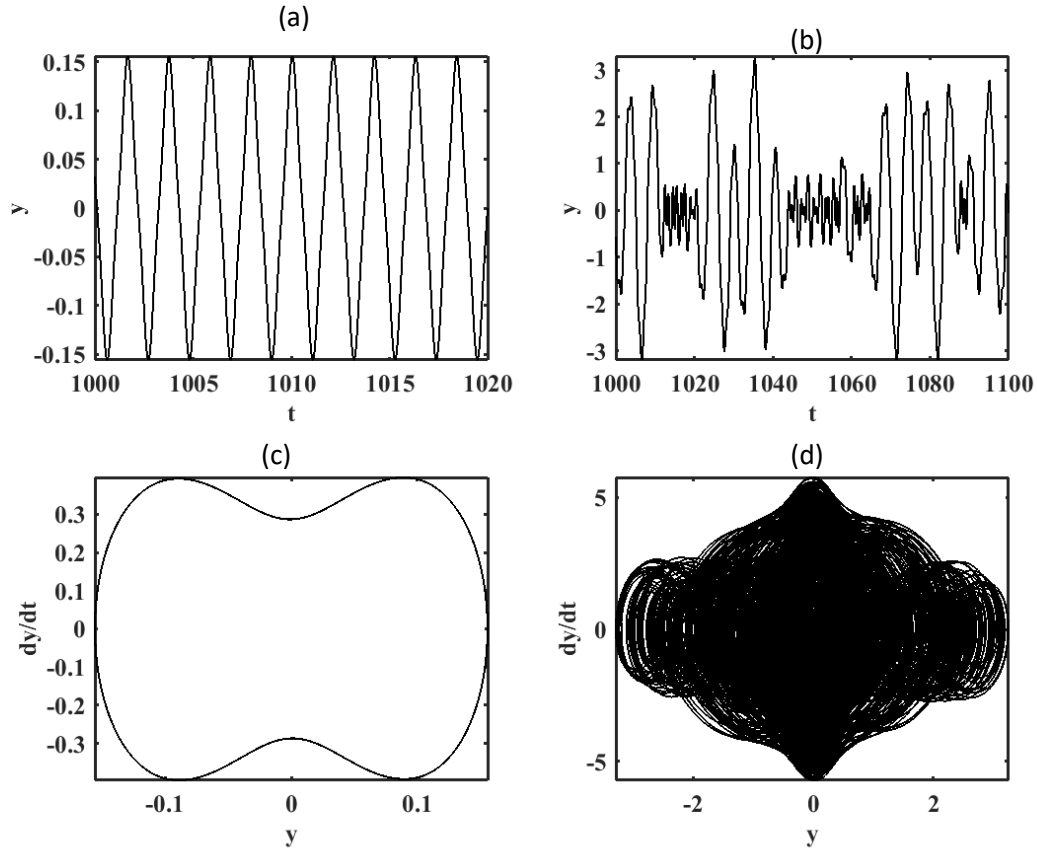


Figure 11 - Time histories and phase portraits in the (y, \dot{y}) plane: period-1T oscillations Figure 11 (a) and 11 (c) with $\varpi=2$. Chaotic oscillations Figure 11 (b) and 11 (d) with $\varpi=6$. Using the parameters of Figure 10.

By using spiral torsion spring, the mechanical rotating arm has the possibility to oscillate with an angle reaching 360° or more, depending on the value of the spring constant and the input voltage. In the absence of the permanent magnets, the device exhibits periodic oscillations when the external source is the sinusoidal input voltage. We observed that in the presence of permanent magnets, chaotic behaviour appears for the magnitude of the external excitation $E \geq 3.5$. These results are very interesting since depending on the application, one can use the chaotic behaviour with small or high value of the angular displacement θ . In the case where chaos is efficient, but with the small values of the magnitude of the external source, one can use the external square signal source with the mathematical expression given by equation (3.12) express as follow.

$$u(t) = u_0 \text{sign}(\sin(\omega t)), \quad (3.12)$$

where

$$\text{sign}(x) = \begin{cases} 1; & \text{if } x > 0 \\ 0; & \text{if } x = 0 \\ -1; & \text{if } x < 0 \end{cases} . \quad (3.13)$$

Replacing the sinusoidal input voltage by a square one, and considering the magnitude of the external excitation, and the normalized frequency as control parameters, one obtains the results presented in Figure 12 and Figure 13. For the square signal, we have non-chaotic oscillations for $E \in [1;2.78]$ and chaotic oscillations for $E \in [2.78;10]$.

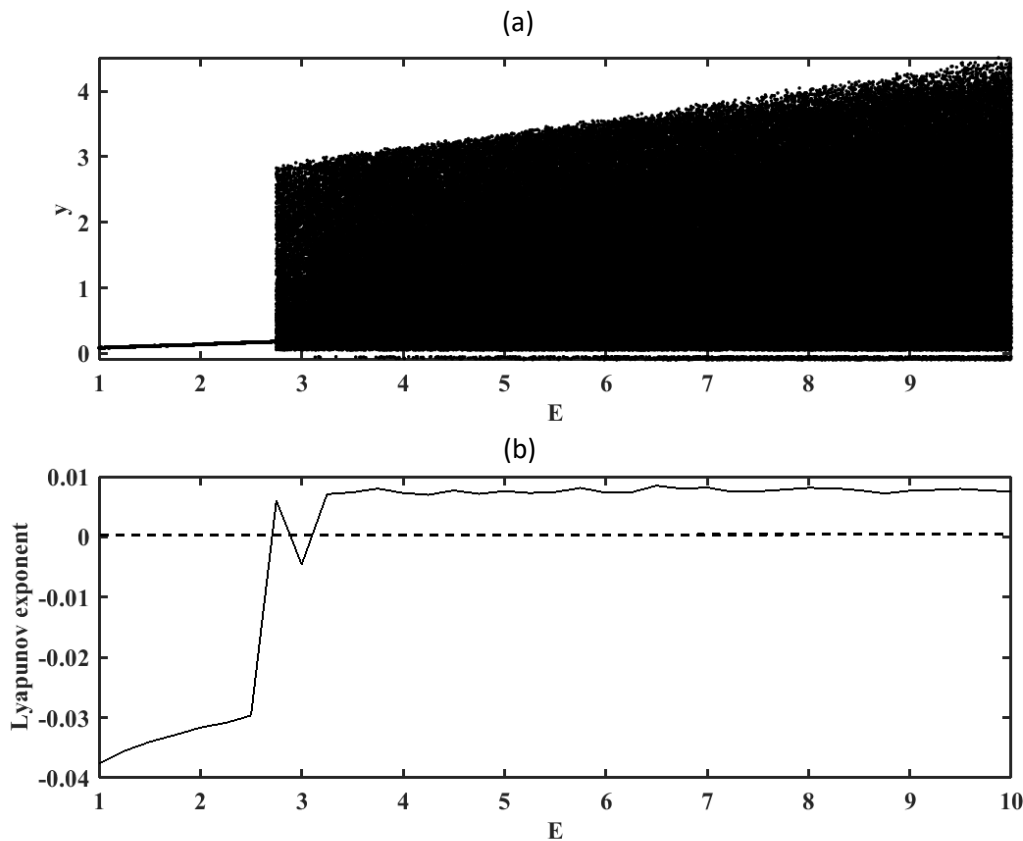


Figure 12 - Bifurcation diagram depicting global maxima of the angular rotating arm displacement (a) and the largest Lyapunov exponent (b) versus the parameter E .

Figure 13 presents the bifurcation diagram and the corresponding Lyapunov exponent when the normalized frequency ϖ is vary. The following transitions are observed. When the normalized frequency ϖ of the external excitation increases from the value $\varpi = 1.0$, the

electromechanical device moves from a periodic state to a chaotic state at $\varpi = 2.35$. This persists until $\varpi = 2.65$ where only periodic oscillations continue to be displayed. From $\varpi = 5.45$, there is a transition from periodic orbit to a chaotic behaviour with some small windows of period-n orbit. It continues to take place until only the periodic dynamical behaviour appeared at $\varpi = 8.4$.

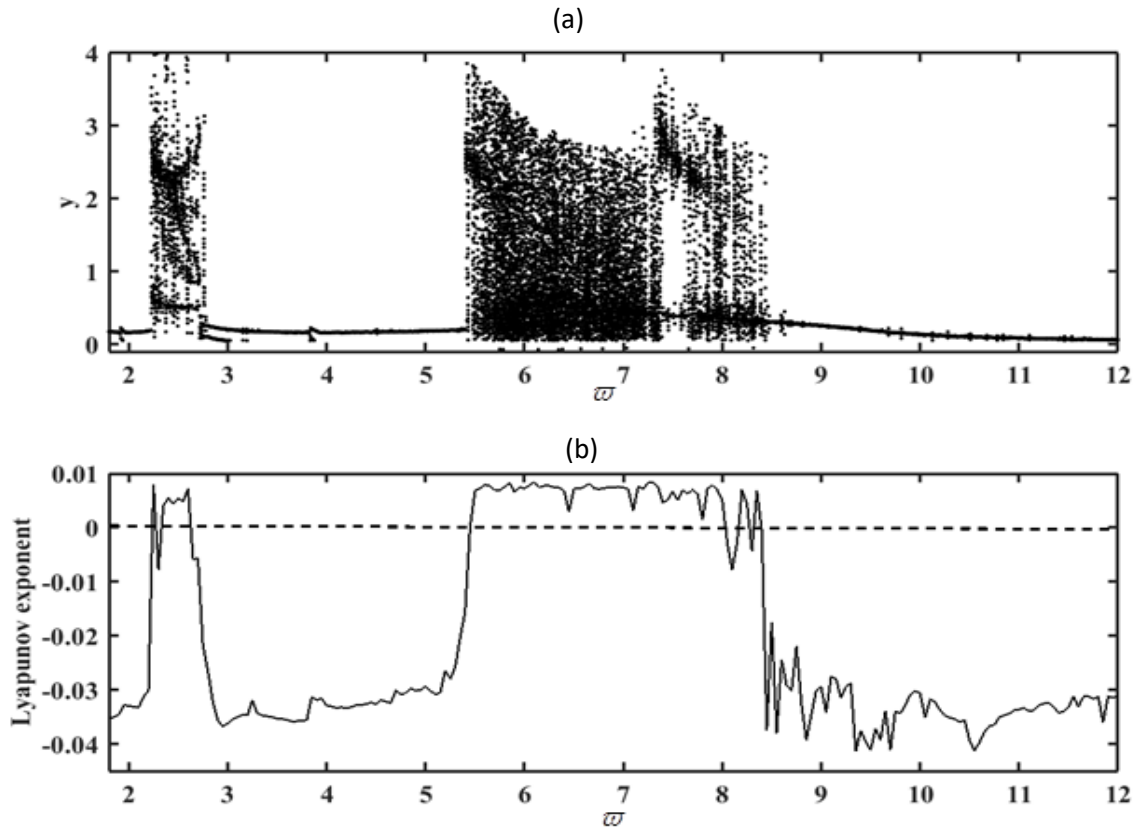


Figure 13 - Bifurcation diagram depicting global maxima ϖ of the angular rotating arm displacement (a) and the largest Lyapunov exponent (b) versus the parameter ϖ with the parameters of Figure 12.

We can note that this device presents the same dynamics as well as for the case where sinusoidal voltage source is used. But with a square wave signal, chaotic behaviour appears for smaller values of the signal amplitude and frequency.

The chaotic dynamics obtained previously corresponds to the dissipative chaos. Because of the bistable nature of the potential energy, one might expect the occurrence of Hamiltonian or Melnikov chaos

3.2.4. The Hamiltonian chaos

The general theory can be found in [80,81]. In the analysis that follows, we will attempt to study the conditions for the appearance of the chaos of Melnikov in the device of Figure 5. Because of the bistable nature of the potential energy, we can observe the occurrence of Hamiltonian or Melnikov chaos. In order to find a mathematical condition for the Melnikov chaos, we need to have an approximate form of the bistable potential from which homoclinic orbits will be calculated. This is a quite complicated issue here because of the complexity of the mathematical expression of the potential energy. However, some crude approximations can be made following the curve of the bistable potential given in Figure 7. We thus approximate the total potential energy equation (3.2) by the following quadratic expression

$$U(\theta) = -\frac{A}{2}\theta^2 + \frac{B}{4}\theta^4, \quad (3.14)$$

Where A and B are positive coefficients. Considering the potential wells of Figure 7, and those derived from equation (3.14), one can write the values of the minima as

$$\theta = \sqrt{\frac{A}{B}} = \pm 0.488. \text{ Taking } A = 0.0238144 \text{ and } B = 0.1 \text{ which satisfied } \sqrt{\frac{A}{B}} = \pm 0.488$$

Although, there is a quantitative difference between the curve generated by equation (3.14) and the potential in Figure 7 (c), equation (3.14) will be used to determine a condition for the appearance of the Hamiltonian chaos.

With the approximate form of the potential energy, the differential equations (3.1) becomes

$$\begin{cases} L \frac{di(t)}{dt} + Ri(t) + K_E \frac{d\theta}{dt} = u(t) \\ J_r \frac{d^2\theta}{dt^2} + c_v \frac{d\theta}{dt} - A\theta + B\theta^3 = K_T i(t) \end{cases} \quad (3.15)$$

In order to find the Melnikov chaos in our system, let us assume that the term $L \frac{di(t)}{dt}$ in equation (3.15) is negligible, and then equation (3.15) is reduced to the single equation (3.16)

$$\frac{d^2\theta}{dt^2} + \left(\frac{c_v}{J_r} + \frac{K_E K_T}{J_r R}\right) \frac{d\theta}{dt} - \frac{A}{J_r} \theta + \frac{B}{J_r} \theta^3 = \frac{u_0 K_T}{J_r R} \cos(\omega t). \quad (3.16)$$

In the non-dimensional form, equation (3.16) takes the form

$$\ddot{y} + \gamma_1 \dot{y} - y + y^3 = \gamma_4 \cos(\Omega \tau), \quad (3.17)$$

where

$$y = \frac{\theta}{\theta_0}; \quad \tau = \omega_0 t; \quad \omega_0 = \sqrt{\frac{A}{J_r}}; \quad \gamma_1 = \frac{c_v + \frac{K_E K_T}{R}}{J_r \omega_0}; \quad \gamma_4 = \frac{u_0 K_T}{J_r \theta_0 R \omega_0^2}; \quad \Omega = \frac{\omega}{\omega_0}; \quad \theta_0 = \omega_0 \sqrt{\frac{J_r}{B}}. \quad (3.18)$$

Equation (3.17) describes the bistable Duffing oscillator. The fixed points $(-1;0)$ and $(1;0)$ are the stable equilibrium points while the fixed point $(0;0)$ is an unstable equilibrium point. Equation (3.17) can be viewed as the Hamiltonian system plus a perturbation consisting of:

$$-\gamma_1 \dot{y} + \gamma_4 \cos(\Omega \tau). \quad (3.19)$$

One can thus use the Melnikov's formalism to find the condition for the appearance of horseshoe chaos [88]. This condition is given by:

$$\gamma_4 \geq \frac{2^{\frac{5}{2}}}{3\pi\Omega^2} \gamma_1 \cosh\left(\frac{\pi\Omega}{2}\right). \quad (3.20)$$

The details for the derivation of equation (3.20) can be found in [110]. A system whose parameters satisfy condition (3.20) presents a chaotic dynamic in a sense that it will present fractality in the basin of attraction.

To validate our analytical study, we numerically simulated equation (3.17) and observed the effects of the control parameters γ_4 on the appearance of the fractality in the basin of attraction. The results are presented in Figure 14, the white and dark regions represent respectively the set of initial conditions that result of motions around the equilibrium points and motion covering both equilibrium points. One notices that the basin of attraction becomes

fractal following the condition defined by equation (3.20). For instance, for $\Omega=2.5$, the fractality appears at $\gamma_4=10$ and $\gamma_4=5$ see (Figure 14 (a) and 14 (b)). We find that the black space increases and the fractality disappear when γ_4 decreases see (Figure 14 (c)). The white space even completely disappears for $\gamma_4=0.02$ see (Figure 14 (d)).

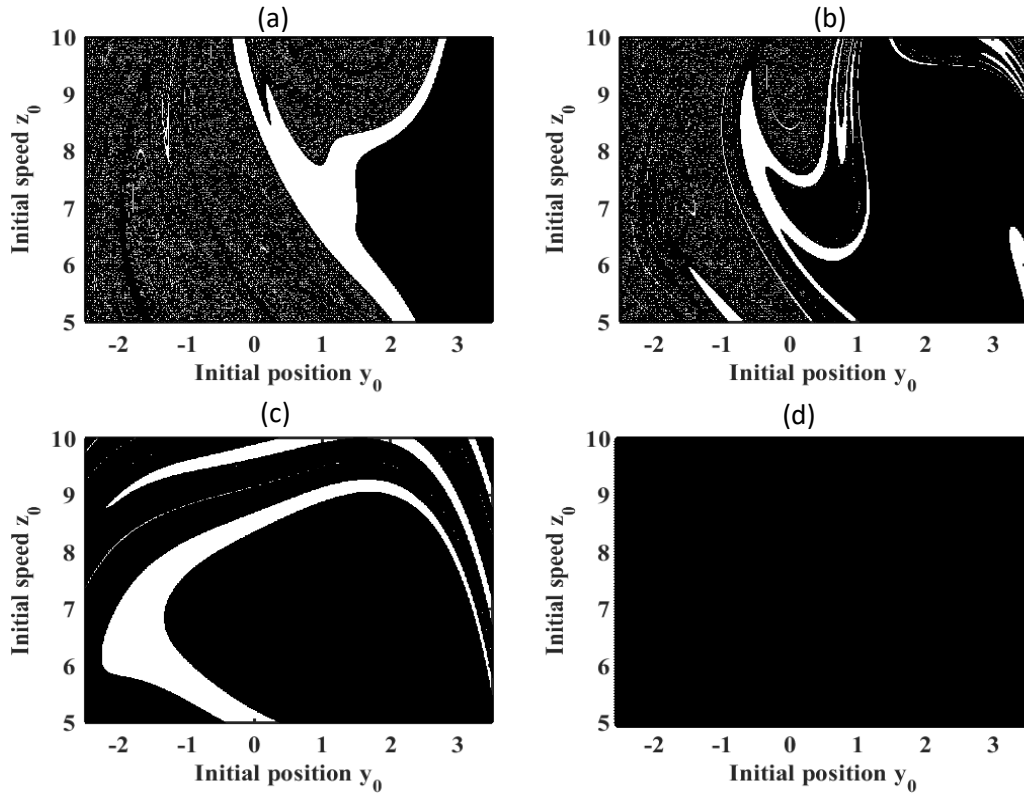


Figure 14 - Variation of the fractal structure of the basin of attraction for $\Omega=2.5$ and (a) $\gamma_4=10$, (b) $\gamma_4=5$, (c) $\gamma_4=1$, (d) $\gamma_4=0.02$. Other parameters of Table 1.

3.3. Dynamical behaviour of a bistable rotating electromechanical system with spring, hysteretic iron-core inductor and delay

3.3.1. System and equations

The electromechanical system with rotating arm is presented in Figure 15. It is constituted by an electrical circuit which is driving a mechanical part. The rotating arm is a thin rod of mass m and length ℓ . The rod has a plate of length $\sigma\ell$ (with $\sigma = \frac{1}{2}$), on which n

electrical windings are applied. When the electrical circuit is connected to a voltage source, it appears a Laplace force in the mechanical part and the Lenz electromotive voltage in the electrical part. Two linear and identical springs of stiffness k are mechanically fixed at the middle ($\ell/2$) of the thin rod. The rotating arm oscillations are due to the combined action of the linear springs and electromagnetic force resulting from two identical and repulsive permanent magnets. This electromechanical system has two degrees of freedom: the electrical current i through the electrical circuit and the angular displacement θ of the rotating arm. The electric circuit used to drive the rotating arm consists of a resistor R , a nonlinear hysteretic iron-core inductor L and a voltage source $u(t)$ all connected in series.

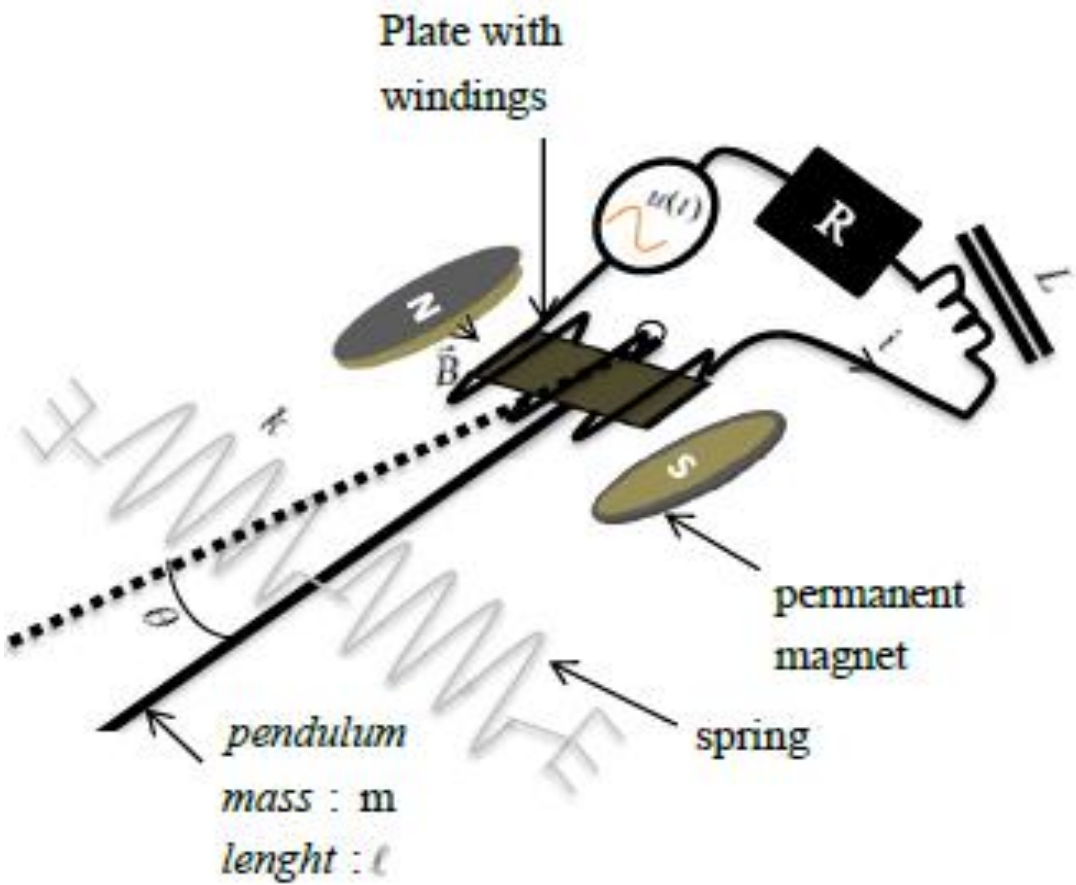


Figure 15 - Electromechanical system with rotating arm.

The parameters of the electromechanical device shown in Figure 15 are listed in Table 2. We choose these values to obtain appropriate angular oscillations with limited magnitude

Parameters	Values	Dimensions
Inductance: L	variable	H
Resistance: R	11	Ω
Mass of the mechanical arm: m	0.15	kg
stiffness coefficient of the spring: k	0.3	N / m
Magnetic field intensity: B	2.2×10^{-2}	T
Length of the mechanical arm ℓ	0.5	m
Average length of winding l	0.24	m
Cross sectional area A of iron core	176.71×10^{-6}	m^2
Number of turn N for the iron core inductor	1000	1
Saturation flux density B_s	0.13	T
Number of electric windings on a plate n	600	1
Frictional coefficient β_1	0.01	Ns / m

Table 2 - Parameters of the electromechanical system

Applying the Kirchhof laws and the Newton second law of dynamics for rotary motions to Figure 15 the electromechanical equations which governed the functioning of the device are given by the following expressions:

$$\left\{ \begin{array}{l} \left[\frac{\mu_0 N^2 A}{l} + \frac{B_s N^2 \alpha A}{2l} \cdot \frac{2}{1 + \cosh\left(\frac{\alpha Ni}{l} - \sigma_1\right)} \right] \frac{di}{dt} + Ri + nB\sigma^2 \frac{\ell^2}{2} \frac{d\theta}{dt} = u(t) \\ J \frac{d^2\theta}{dt^2} + \frac{\beta_1 \ell}{2} \frac{d\theta}{dt} + k \frac{\ell^2}{4} \sin(\theta) \cos(\theta) - \frac{niB\sigma^2 \ell^2}{2} = 0 \end{array} \right. , \quad (3.21)$$

Where $J = \frac{1}{3} m \ell^2$ is the total inertia moment of the studied device. We assume that the total mass of the conducting wire and the plate bathing in the magnetic field can be neglected compared to the rotating arm mass. The rotating arm moves in a viscous medium with frictional coefficient β_1 . Using the dimensionless variables given in equation (3.3) with the normalized current given as:

$$i_0 = \frac{l}{\alpha N}. \quad (3.22)$$

Replacing equation (3.3) into equation (3.21) taking in to account equation (3.22), one obtains the following system of dimensionless equations for the electromechanical system:

$$\left\{ \begin{array}{l} \left[(1-\eta) + \frac{2\eta}{1 + \cosh(x - \sigma_2 \text{sign}(\dot{x}))} \right] \dot{x} = -\lambda \dot{y} - x + E \sin(\bar{\omega}\tau) \\ \ddot{y} = -\beta_3 \dot{y} - \beta_2 \sin(\theta_0 y) \cos(\theta_0 y) + \beta_0 x \end{array} \right. , \quad (3.23)$$

with:

$$\beta_0 = \frac{nB\sigma^2 \ell^2 i_0}{2J\omega_e^2 \theta_0}; \quad \beta_2 = \frac{k\ell^2}{4J\theta_0\omega_e^2}; \quad \bar{\omega} = \frac{2\pi f}{\omega_e}; \quad \lambda = \frac{l(1-\eta)nB\sigma^2 \ell^2 \theta_0}{2\mu_0 N^2 A i_0}; \quad \sigma_2 = \beta\omega_e i_0;$$

$$\beta = 88.42 \times 10^{-2}; \quad \omega_e = \frac{Rl(1-\eta)}{\mu_0 N^2 A}; \quad \eta = \frac{B_s \alpha}{2\mu_0 + B_s \alpha}; \quad \beta_3 = \frac{\beta_1 \ell}{2J\omega_e}; \quad E = \frac{u_0 l(1-\eta)}{\mu_0 N^2 A i_0 \omega_e}; \quad (3.24)$$

$$\alpha = 88.23 \times 10^{-4} m.A^{-1}$$

In order to have the electromechanical rotating arm with chaotic oscillations for small values of the control parameters, the previous device is changed into the one of Figure 16 where one permanent magnet is fixed at the free end of the mechanical arm. In the right and in the left sides of the mechanical arm, at equal distances to the equilibrium position, there are two other permanent magnets also fixed somewhere in the whole system.

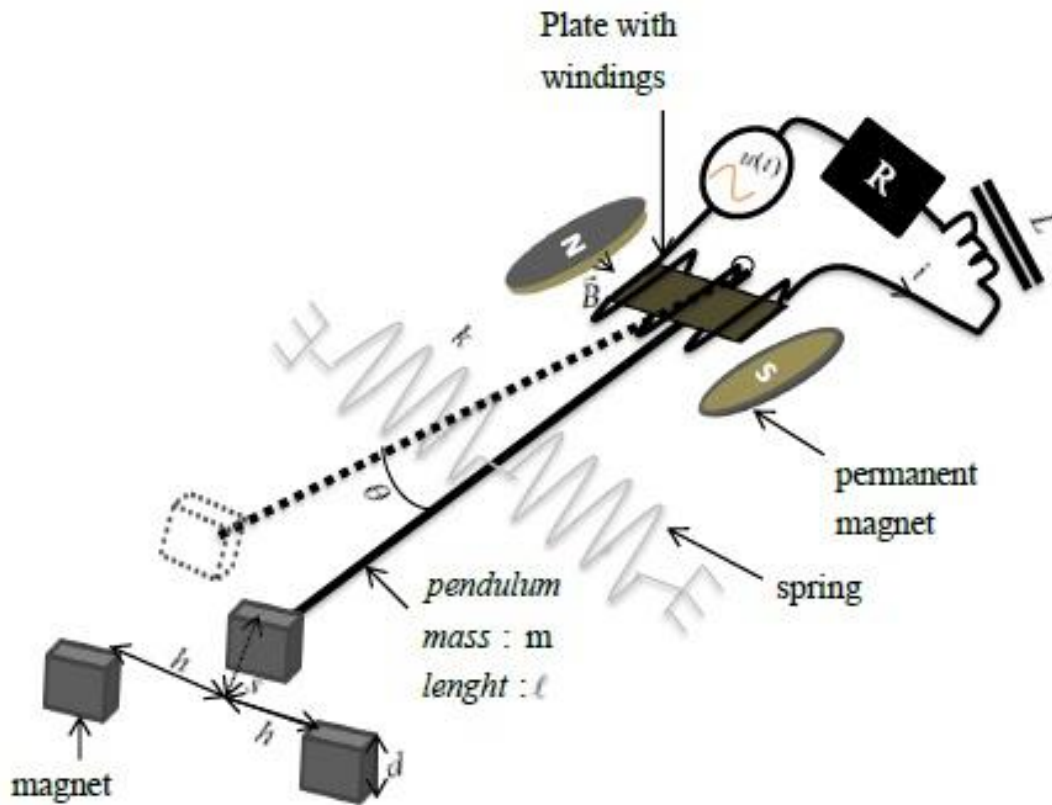


Figure 16 - Electromechanical rotating arm with three permanent magnets.

The values and dimensions of the new parameters of the device are:

Parameters	Values	Dimensions
Mass of the mechanical arm: m	0.3	kg
Magnetic moment M_A of the magnet	1.2	$A.m^2$
Magnets position h (see Figure.16)	0.01	m
Width d of the magnet	0.01	m
Distance S of the free end of the arm and middle of the distance between the magnets	0.02	m

Table 3 - New parameters of the electromechanical system (some of these parameters are indicated in Figure 16)

The dimensionless form of the mathematical model of the device is described using the following system:

$$\left\{ \begin{array}{l} \left[(1-\eta) + \frac{2\eta}{1 + \cosh(x - \sigma_2 \text{sign}(\dot{x}))} \right] \dot{x} = -\lambda \dot{y} - x + E \text{sign}(\sin(\bar{\omega}\tau)) \\ \ddot{y} = -\beta_3 \dot{y} - \beta_2 \sin(\theta_0 y) \cos(\theta_0 y) - \beta g(y\theta_0) + \beta_0 x \end{array} \right. , \quad (3.25)$$

with

$$g(y\theta_0) = \left[\begin{array}{l} \left(\frac{(1 + p_1 \sin y\theta_0 - p_2 \cos y\theta_0)^{-\frac{3}{2}}}{a} + \frac{(1 + q_1 \sin y\theta_0 - q_2 \cos y\theta_0)^{-\frac{3}{2}}}{b} \right) \sin y\theta_0 \\ + \frac{3}{2} \left(\frac{(p_1 \sin y\theta_0 - p_2 \cos y\theta_0)(1 + p_1 \sin y\theta_0 - p_2 \cos y\theta_0)^{-\frac{5}{2}}}{a} + \frac{(q_1 \sin y\theta_0 - q_2 \cos y\theta_0)(1 + q_1 \sin y\theta_0 - q_2 \cos y\theta_0)^{-\frac{5}{2}}}{b} \right) \cos y\theta_0 \end{array} \right] ; \quad \text{and}$$

$$\beta_4 = \frac{\mu_0 M_A^2 \ell}{2\pi J \theta_0 \omega_e^2}.$$

3.3.2. Dynamic in absence of permanent magnets

In this subsection, we assume that the device designed in Figure 15 exhibits with small angular displacement of the rotating arm (e.g., less than 10°), one can have: $\cos(\theta) = 1$; $\sin(\theta) = \theta$. As simplifying conditions, let the parameter β (it is one of the parameters appearing in the relation between the magnetic induction and the magnetic fields suggested by the authors in [44]) be neglected and for the smaller values of x ($\cosh(x) = 1$). Equation (3.23) takes the reduced form

$$\left\{ \begin{array}{l} \dot{x} = -\lambda \dot{y} - x + E \sin(\bar{\omega}\tau) \\ \ddot{y} = -\beta_3 \dot{y} - \beta_2 \theta_0 y + \beta_0 x \end{array} \right. . \quad (3.26)$$

The presence of the sinusoidal input voltage gives rise to oscillatory states that can be approximated by the mathematical relations of the form

$$\begin{cases} x(\tau) = A_0 \sin(\varpi\tau) + B_0 \cos(\varpi\tau) \\ y(\tau) = A_1 \sin(\varpi\tau) + B_1 \cos(\varpi\tau) \end{cases}, \quad (3.27)$$

where A_0 ; A_1 ; B_0 ; B_1 are unknown parameters to be determined; $y_{\max} = \sqrt{A_1^2 + B_1^2}$ represents the maximal amplitude of y and $x_{\max} = \sqrt{A_0^2 + B_0^2}$ represents the maximal amplitude of x . Substituting (3.27) into (3.26) and next balancing the harmonic terms $\sin(\varpi\tau)$ and $\cos(\varpi\tau)$, we get

$$\begin{aligned} A_0 &= \frac{(\varpi^4 + \beta_2^2 + (\beta_3\beta_0\lambda + \beta_3^2 - 2\beta_2)\varpi^2)E}{\varpi^6 + (\beta_3^2 - 2\beta_0\lambda - 2\beta_2 + 1)\varpi^4 + (\beta_3^2 + 2\beta_2\beta_0\lambda - 2\beta_2 + \beta_2^2 + 2\beta_3\beta_0\lambda + \beta_0^2\lambda^2)\varpi^2 + \beta_2^2} \\ B_0 &= \frac{(\varpi^4 + \beta_2\beta_0\lambda + \beta_2^2 + (-\beta_0\lambda + \beta_3^2 - 2\beta_2)\varpi^2)E\varpi}{\varpi^6 + (\beta_3^2 - 2\beta_0\lambda - 2\beta_2 + 1)\varpi^4 + (\beta_3^2 + 2\beta_2\beta_0\lambda - 2\beta_2 + \beta_2^2 + 2\beta_3\beta_0\lambda + \beta_0^2\lambda^2)\varpi^2 + \beta_2^2} \quad (3.28) \\ A_1 &= \frac{((1 + \beta_3)\varpi^2 - \beta_2)\beta_0 E}{\varpi^6 + (\beta_3^2 - 2\beta_0\lambda - 2\beta_2 + 1)\varpi^4 + (\beta_3^2 + 2\beta_2\beta_0\lambda - 2\beta_2 + \beta_2^2 + 2\beta_3\beta_0\lambda + \beta_0^2\lambda^2)\varpi^2 + \beta_2^2} \\ B_1 &= \frac{(\varpi^2 - \beta_3 - \beta_0\lambda - \beta_2)\beta_0 E\varpi}{\varpi^6 + (\beta_3^2 - 2\beta_0\lambda - 2\beta_2 + 1)\varpi^4 + (\beta_3^2 + 2\beta_2\beta_0\lambda - 2\beta_2 + \beta_2^2 + 2\beta_3\beta_0\lambda + \beta_0^2\lambda^2)\varpi^2 + \beta_2^2} \end{aligned}$$

Maximal amplitudes x_{\max} and y_{\max} will be represented in terms of the frequency ϖ in Figure 17.

The frequency-responses of the angular displacement and current (calculated from equation (3.27) and the numerical simulation of the differential equation (3.26)) are plotted in Figure 17, when the normalized frequency ϖ varies. It appears that, when ϖ increases from 0 to 7, the response amplitude y_{\max} decreases while the response amplitude x_{\max} increases to its maximal amplitude, and decreases from a higher amplitude (0.48) to a lower amplitude.

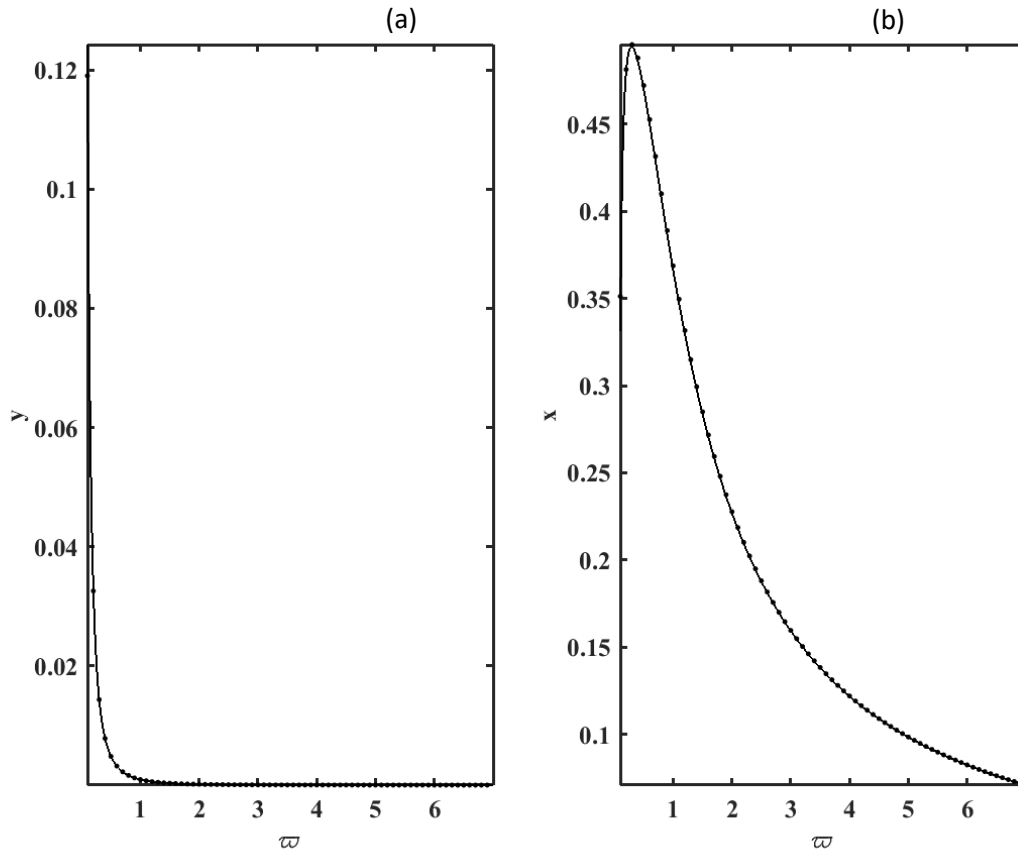


Figure 17 - Frequency-responses of the (a) angular displacement (b) electrical current with the parameters values of Table 3, for the magnitude of the external excitation $E=0.5$. (the point (\cdot) for the numerical simulation of the differential equation (3.26) and the lines $(-)$ for the analytical expression (3.27).

Now, we consider large values of the magnitude E . To analyse the dynamical behaviour of the device, the Runge-Kutta algorithm is used to solve numerically the dimensional differential equation (3.26) and thereafter, the bifurcation diagram and Lyapunov exponent are used to find the regions where the system is periodic or chaotic. The bifurcation diagram of Figure 18 (a) shows that, the device exhibits period- nT oscillation when $\varpi \in [0.01; 0.7]$. This behaviour is confirmed by the Lyapunov exponent (see Figure 18 (b)) which presents a negative value when $\varpi \in [0.01; 0.7]$.

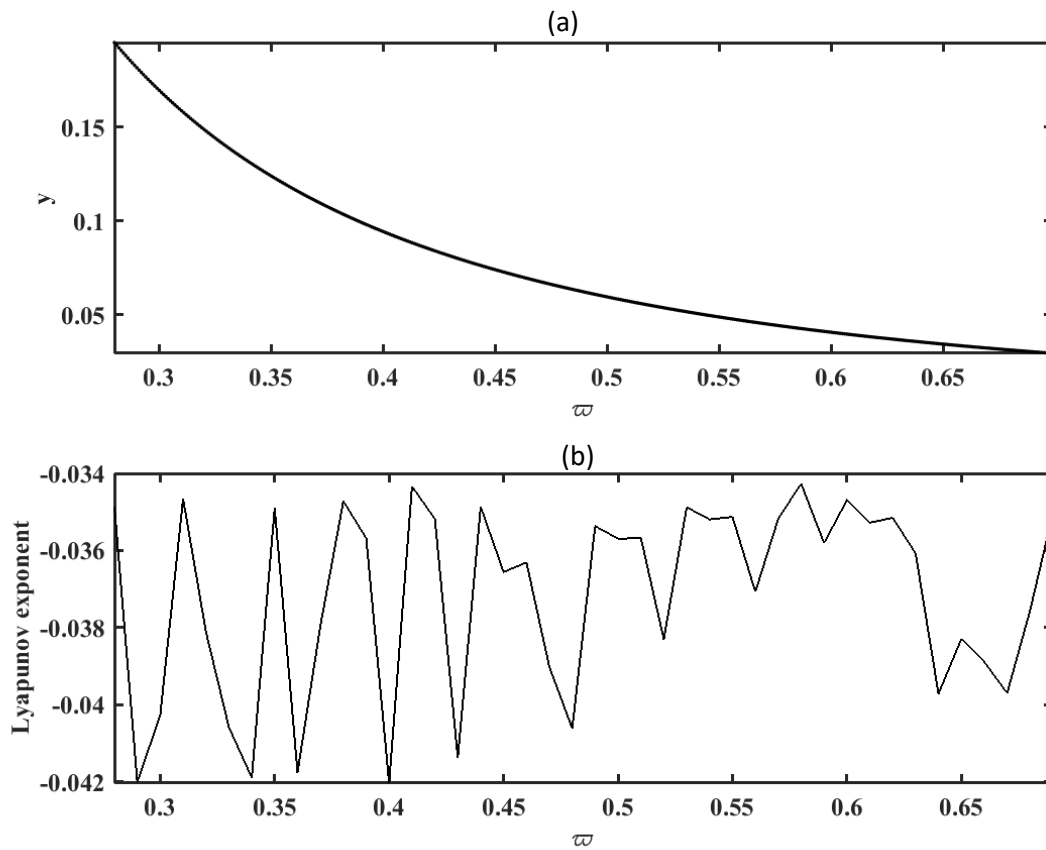


Figure 18 - Bifurcation diagram depicting global maxima of the angular rotating arm displacement (a) and the largest Lyapunov exponent (b) versus the parameter ϖ for $E=6$. With the parameters of Table 2.

Considering the dimensionless magnitude of the external excitation E as the control parameter, Figure 19 (a) shows the bifurcation diagram plotted in terms of the dimensionless angular displacement.

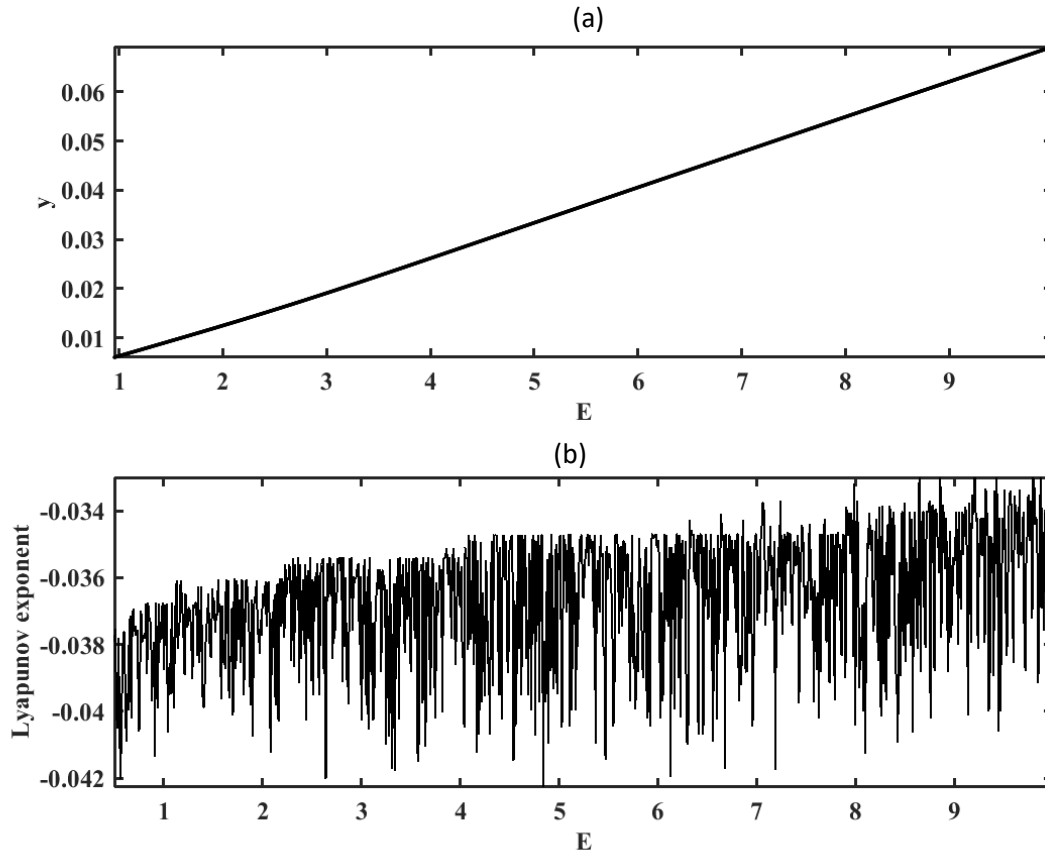


Figure 19 - Bifurcation diagram depicting global maxima of the angular rotating arm displacement (a) and the largest Lyapunov exponent (b) versus the parameter of Figure 18 and for $\varpi=0.6$.

As E increases from 0.5 to 10, the device exhibits period- nT oscillations. This behaviour is confirmed by Figure 19 (b) where its Lyapunov exponent is always negative.

3.3.3. Inducing chaos using three magnets.

The aim of this section is to analyse the dynamics of an electromechanical rotating system with a nonlinear hysteretic iron-core inductor when three permanent magnets are added at the end and in front of the rotating arm. Potential energy is still the equation (3.2). These potential energies as well as the total potential energy are respectively represented in Figure 20 (a), 20 (b) and 20 (c) taking into account the parameters of this new device with permanent magnets. The association of the elastic potential energy and mechanical potential due to magnets leads to the bistable nature of the total potential energy.

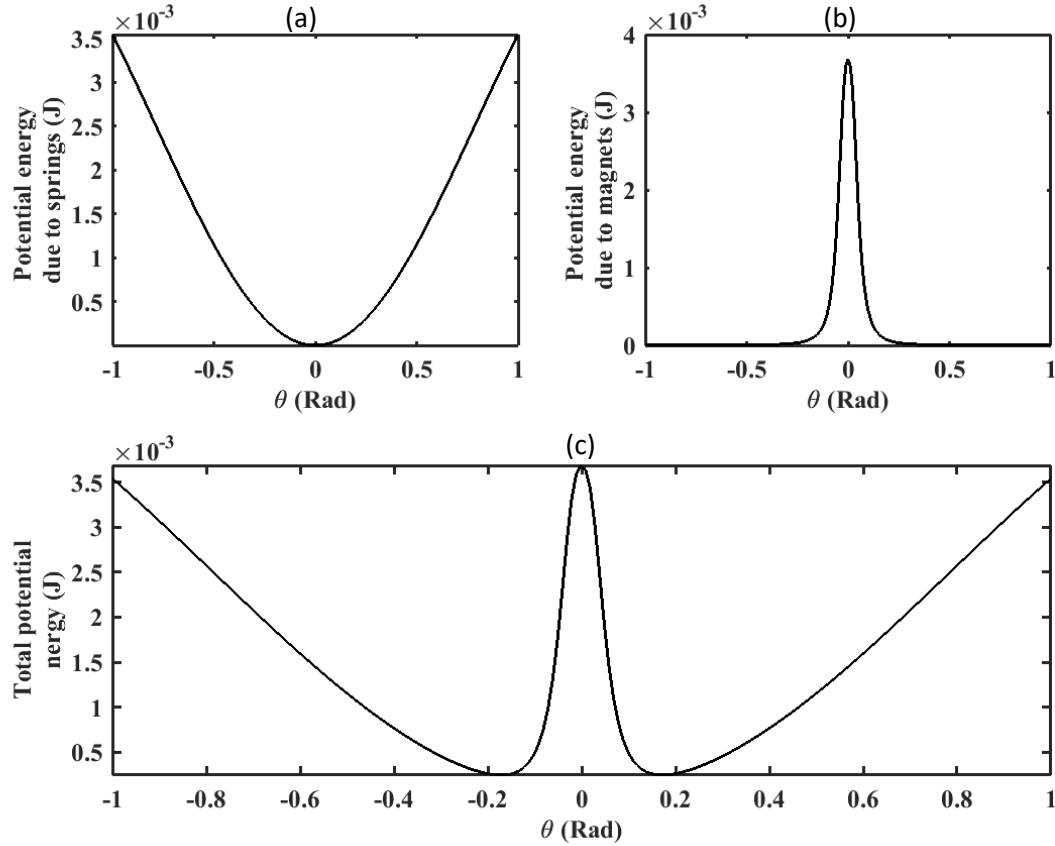


Figure 20 - Elastic potential energy (a), magnetic potential energy (b) and magneto elastic potential energy (c) as function of the angular displacement.

The total potential energy is sinusoidal and equations (3.26) has many periodic solutions. However, in an interval of length 2π , the rotating arm presents two stable points located on both sides of an unstable point Figure 20 (c). When the amplitude of the motion is very large, the unstable fixed point disappears, this is an interesting phenomenon. In this case, the arm shows a complete rotation. If these rotations are harmful, they should be avoided. Here, the external sine wave generator is replaced by a square one. The dimensionless mathematical model of the device is described by the following system:

$$\left\{ \begin{array}{l} \left[(1-\eta) + \frac{2\eta}{1 + \cosh(x - \sigma_2 \text{sign}(\dot{x}))} \right] \dot{x} = -\lambda \dot{y} - x + E \text{sign}(\sin(\bar{\omega}\tau)) \\ \ddot{y} = -\beta_3 \dot{y} - \beta_2 \sin(\theta_0 y) \cos(\theta_0 y) - \beta g(y\theta_0) + \beta_0 x \end{array} \right. \quad (3.29)$$

Figure 21 shows the bifurcation diagram depicting global maxima of the angular rotating arm displacement and its corresponding Lyapunov exponent versus the parameter E .

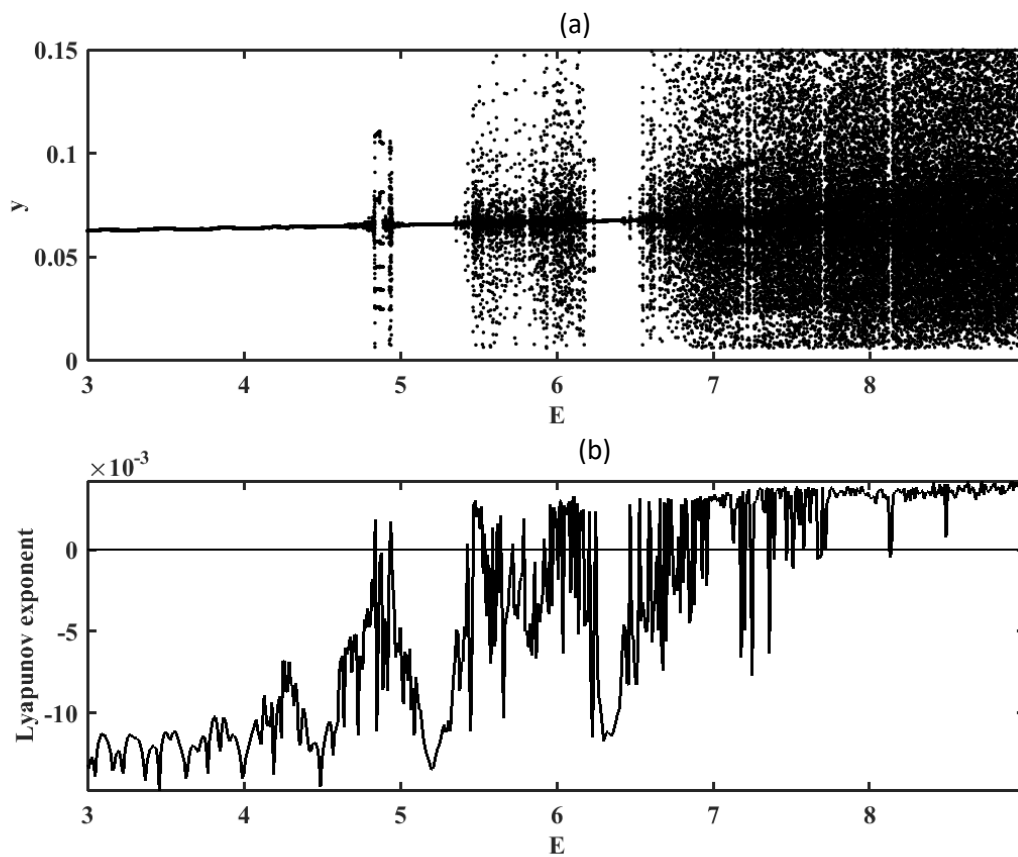


Figure 21 - Bifurcation diagram depicting global maxima of the angular rotating arm displacement (a) and the largest Lyapunov exponent (b) versus the parameter E obtained for $\varpi=0.6$. With the parameters of Table 2.

Figure 22 shows some typical time histories and phase portraits of the rotating arm motion for different values of E . Figure 22 (a) and 22 (c) show periodic 1T oscillations while Figure 22 (b) and 22 (d) show chaotic oscillations.

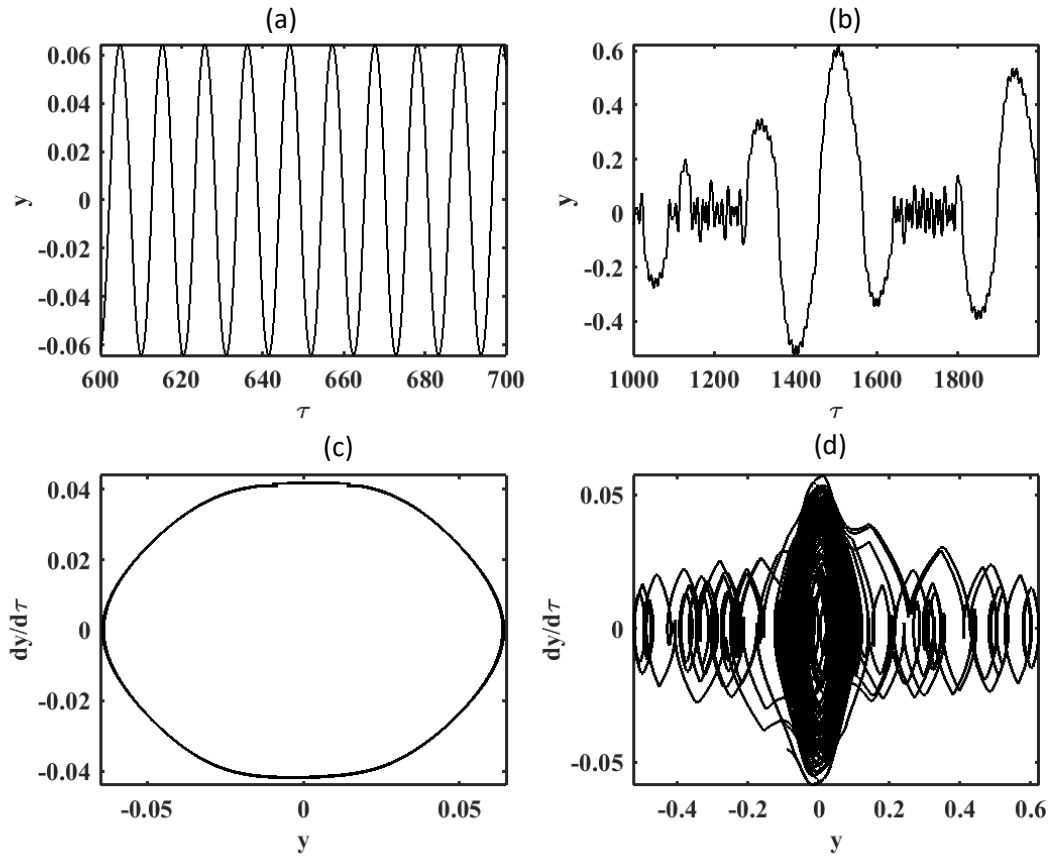


Figure 22 - Time histories(a), (b) and phase portraits (c), (d) obtained with the parameters of Figure 21 and for $E=4.0$ (a), (c); $E=9.0$ (b), (d).

Figure 23 (a) shows the bifurcation diagram of the angular displacement of the rotating arm when the normalized frequency ϖ varies. The behaviour of the device shows non-chaotic oscillations for $\varpi \in [0.2; 0.51]$ and chaotic oscillations for $\varpi \in [0.52; 0.6]$. It can be well observed that the corresponding Lyapunov exponent plotted in Figure 23 (b) converges well to a positive value only when $\varpi \in [0.52; 0.6]$. Figure 24 shows some typical time histories and phase space of the rotating arm motion for different values of ϖ . Figure 24 (a) and 24 (b) show periodic 1T oscillations while Figure 24 (b) and 24 (d) show chaotic oscillations.

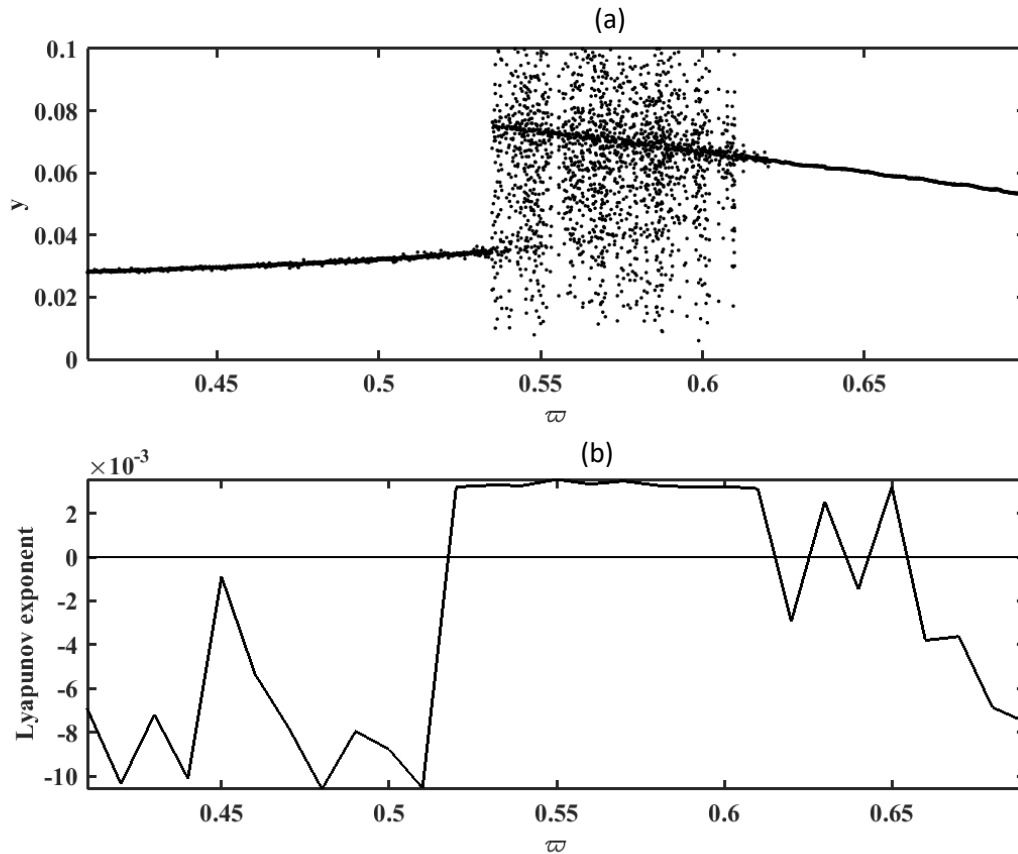


Figure 23 - Bifurcation diagram depicting global maxima of the angular rotating arm displacement (a) and the largest Lyapunov exponent (b) versus the parameter ϖ obtained with $E=6$. With the parameters of Table 2.

With the dimensionless value of the angular rotating arm displacement $y = 0.2$, we obtain from equation (3.18), the corresponding real value $\theta = 0.157$ rad, which is less than 1 rad. Comparing with our study, we can conclude that, for the chosen parameters, the rotating arm does not exhibit complete rotation. The numerical simulation shows that the set of equation (3.29), can lead to complex dynamical behaviours such as nT periodic oscillations and chaotic oscillations. It was observed that, without the three permanent magnets, the system shows a chaotic behaviour for appropriate range of large values of the normalized frequency and magnitude of the external excitation source. When three permanent magnets are added, the system shows a chaotic behaviour for appropriate range of small values of the normalized frequency and magnitude of the external excitation. The bifurcation diagrams can be obtained for other sets of parameters.

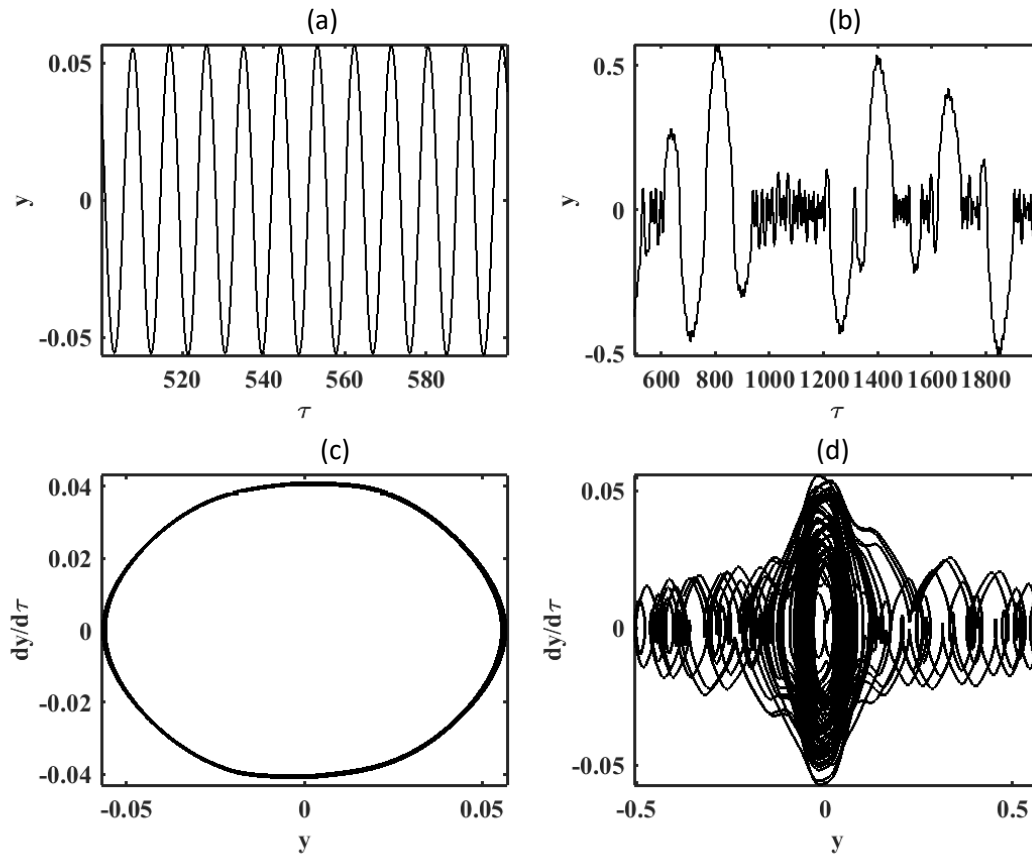


Figure 24 - Time histories (a), (b) and phase portraits (c), (d) obtained for $\varpi=0.69$ (a), (c); $\varpi=0.57$ (b), (d).

In this section, we have showed that, for appropriate range of parameters, chaos can arise even for motion without complete rotations with small value of the control parameters. This is particularly interesting if the rotating arm is used to mix different liquids and powder. The magnitude E and the normalized frequency ϖ of the external source are used as control parameters. We have confirmed our hypothesis by the bifurcation diagram of the angular displacement of the rotating arm and the Lyapunov exponent.

3.3.4. Chaotic dynamics generated from delay

Dynamical systems occur in a wide variety of physical, chemical, engineering, economics and biological systems. There are many examples where delay plays an important role. Some of these examples are listed and presented by M. Lakshamanan and D. V. Senthilkumar in [111] and some others in ref. [112-114]. The mathematical description of delay dynamical systems will naturally involve the

delay parameter in some specified way. This can be in the form of differential equations with delay [89, 115-117]. Delay differential equations with multiple delays are represented by an equation with more than one positive delays [117-120]. Delay differential equations with time-dependent delay where time-delays are explicitly dependent on time. Time dependent delays depend on the relative distance between the drive and response systems [121-123]. As a specific system parameter, delay can lead to bifurcation, oscillation and also to chaotic or non-chaotic behaviour.

Mechatronic delay generator

One can investigate another way of generating chaos in the EMS device by using a mechatronic delay generator. This can also be seen as the enhancement of complexity of the device. Purposely mechatronic generator is a velocity sensor, such as a tachometer where the measured angular velocity is proportional to the output voltage. As well as in electricity network, the propagation time of signal through the transmission line from a subunit to another is an interesting parameter that can strongly influence the dynamical behaviour of the device. The time delay here can be due to an embedded control system that serves as the communication system taking a message at the source (tachogenerator) and sending it to the receiver (electrical part of the electromechanical rotating arm). The internal generated voltage $U(t)$ from the tachometer is given by [124]:

$$U(t) = \nu \dot{\theta}(t - \tau_i). \quad (3.30)$$

This is equivalent to the e.m.f of a DC motor. ν is the conversion gain (Volts. second/radians), i.e. a specific-fixed value for a given tachogenerator. $\dot{\theta}(t - \tau_i)$ is the input angular speed (for the thin rod) and τ_i the time delay.

Here we consider the presence of the three permanent magnets, at the free end of the thin rod. In presence of delay, one can derive the equations describing the dynamics of the electromechanical system as given by the following equations:

$$\left\{ \begin{array}{l} \left[(1-\eta) + \frac{2\eta}{1 + \cosh(x - \sigma_2 \text{sign}(\dot{x}))} \right] \dot{x} = -\lambda \dot{y} - x + E \text{sign}(\sin(\bar{\omega}\tau)) + \xi \Omega(\tau - \tau_i) \\ \ddot{y} = -\beta_3 \dot{y} - \beta_2 \sin(\theta_0 y) \cos(\theta_0 y) - \beta g(y\theta_0) + \beta_0 x \end{array} \right. \quad (3.31)$$

Effects of delay on the dynamical behaviour

In this subsection, the EMS device is still driven by a square wave excitation. Figure 25 (a) shows the bifurcation diagram of the dimensionless angular displacement y when the parameter E varies. From this Figure 25, the behaviour of the device shows chaotic oscillations for $E \in [4; 10]$ and non-chaotic oscillations for $E \in [0.5; 3.98]$. These behaviours are confirmed by the corresponding Lyapunov exponent in Figure 25 (b). For a long delay ($\tau_i = 20$), induced by the mechatronic generator, chaotic behaviour appears for small value $E=4$ (compared to the case without delay $E=5.41$) of the magnitude of the external excitation.

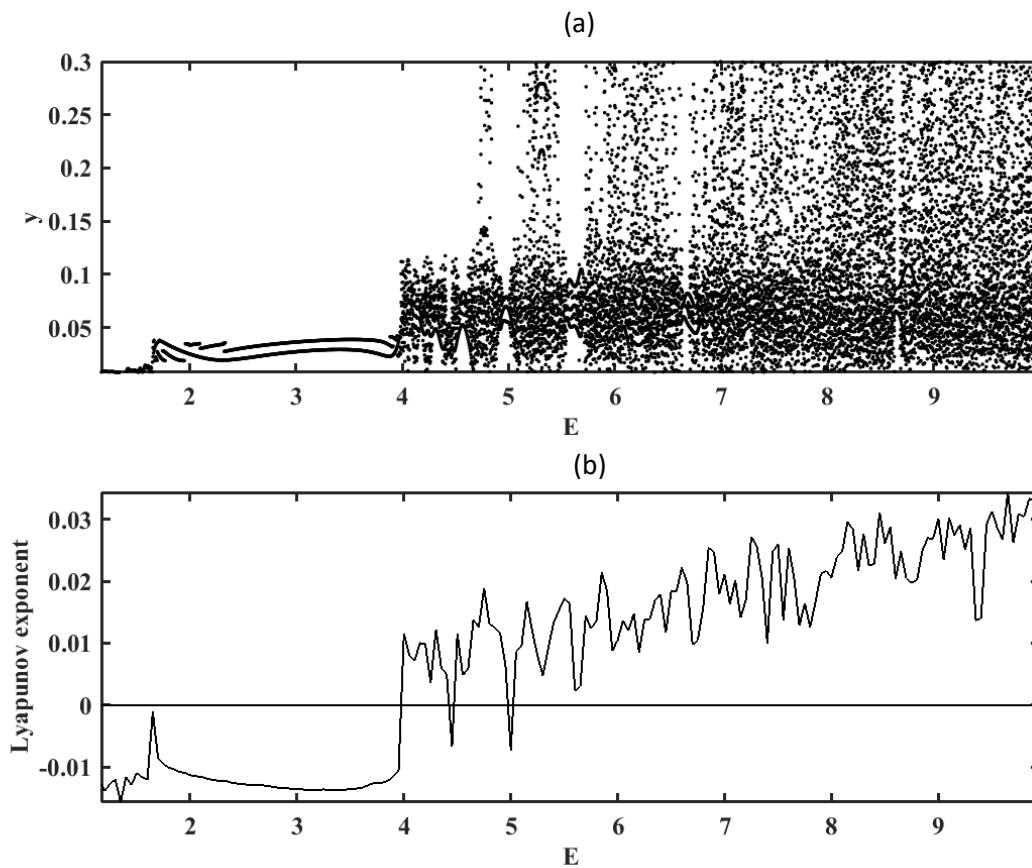


Figure 25 - Bifurcation diagram depicting global maxima of the angular rotating arm displacement (a) and the largest Lyapunov exponent (b) versus the parameter E obtained with the parameters of Figure 24 and for $\varpi=0.57$; $\nu=0.085$; $\tau_i=20$.

Similarly, Figure 26 (a) shows the bifurcation diagram of the angular displacement of the rotating arm when the normalized frequency ϖ varies. The behaviour of the device shows

non-chaotic oscillations for $\varpi \in [0.4; 0.56] \cup [0.580; 0.582] \cup [0.59; 0.65]$ and chaotic oscillations for $\varpi \in [0.570; 0.579] \cup [0.580; 0.591]$. It can be well observed that the corresponding Lyapunov exponent plotted in Figure 26 (b) converges well to a positive value only when $\varpi \in [0.570; 0.579] \cup [0.580; 0.591]$. For smallest value of the dimensionless magnitude of the external excitation $E = 4$; the device exhibits chaotic behaviour.

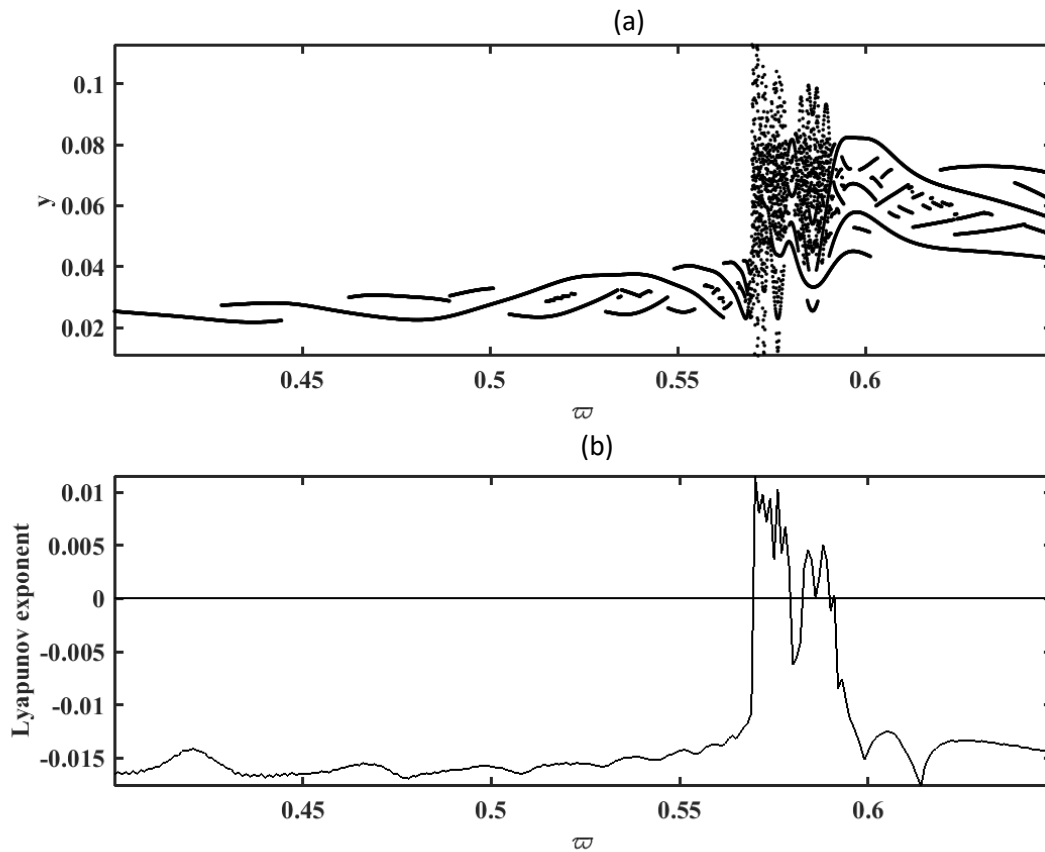


Figure 26 - Bifurcation diagram depicting global maxima of the angular rotating arm displacement (a) and the largest Lyapunov exponent (b) versus the parameter ϖ obtained with the parameters of Figure 25 and for $E=4$.

The electromechanical pendulum arm can be use to homogenise different liquid and/or powder. The results obtained from Figure 25 and Figure 26 are very interesting since the device can be use either in regular or chaotic dynamics.

3.4. Analysis of an electromechanical system with translational and pendulum motion

3.4.1. Electromechanical system and equations

The device is an electrodynamic transducer as shown in Figure 1. This transducer is constituted by an electrical part and a mechanical part magnetically coupled by a permanent magnet.

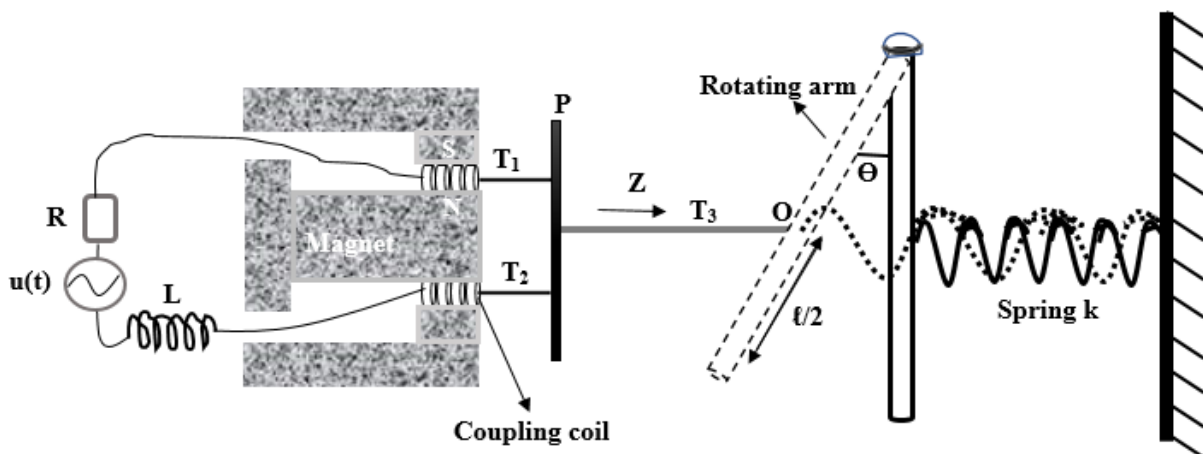


Figure 27 - Electromechanical device

The electrical part of the system consists of a resistor R , an inductor L , and an external voltage source $u(t)$ all connected in series. The ends of this series of dipoles are immersed in the coupling magnet and extend in the form of two coils with which certain elements of the mechanical part will oscillate.

The mechanical part consists of a translational rod that activates the pendulum or pendulum arm of length ℓ and mass m see Figure 27. This pendulum arm returned to its equilibrium position by a spring of stiffness k , connected by its free end to the rotating arm and fixed at the other end (see Figure 27). The center (O) of the pendulum arm being connected to the rod P , perform the same movement parameterized by the abscissa Z . The pendulum arm performs a rotational movement of angle θ around its vertical position. It suffers viscous friction (characterized by the coefficient of viscosity λ). In this study, we assume that T_1 , T_2 , T_3 , and P have a negligible mass and the role of T_3 is to transmit the Laplace force to the pendulum arm. The relation between the translational displacement Z and the angular displacement θ is:

$$Z = \frac{\ell}{2} \sin(\theta) \quad (3.32)$$

In this electromechanical model, all the components have linear characteristics.

The parameters of the electromechanical device shown in Figure 27 are listed in Table 1. We choose these values to obtain appropriate angular oscillations with limited magnitude

Parameters	Values	Dimensions
Inductance: L	0.05	H
Resistance: R	2	Ω
Mass of the pendulum arm: m	0.05	kg
stiffness coefficient of the spring: k	variable	N / m
Magnetic field intensity: B	1	T
Length of the pendulum arm ℓ	0.8	m
Average length of winding in magnetic field l	0.5	m
Frictional coefficient λ	0.04	Ns / m

Table 4 - Parameters of the electromechanical system

The coupling between the electrical part and the mechanical part generates on the mechanical part a Laplace force:

$$\vec{f} = i\vec{l} \wedge \vec{B} \quad (3.33)$$

where l is the length of the winding in the magnetic field \vec{B} of the magnet. $i\vec{l}$ is orthogonal to \vec{B} and $\vec{f} = f(i)\vec{z}$, with $f(i) = lBi$ where \vec{z} is the unit vector along the horizontal axis.

In the electric part, an electromotive induction force is obtained by the Lenz law:

$$e = -\vec{l} \cdot (\vec{B} \wedge \dot{\vec{Z}}) \quad (3.34)$$

Since $(i\vec{l}, \vec{B}, \dot{\vec{Z}})$ is a direct trihedral, $e(\dot{\vec{Z}}) = -lB\dot{Z}$.

To establish the electrical equation governing the dynamics of the system, we use voltage Kirchhoff's law on the electrical part and obtain:

$$L \frac{di}{dt} + Ri + lB\dot{Z} = u(t) \quad (3.35)$$

where in the left, the first term is the voltage across the inductor, the second term is the ohmic voltage and the third term represents the coupling term between the electrical and mechanical parts. The dot over a variable represents a time derivative.

To establish the equation governing the dynamics of the mechanical arm, we use the Newton's second law of dynamics for rotational motion taking into account the Laplace force. One obtains:

$$J \frac{d^2\theta}{dt^2} + \lambda \frac{\ell^2}{4} \frac{d\theta}{dt} + kZ \frac{\ell}{2} \cos(\theta) + mg \frac{\ell}{2} \sin \theta - \frac{\ell}{2} \cos(\theta)(lBi) = 0 \quad (3.36)$$

where $J = m \frac{\ell^2}{3}$ is the moment of inertia of the pendulum arm. Considering $u(t)$ as a sinusoidal voltage in the form $u_0 \sin(\omega t)$ (u_0, ω being respectively, the amplitude and the frequency, and t the time), then replacing equation (3.32) into equation (3.35) and (3.36), one obtains the electromechanical equations which govern the functioning of the device given in Figure 27:

$$\begin{cases} L \frac{di}{dt} + Ri + lB \left(\frac{\ell}{2} \cos(\theta) \frac{d\theta}{dt} \right) & = u_0 \sin(\omega t) \\ J \frac{d^2\theta}{dt^2} + \lambda \frac{\ell^2}{4} \frac{d\theta}{dt} + k \frac{\ell^2}{4} \sin(\theta) \cos(\theta) + \frac{mg\ell}{2} \sin(\theta) - \frac{\ell}{2} \cos(\theta)(lBi) = 0 \end{cases}, \quad (3.37)$$

Denote:

$$\begin{aligned} \bullet &= \frac{d}{d\tau}; \bullet\bullet = \frac{d^2}{d\tau^2}; x = \frac{i}{i_0}; t = \frac{\tau}{\omega_e}; y = \frac{\theta}{\theta_0}; \omega_e = \frac{R}{L}; E_0 = \frac{u_0}{L\omega_e i_0}; \theta_0 = 0.25 \\ \lambda_1 &= \frac{lB\theta_0}{2Li_0}; \gamma_2 = \frac{\lambda\ell^2}{4J\omega_e}; \omega_1^2 = \frac{k\ell^2}{4J\theta_0\omega_e^2}; \omega_2^2 = \frac{mg\ell}{2J\theta_0\omega_e^2}; \lambda_2 = \frac{lBi_0}{2J\theta_0\omega_e^2}; i_0 = 0.1 \end{aligned} \quad (3.38)$$

ω_e is the frequency of the electrical part, i_0 is the normalization current of the electrical part and θ_0 is the normalized angular displacement. Taking into account equation (3.38), the differential equations (3.37) are reduced to the following set of non-dimensional differential equations:

$$\begin{cases} \dot{x} + x + \lambda_1 \cos(y\theta_0) \dot{y} & = E_0 \sin(\omega\tau) \\ \ddot{y} + \gamma_2 \dot{y} + \omega_1^2 \sin(y\theta_0) \cos(y\theta_0) + \omega_2^2 \sin(y\theta_0) - \lambda_2 \cos(y\theta_0) x = 0 \end{cases} \quad (3.39)$$

γ_2 is the dissipative coefficient of the mechanical parts. λ_1, λ_2 are the electromechanical coupling coefficients.

The investigation of the dynamical behavior of this device is done considering the frequency and the maximal amplitude of the external excitation as control parameters. Figure 28 shows some phase portraits for different values of E_0 .

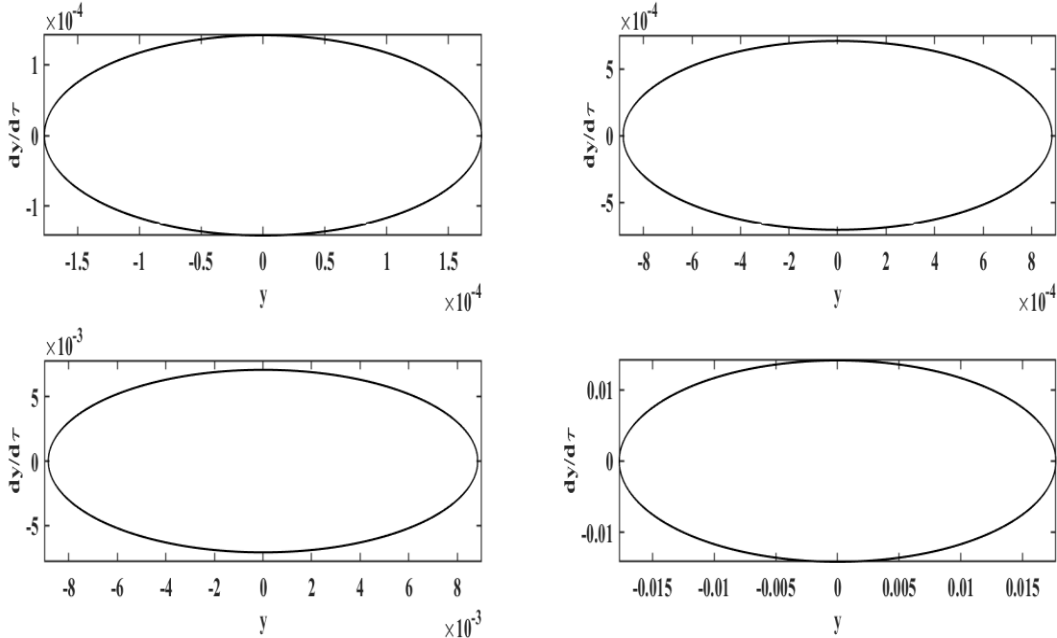


Figure 28 - phase portraits obtained with the parameters of Table 4. $E_0 = 0.1$ (a), $E_0 = 0.5$ (b), $E_0 = 5.0$ (c), $E_0 = 10$ (d) and $\varpi = 0.8$

For the small and high values of E_0 , one observe 1T periodic oscillations. Similarly, Figure 29 shows some phase portraits for different values of ϖ .

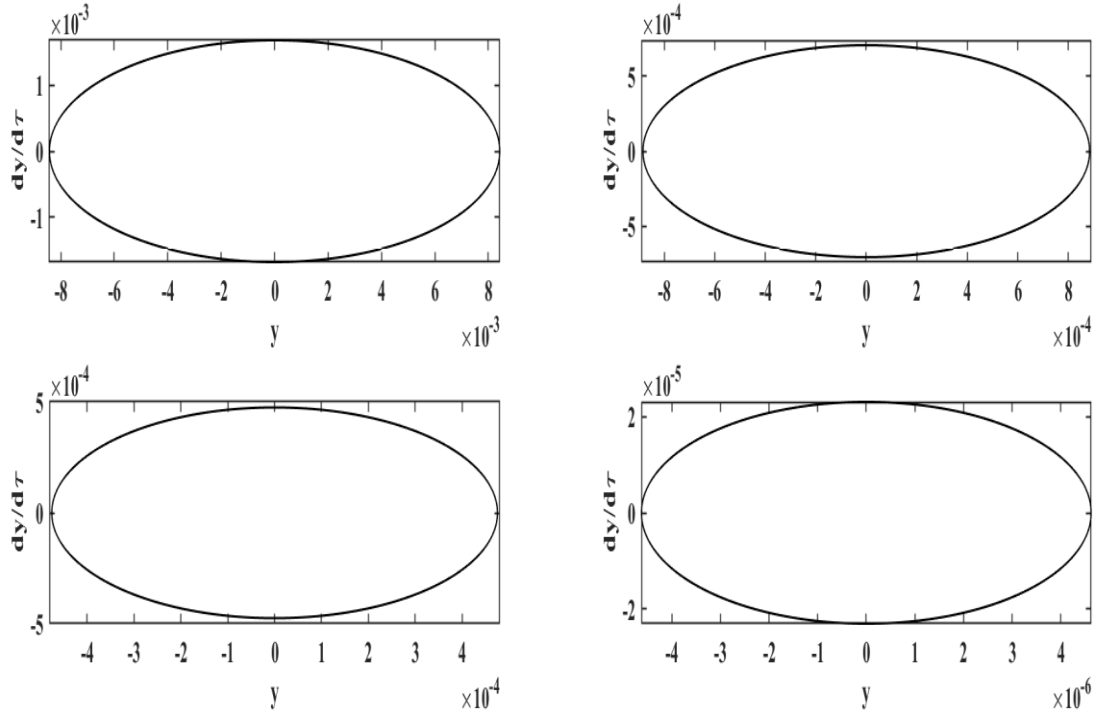


Figure 29 - phase portraits obtained with the parameters of Table 4. $\varpi = 0.2$ (a), $\varpi = 0.8$ (b), $\varpi = 1.0$ (c), $\varpi = 5.0$ (d) and $E_0 = 0.5$

For some different values of ϖ , Figure 29 shows that the device exhibit with periodic 1T oscillations.

Oscillatory states

Assuming that the pendulum arm performs small angular displacement, y is small and the following approximations can be considered: $\sin(y\theta_0) \approx y\theta_0$ and $\cos(y\theta_0) \approx 1$. Taking into account these approximations, equations (3.45) become:

$$\begin{cases} \dot{x} + x + \lambda_1 \dot{y} & = E_0 \sin(\varpi\tau) \\ \ddot{y} + \gamma_2 \dot{y} + \omega_0^2 y \theta_0 - \lambda_2 x & = 0 \end{cases} \quad (3.40)$$

With $\omega_0^2 = \omega_1^2 + \omega_2^2$

Equations (9) presents in the absence of the input voltage $u(t)$ a single stationary point ($x = 0, y = 0, \frac{dy}{d\tau} = 0$) which is asymptotically stable. The presence of the sinusoidal input voltage gives rise to the oscillatory steady state.

We use the well-known method of harmonic balance to establish the equations characterizing the amplitudes of the harmonic oscillations as a function of the frequency ϖ . To do this we express x and y in the form:

$$\begin{cases} x = a_1 \cos(\varpi t) + a_2 \sin(\varpi t) \\ y = b_1 \cos(\varpi t) + b_2 \sin(\varpi t) \end{cases} \quad (3.41)$$

The maximal amplitudes A and B of these oscillations are defined by $A^2 = a_1^2 + a_2^2$ and $B^2 = b_1^2 + b_2^2$. Replacing equations (3.41) into equations (3.40), and equating the sine ($\sin(\varpi t)$) and cosine ($\cos(\varpi t)$) terms separately, it comes that the unknown parameters a_1 ; a_2 ; b_1 ; b_2 satisfies the following expressions:

$$\begin{aligned} a_1 &= \frac{-E_0 \varpi (\varpi^4 + \gamma_2^2 \varpi^2 - 2\varpi^2 \omega_0^2 \theta_0 + \omega_0^4 \theta_0^2 + \omega_0^2 \theta_0 \lambda_2 \lambda_1 - \lambda_2 \lambda_1 \varpi^2)}{D} \\ a_2 &= \frac{(\varpi^4 + \gamma_2^2 \varpi^2 - 2\varpi^2 \omega_0^2 \theta_0 + \gamma_2 \varpi^2 \lambda_2 \lambda_1 + \omega_0^4 \theta_0^2) E_0}{D} \\ b_1 &= \frac{(\varpi^2 - \gamma_2 - \omega_0^2 \theta_0 - \lambda_2 \lambda_1) \varpi \lambda_2 E_0}{D} \\ b_2 &= \frac{-\lambda_2 E_0 (-\omega_0^2 \theta_0 + \varpi^2 + \varpi^2 \gamma_2)}{D} \end{aligned} \quad (3.42)$$

with

$$\begin{aligned} D &= \varpi^6 - 2\varpi^4 \omega_0^2 \theta_0 + 2\gamma_2 \varpi^2 \lambda_2 \lambda_1 - 2\varpi^4 \lambda_2 \lambda_1 + \varpi^4 + \omega_0^4 \theta_0^2 \varpi^2 + \lambda_2^2 \lambda_1^2 \varpi^2 + \\ &\quad 2\omega_0^2 \theta_0 \lambda_2 \lambda_1 \varpi^2 + \gamma_2^2 \varpi^2 - 2\varpi^2 \omega_0^2 \theta_0 + \omega_0^4 \theta_0^2 + \gamma_2^2 \varpi^4 \end{aligned}$$

We analyze the behavior of A and B when the normalized frequency of the external excitation ϖ is varied and the results are presented in Figure 30.

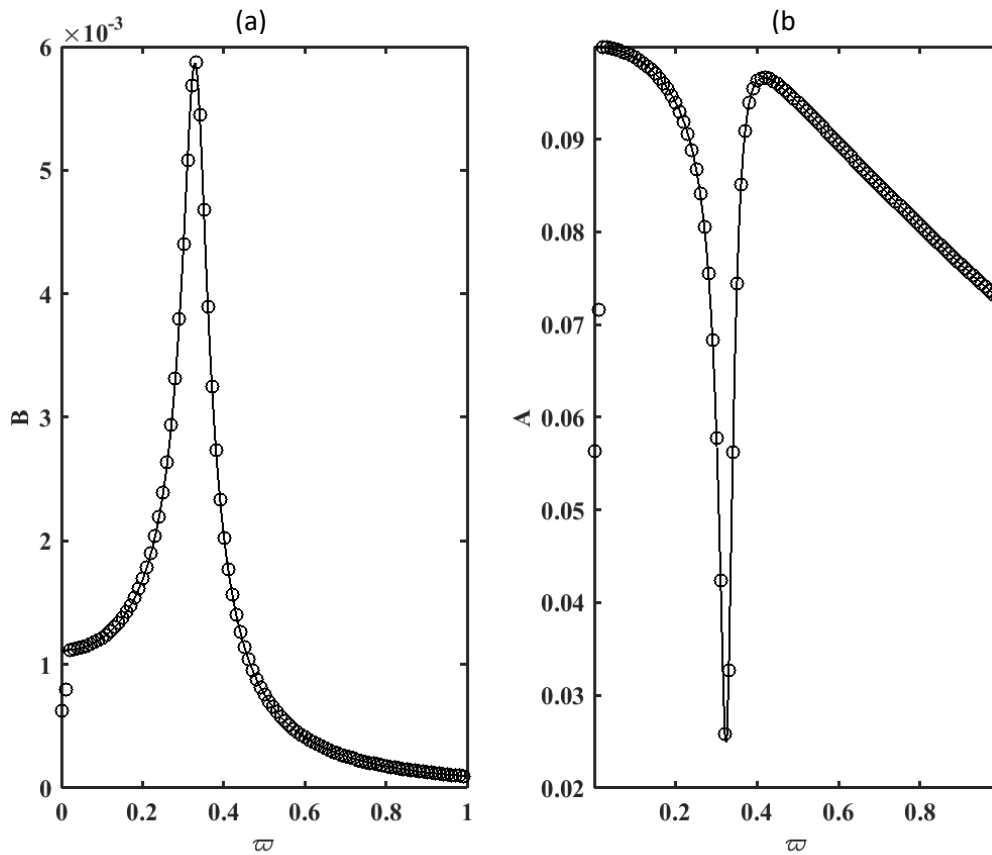


Figure 30 – Frequency-responses of the (a) angular displacement (b) electrical current: curves from the harmonic balance approximations (-) and curves from the direct numerical simulations (o) with the parameters of Table 4 and $E0=0.1$

Figure 30, shows that when the high amplitude is attained in the mechanical part, for the frequency close to ω_0 , the amplitude of the electrical signal is at its lowest value.

3.4.2. Effects of the bistable potential energy

In order to make the electromechanical pendulum arm oscillations chaotic, the previous device is changed into the one of Figure 31 where one permanent magnet is fixed at the free end of the pendulum arm (the mass of the pendulum arm will therefore increase). In the right and in the left sides of the pendulum arm, at equal distances to the equilibrium position, there are two other permanent magnets. The electric part is the same as previously. Because of the magnet at the end of the rotating arm the mass of the rotating arm increases from 0.05 kg to 0.07 kg .

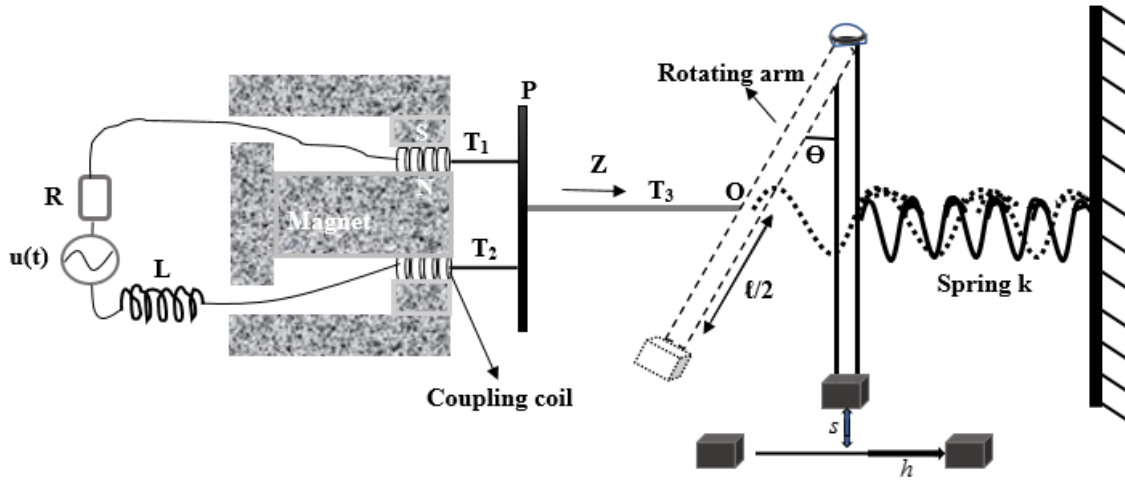


Figure 31 - Electromechanical device with bistable potential

Equations

This configuration of additional permanent magnets with spring has been used in [16]. The authors demonstrated that, the association of permanent magnets with linear spring leads to the bistable nature of the potential energy which can be expressed as:

$$U(\theta) = -\frac{a}{2}\theta^2 + \frac{b}{4}\theta^4 \quad (3.43)$$

where a and b are positive coefficients. The values of the minima are given as $\theta = \pm\sqrt{\frac{a}{b}}$. We

assume that the magnets are close enough so that even if the angles are small

($\sin(y\theta_0) \approx y\theta_0, \cos(y\theta_0) \approx 1$), the effect of the bi-stability remains valid. Assuming that the parameters of the device present in Figure 3 are chosen as $a=1.0$ and $b=50.0$, the minima are $\theta = \pm 0.141 \text{ radian} \approx 8^\circ$.

Applying voltage Kirchhoff's law on the electrical part and Newton second law for the rotational movement to the pendulum arm, the electromechanical equations that govern the functioning of the device shows in Figure 3 are:

$$\begin{cases} L \frac{di}{dt} + Ri + \frac{lB\ell}{2} \cos(\theta) \frac{d\theta}{dt} = u_0 \sin(\omega t) \\ J \frac{d^2\theta}{dt^2} + \lambda \frac{\ell^2}{4} \frac{d\theta}{dt} + \frac{dU(\theta)}{d\theta} - \frac{\ell}{2} \cos(y\theta_0)(lBi) = 0 \end{cases} \quad (3.44)$$

Using the dimensionless variables given in equations (3.38), considering the case of small angular displacement ($\sin(y\theta_0) \approx y\theta_0, \cos(y\theta_0) \approx 1$), equations (3.44) take the following form:

$$\begin{cases} \dot{x} + x + \lambda_1 \dot{y} & = E_0 \sin(\varpi\tau) \\ \ddot{y} + \gamma_2 \dot{y} - \sigma y + \alpha y^3 = \lambda_2 x \end{cases} \quad (3.45)$$

with, $\sigma = \frac{a}{J\omega_e^2}$ and $\alpha = \frac{b\theta_0^2}{J\omega_e^2}$

We remind that despite the angle is small, we have assumed that the magnets are disposed so that the effects of the bistable potential are still operating.

Bifurcation diagram and Lyapunov exponent

The dynamical behaviors of the system mathematically represented by equations (3.45) are illustrated using numerical simulation to present bifurcation diagrams, Lyapunov exponent, phase portraits, and time histories. In this subsection, parameters E_0 and ϖ are chosen as the control parameters.

Analysis with respect to parameter E_0

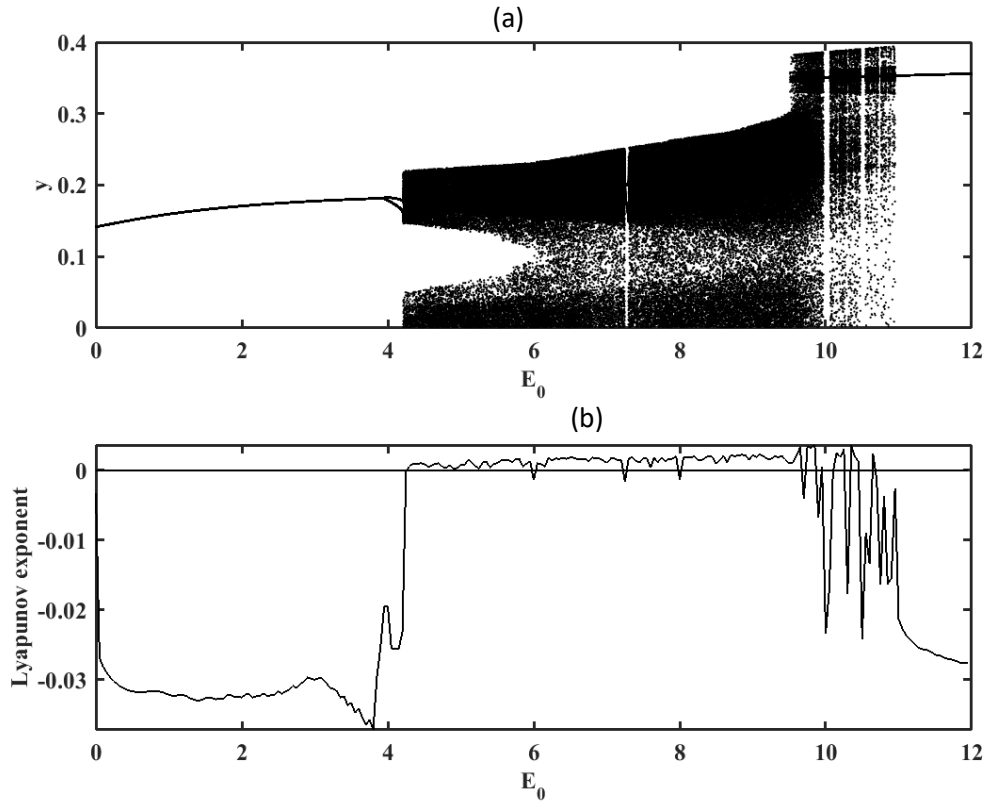


Figure 32 - Bifurcation diagram depicting the global maxima of the angular pendulum arm displacement (a) and the largest Lyapunov exponent (b) versus the amplitude E_0 with the parameters of table 4, for $m=0.07$ and $\varpi=0.35$

Figure 32 shows that, as the amplitude of the external excitation E_0 varies from 0.0 to 12.0, the bifurcation diagram of the angular displacement pendulum arm reveals nT period-oscillations behavior for $E_0 \in [0.0, 4.25] \cup [10.5, 12.0]$. Chaos appears in the electromechanical pendulum arm when $E_0 \in [3.7, 8.88]$ characterized by the positive values of the Lyapunov exponent. For $E_0 \in [9.65, 10.45]$, one observes chaos oscillations with some windows of nT period-oscillations. This chaotic state is particularly of interest when the electromechanical pendulum arm is used for industrial operations such as the mixing of different liquids, chemicals or powders. Figure 33 shows some Time histories and corresponding phase portraits. Figure 34 shows the Poincarré map for the chaotic attractor [125,126].

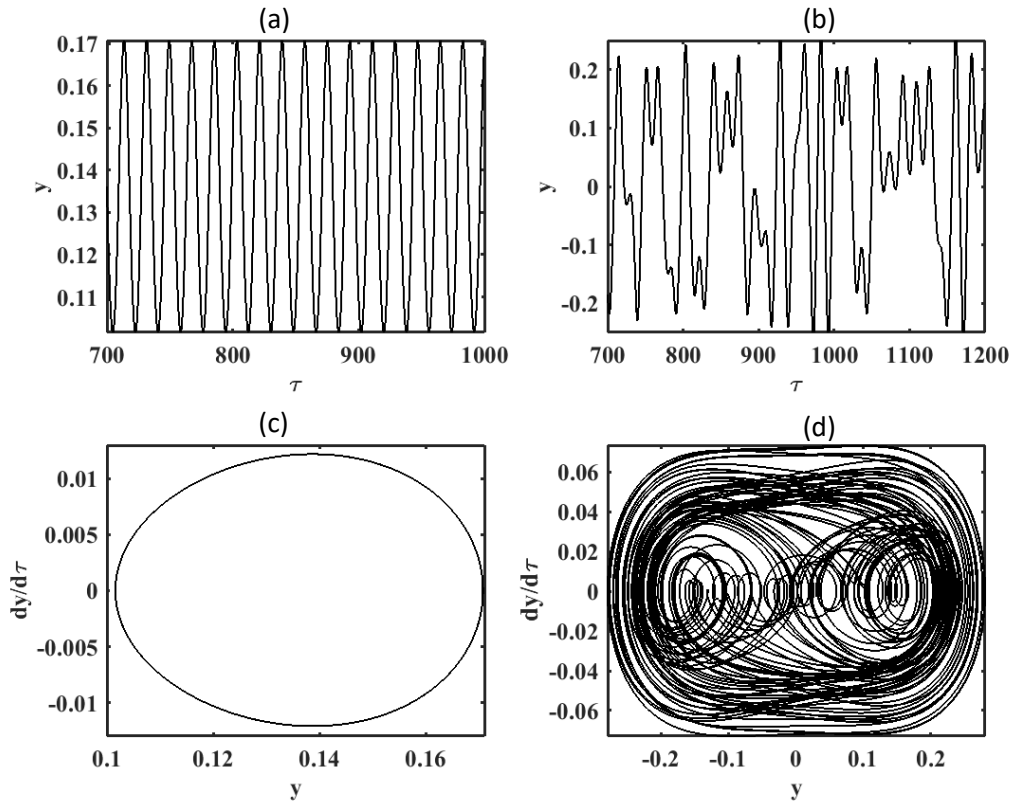


Figure 33: Time histories (a), (b) and phase portraits (c), (d) obtained with the parameters of Figure 4 and (a), (c); (b), (d)

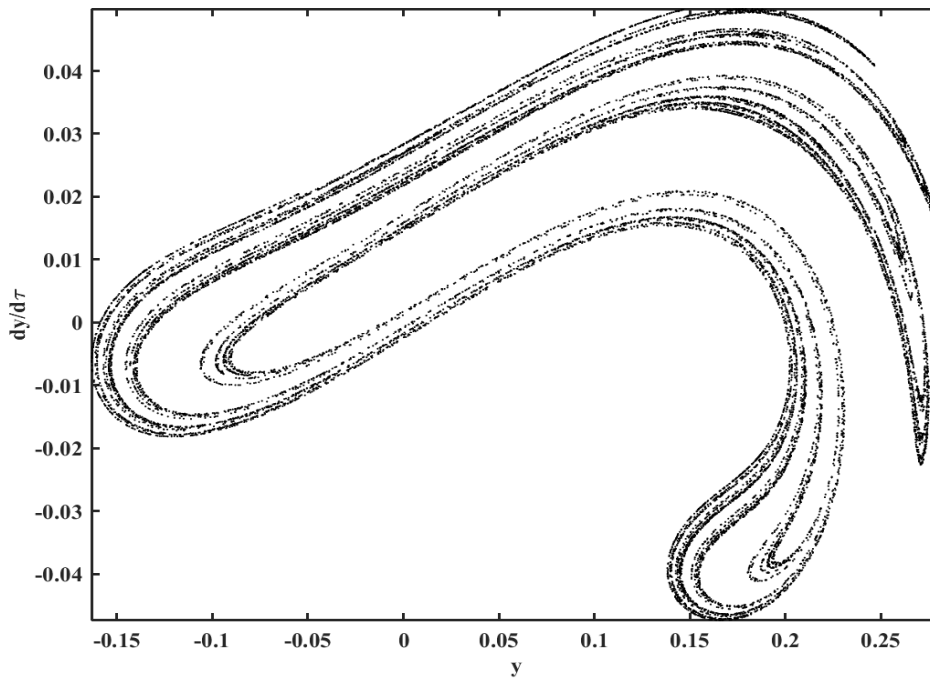


Figure 34 - The Poincaré map of a chaotic state with the parameters of Figure 5 and for $\varpi=0.35$, $E0=9.0$.

Analysis with respect to parameter ϖ

In Figure 35 the bifurcation diagram and the corresponding Lyapunov exponent of the angular rotating movement when the parameter ϖ varies. One finds in Figure 35 (a) that, when $\varpi \in [0.2, 0.295] \cup [0.524, 1]$ nT period-oscillations. For $\varpi \in [0.3, 0.519]$, the device shows chaotic oscillations with some windows of non-chaotic oscillations. These behaviors are confirmed by Figure 35 (b) in which the variation of the Lyapunov exponent is plotted.

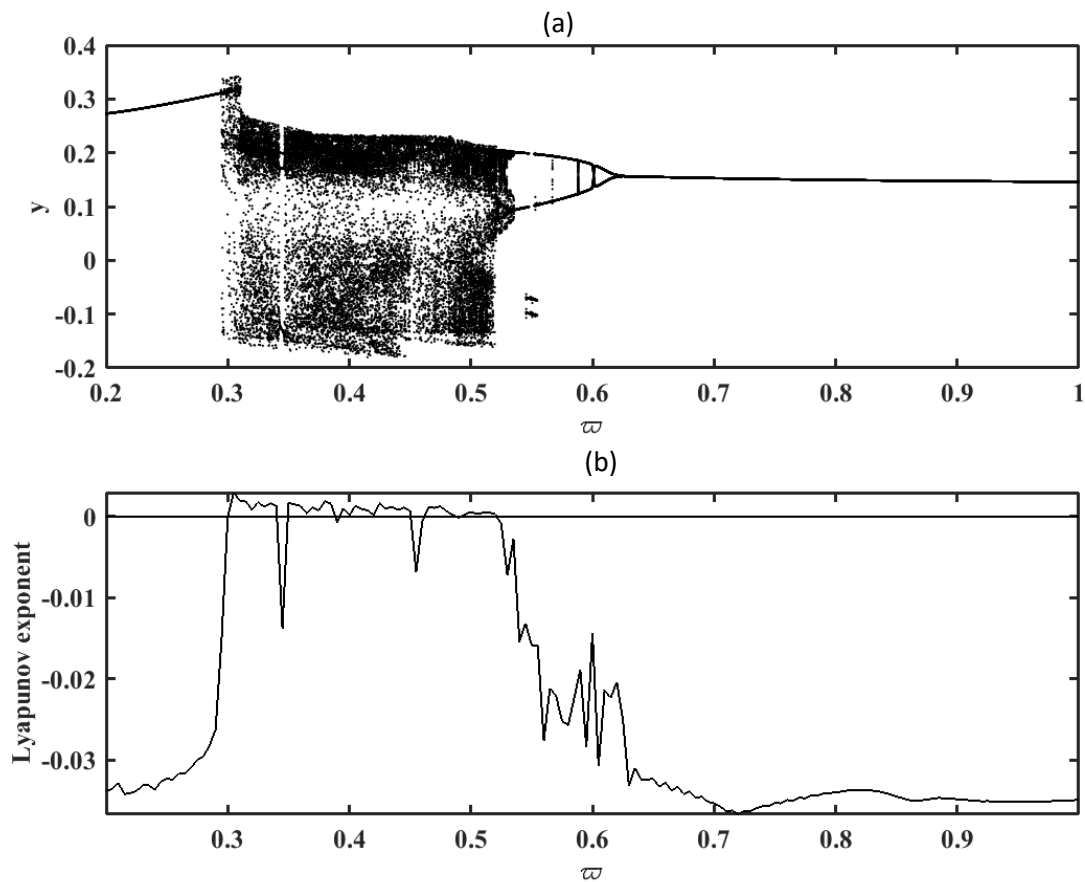


Figure 35 - Bifurcation diagram depicting global maxima of the angular pendulum arm displacement (a) and the largest Lyapunov exponent (b) versus the parameter ϖ with the parameters of Figure 32 and for $E0=9.0$

3.4.3. Electromechanical device with hysteretic iron-core inductor

In absence of the permanent magnets

The electromechanical device with hysteretic iron core is present in Figure 36 Here, the previous inductor is replaced by the iron-core inductor.

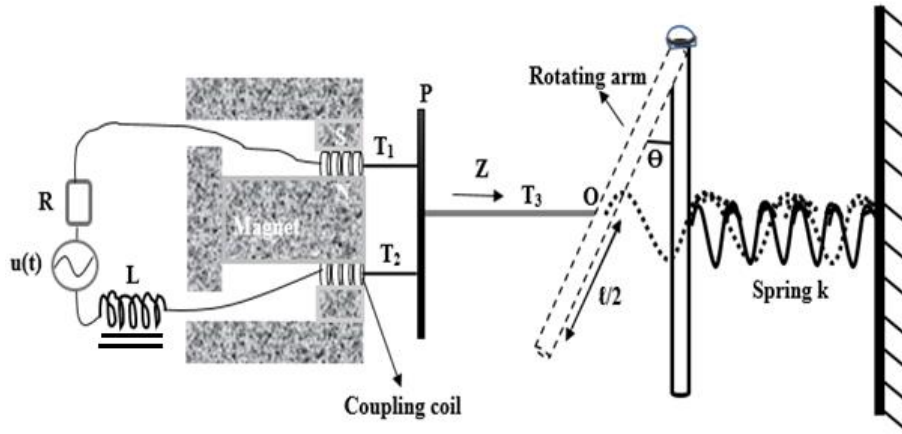


Figure 36 - Electromechanical pendulum arm with hysteretic iron core inductor

As the ferromagnetic circuit is made of steel or iron sheet, the flux through the iron core is not always constant, but can vary with the current. It is therefore interesting to analyze the effects of such behavior on the dynamical behaviors of the device to delineate the domains of regular periodic dynamics and that of chaotic dynamics when the device parameters change.

We assume that the ferromagnetic core inductance L in equation (3.44) is a function of the current in the electrical circuit [87]:

$$L = \left[\frac{\mu_0 N^2 A}{l_e} + \frac{B_s N^2 \alpha_0 A}{2l_e} \cdot \frac{2}{1 + \cosh\left(\frac{\alpha_0 Ni}{l_e} - \sigma_1\right)} \right] \quad (3.46)$$

where $\sigma_1 = \beta_0 \text{sign}\left(\frac{di}{dt}\right)$, $\mu_0 = 4\pi \cdot 10^{-7}$ H/m is the air permeability, α_0 are constants. N is the number of turns for the iron core inductor, A is the cross sectional area of the iron core, B_s is the saturation flux density, and l_e the average length of winding of the iron core.

The new parameters are listed in Table 2.

Parameters	Values	Dimensions
Mass of the pendulum arm: m	0.07	kg
Cross sectional area A of iron core	176.71×10^{-6}	m^2
Number of turn N for the iron core inductor	variable	1
Saturation flux density B_s	0.13	T
the average length of winding of the iron core l_e	0.5	m

Table 5 - Parameters of the electromechanical system

The iron core inductor modified only the electrical part of the device which becomes

$$\left[\frac{\mu_0 N^2 A}{l_e} + \frac{B_s N^2 \alpha_0 A}{2l_e} \cdot \frac{2}{1 + \cosh\left(\frac{\alpha_0 N i}{l_e} - \sigma_1\right)} \right] \frac{di}{dt} + Ri + \frac{l\ell B}{2} \cos(\theta) \frac{d\theta}{dt} = u(t) \quad (3.47)$$

Considering the sinewave as the external source, the dimensionless electromechanical equations, which govern the functioning of the studied device are written as follows:

$$\left\{ \begin{array}{l} \left[(1-\eta) + \frac{2\eta}{1 + \cosh(x - \sigma_2 \text{sign}(\dot{x}))} \right] \dot{x} + x + \lambda_0 y = E_0 \sin(\varpi\tau) \\ \ddot{y} + \gamma_2 \dot{y} + \omega_1^2 \sin(y\theta_0) \cos(y\theta_0) + \omega_2^2 \sin(y\theta_0) - \lambda_2 \cos(y\theta_0)x = 0 \end{array} \right. \quad (3.48)$$

with

$$\begin{aligned} \omega_e &= \frac{Rl_e(1-\eta)}{\mu_0 N^2 A}; \quad \lambda_0 = \frac{l_e(1-\eta)lB\ell\theta_0}{2\mu_0 N^2 Ai_0}; \quad \sigma_2 = \beta_0 \omega_e i_0; \quad \beta_0 = 88.42 \times 10^{-2} \\ E &= \frac{u_0 l(1-\eta)}{\mu_0 N^2 Ai_0 \omega_e}; \quad \alpha_0 = 88.23 \times 10^{-4}; \quad \eta = \frac{B_s \alpha_0}{2\mu_0 + B_s \alpha_0}; \quad i_0 = \frac{l_e}{\alpha_0 N} \end{aligned} \quad (3.49)$$

One observed that the frequency of the electrical part changes the value and then all constants as well as λ_2 , γ_2 , ω_0 and α depending on that frequency will also change their values. The aim of this section is to investigate the effect of the hysteretic iron-core on the studied electromechanical device considering the maximal amplitude and the frequency of the external excitation.

In Figure 37, We plot phase portrait of the device considering the same values of the maximal external amplitude than the one used in Figure 28. One observe multiperiodic oscillations in Figures 37 (a), (b) and quasiperiodic oscillations in Figure 37 (c), (d).

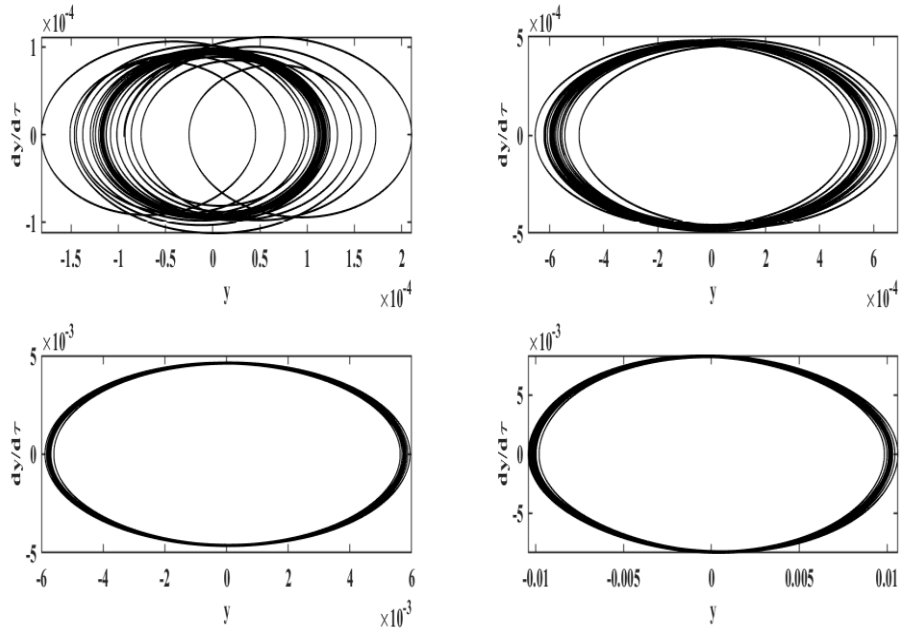


Figure 37 - Phase portraits obtained with the parameters of Table 5. $E_0=0.1$ (a), $E_0=0.5$ (b), $E_0=5.0$ (c), $E_0=10.0$ (d) and $\varpi=0.8$.

Figure 37 Presents some phase portraits for the same values of ϖ than the one considering in Figure 28

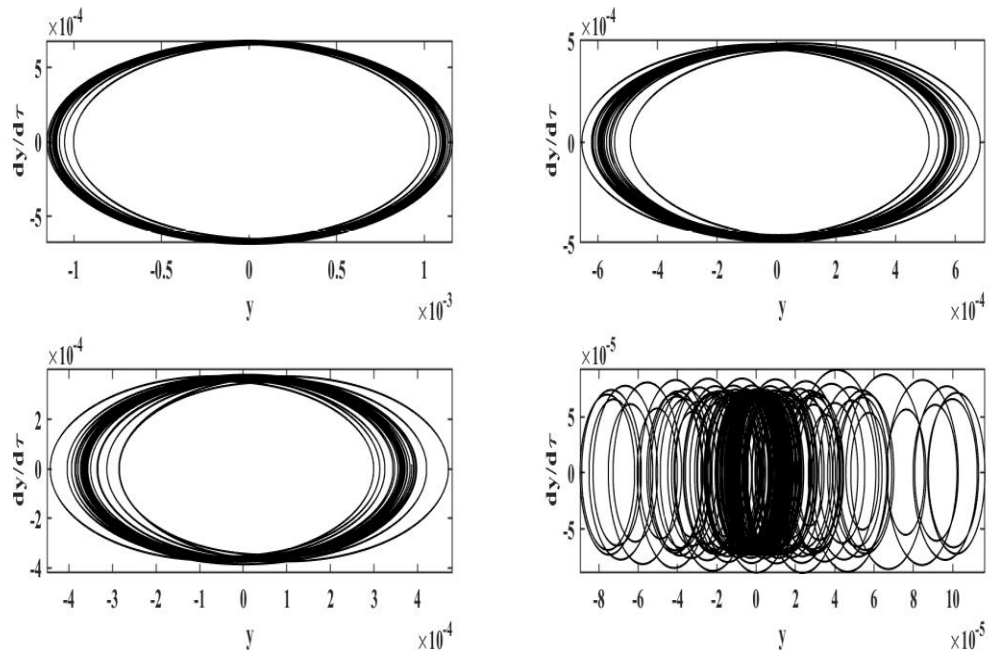


Figure 38 - Phase portraits obtained with the parameters of Table 4, Table 5. $\varpi=0.2$ (a), $\varpi=0.8$ (b), $\varpi=1.0$ (c), $\varpi=5.0$ (d) and $E_0=5.0$.

Compared to the case in the absence of the iron-core inductor, the device exhibits multiperiodic oscillations. So the iron core inductor enhances the complexity of the pendulum's arm vibration.

In presence of permanents magnets

The studied device is the one presented in Figure 39. Here three permanents magnets are added to the previous one.

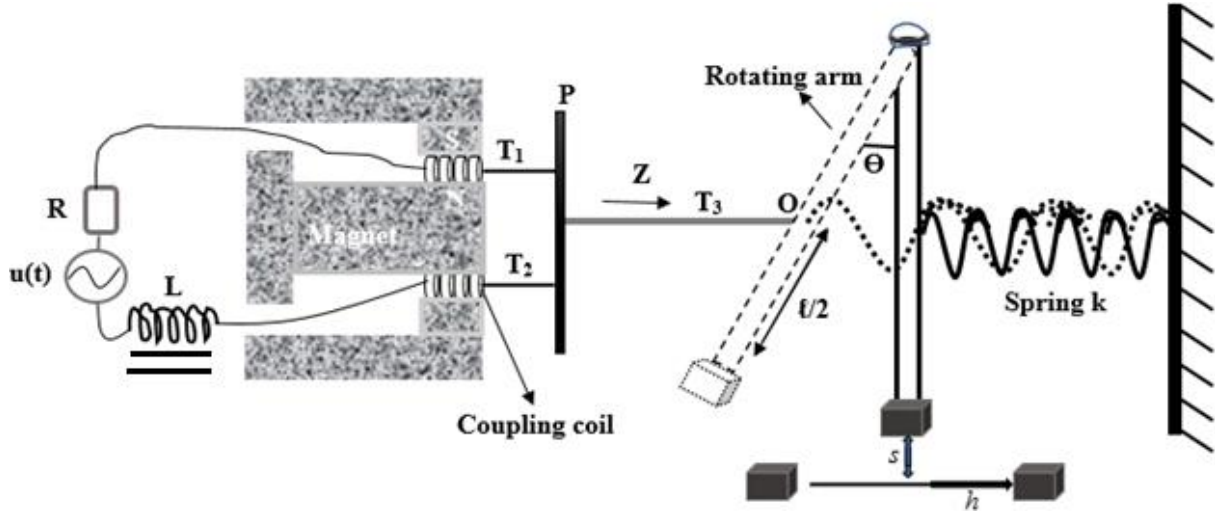


Figure 39 - Electromechanical pendulum arm with hysteretic iron core inductor and bistable potential energy.

In presence of the permanents magnets, only the mechanical part change and became the same than the one Figure 31 and the electromechanical equations that governing the functioning of the device are:

$$\left\{ \begin{array}{l} \left[(1-\eta) + \frac{2\eta}{1 + \cosh(x - \sigma_2 \text{sign}(\dot{x}))} \right] \dot{x} + x + \lambda_0 y = E_0 \sin(\omega\tau) \\ \ddot{y} + \gamma_2 \dot{y} - \sigma y + \alpha y^3 = \lambda_2 x \end{array} \right. \quad (3.50)$$

The aim of this section is to find how chaos arises in our device when the parameters of the iron core inductor vary. We have focused the attention on the variation of the number N of turns. Figure 40 shows that, as N varies from 400 to 850, nT period-oscillations behavior exist for $N \in [200, 380] \cup [705, 760]$ while chaos appears when $N \in [380, 504] \cup [770, 840]$.

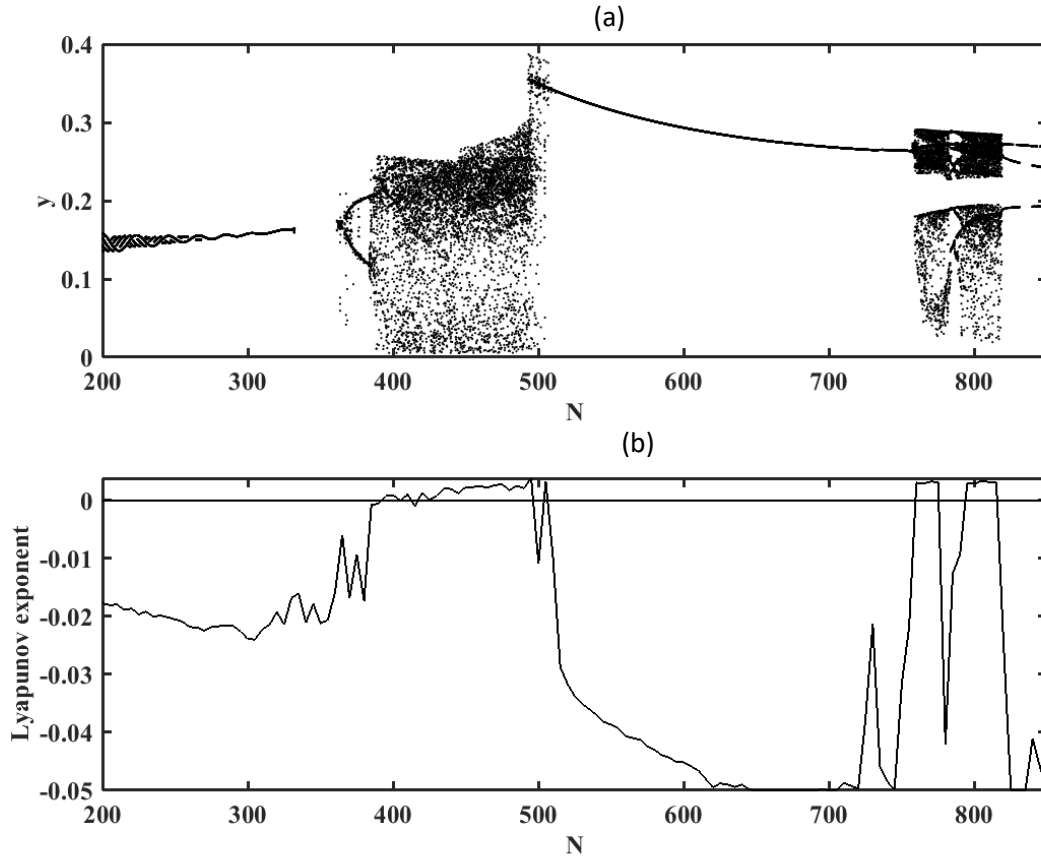


Figure 40 - Bifurcation diagram depicting global maxima of the angular pendulum arm displacement (a) and the largest Lyapunov exponent (b) versus the parameter N obtained with the parameters of Table 4, Table 5 and for $\varpi=0.35$, $E0 =9.0$.

3.4.4. Effect of the delay on electromechanical system

As it has appeared in the above analysis, chaos has been observed in the electromechanical systems when some parameters of the device vary. One can investigate another way of generating chaos in the same device by using a mechatronic delay generator. This can also be seen as the enhancement of complexity of the device. Purposely mechatronic generator is a velocity sensor, such as a tachometer where the measured angular velocity is proportional to the output voltage of the meter. The internal generated voltage $U(t)$ in a tachometer is given by equation (3.36):

In presence of delay, the equations describing the dynamics of the electromechanical system are the following:

$$\begin{cases} \dot{x} + x + \lambda_0 y & = E_0 \sin(\varpi\tau) + \xi \dot{y}(\tau - \tau_0) \\ \ddot{y} + \gamma_2 \dot{y} + \omega_1^2 \sin(y\theta_0) \cos(y\theta_0) + \omega_2^2 \sin(y\theta_0) - \lambda_2 \cos(y\theta_0)x = 0 \end{cases} \quad (3.51)$$

with: $\xi = \frac{\nu l_e (1 - \eta)}{\mu_0 N^2 A i_0}$

Figure 41 presents the behavior of the device when the delay is considered as control parameter.

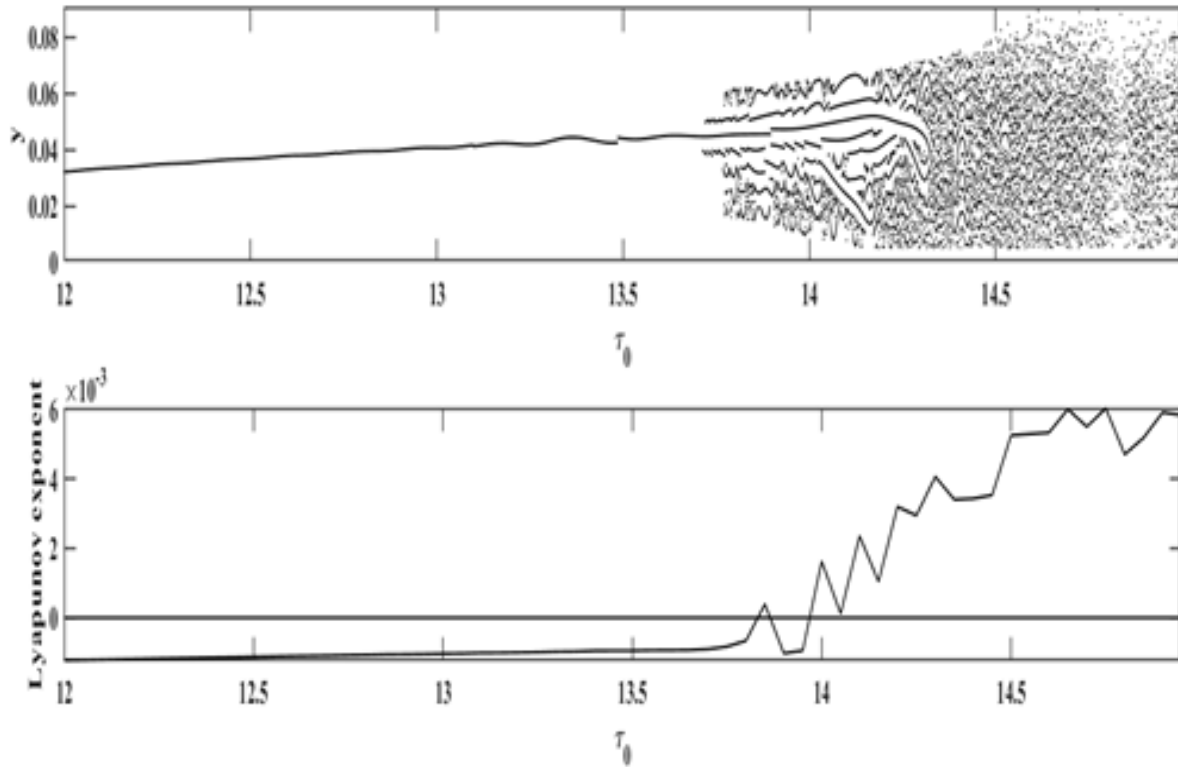


Figure 41 - Bifurcation diagram depicting global maxima of the angular pendulum arm displacement (a) and the largest Lyapunov exponent (b) versus the parameter τ obtained with the parameters of Table 4 and for $\varpi=0.8$, $E0 =0.5$.

. Figure 41 shows that, as τ_0 varies from 12 to 15, nT period-oscillations behavior exist for $\tau_0 \in [12;13.87]$ while chaos appears when $\tau_0 \in [13.871;15]$. To complement the results presented in Figure 41, Time histories and corresponding phase portraits are displayed in Figure 42, they are indicating chaotic states and periodic oscillations.

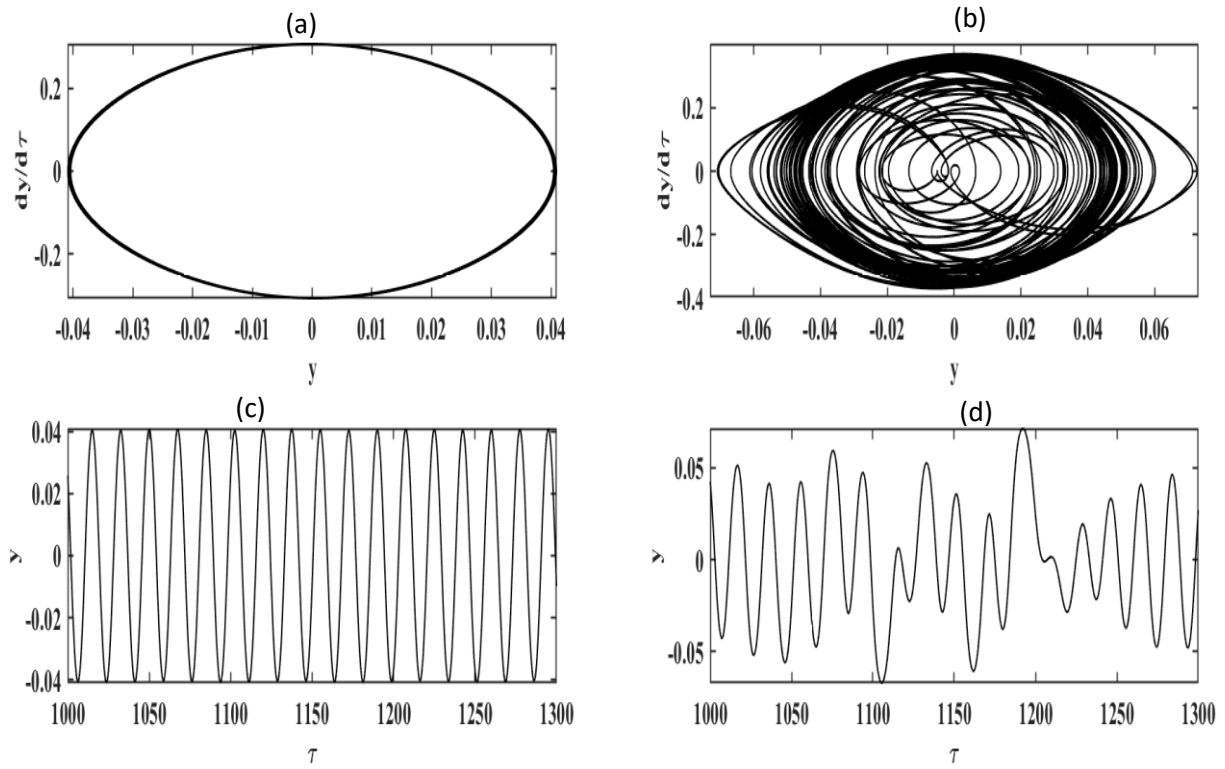


Figure 42 - Phase portraits (a), (b) and Time histories (c), (d) obtained with the parameters of Figure 41 and $\tau_0=13$ (a), (c); $\tau_0=14.5$ (b), (d).

Figure 42 (a) and 9 (c) show 1T-periodic oscillations while Figure 42 (b) and 42 (d) demonstrate chaotic oscillations.

Case with bistable potential energy and hysteretic iron core inductor.

By a adding three permanents magnets and the hysteretic iron core inductor, this subsection present how the device behave when some control parameter vary. The dynamical behaviour of the device is mathematically describe by the following set of differential equation (3.52).

$$\left\{ \begin{array}{l} \left[(1-\eta) + \frac{2\eta}{1 + \cosh(x - \sigma_2 \text{sign}(\dot{x}))} \right] \dot{x} + x + \lambda_0 y = E_0 \sin(\omega\tau) + \xi \dot{y}(\tau - \tau_0) \\ \ddot{y} + \gamma_2 \dot{y} - \sigma y + \alpha y^3 = \lambda_2 x \end{array} \right. \quad (3.52)$$

Figure 43 (a) shows the bifurcation diagram plotted in terms of the non-dimensional angular displacement y as τ_0 increases. One finds that, when $\tau_0 \in [21.5, 21.7]$ the system shows nT period-oscillations while chaos appears for $\tau_0 \in [21.7, 22.5]$ with some windows of nT period-oscillations. These behaviors are confirmed by Figure 41 (b) in which the variation of the Lyapunov exponent is plotted.

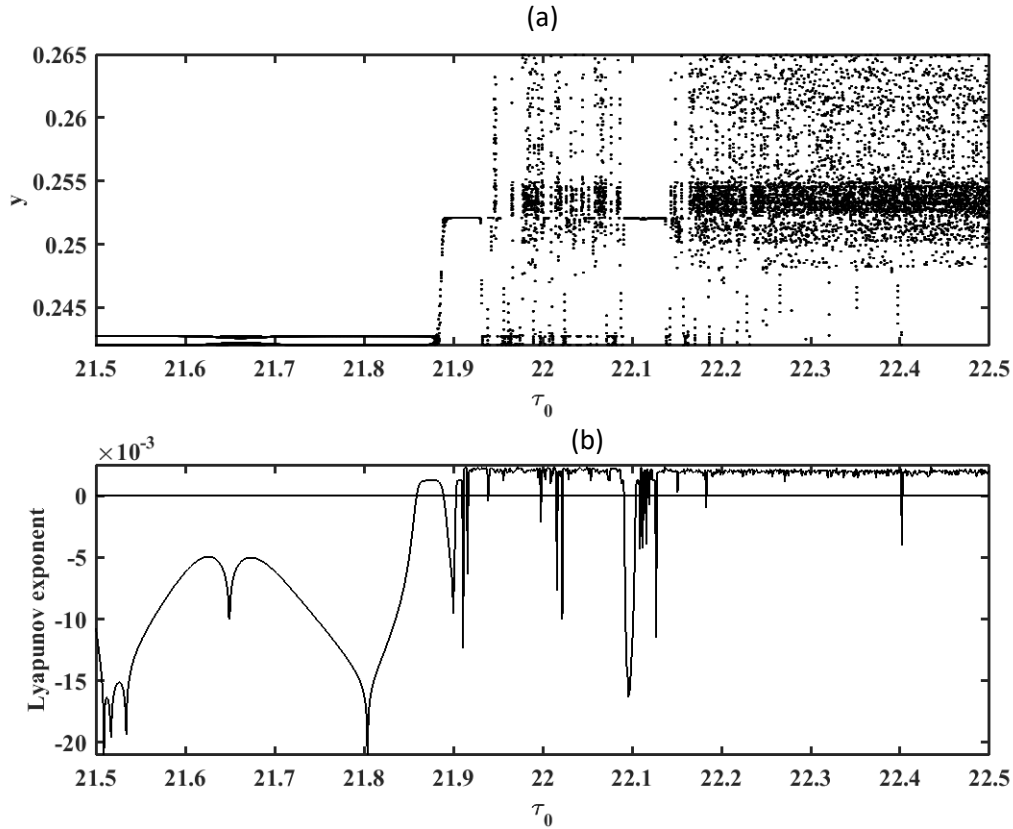


Figure 43 - Bifurcation diagram depicting global maxima of the angular pendulum arm displacement (a) and the largest Lyapunov exponent (b) versus the delay obtained with the parameters of Table 4, Table 5 and for $N=780$, $\varpi=0.35$, $E0 = 7.7$, $v=0.25$

3.5. Conclusion

We have studied the dynamical behaviours of three EMS with rotating arm. Bifurcation diagrams and corresponding Lyapunov exponent diagrams have been used to find, in the parameters spaces, the domains of periodic and chaotic states. The results obtained are interesting since they give the parameters ranges where the device can be used either in the regular dynamics or in the chaotic states. For the three EMS with rotating arm, good agreements have been found between the results from the analytical treatment and the ones from the numerical simulations. Melnikov chaos has been used in the first device to show analytically the existence of horseshoes chaos dynamics.



GENERAL CONCLUSION



General conclusion

This thesis was motivated by the design of three EMS having each a mobil arm actuated by an electric circuit for easy domestic and industrial appliances such as vibrating sieve and mixer. Thereafter, a theoretical investigation of their dynamical behaviours has been done

We have first presented a new electromechanical rotating arm with bistable potential energy generated by the combined action of a spiral spring and magnets appropriately placed in the device. We have studied the dynamical behaviour of the device both in the absence and in the presence of the magnets. The device has been seen to generate complex behaviours including chaos and angular oscillations with amplitude greater than one turn. In the absence of magnets, the device presents a single stable point and exhibit periodic behaviour. In presence of magnets, we numerically show that the association of elastic potential energy and mechanical potential energy due to the magnets leads to the bistable nature of the total potential energy. This bistability is responsible for the generation of chaotic dynamics in the electromechanical system. By using square excitation, the device presents chaotic behaviour for smaller values (compared to the case of sinusoidal source) of the excitation amplitude and frequency. It has also been shown that the electromechanical system can show Hamiltonian chaos characterized by the fractality of the basin of attraction.

Secondly, we have considered the dynamical behaviour of an electromechanical rotating arm with a nonlinear hysteretic iron-core inductor. The results obtained are interesting since for the chosen parameters, the device can be used either in the regular dynamics or in the chaotic states with rotating angular displacement less than 90° . For small value of the magnitude of the external excitation, a good agreement has been found between the results from the analytical treatment and the ones from the numerical simulations. The effects of the three permanent magnets at the end of the rotating arm have been examined. We numerically show that the association of elastic potential energy due to springs and mechanical potential energy due to the magnets leads to the bistable nature of the total potential energy. The numerical simulation shows that the presence of the magnets leads as in the first device to complex dynamical behaviours such as nT periodic oscillations and the system exhibits chaotic behaviour. The effects of the delay induced by the mechatronic delay generator were also examined. One observed that, by taking into account the delay, the device also exhibits regular and chaotic

oscillations. In this case, depending on the chosen parameters, the chaotic behaviour appeared for smaller values (compared to the case without delay) of the control parameters (magnitude of the external excitation and normalized frequency).

The dynamics of a pendulum arm actuated by an electromechanical transducer has been investigated in the third device. In order to induce chaos dynamics in the system, we also introduce a bistable potential by adding three permanent magnets at the end of the pendulum arm. The numerical simulation shows that the presence of the additional magnets leads to complex dynamical behaviors such as nT periodic oscillations and chaos when the sine wave is the input voltage. Secondly, we assume that the magnetic circuit is saturated and found that some values of the iron core turns can lead the system to chaotic states. Thirdly, it has been found that a feedback delay signal proportional to the pendulum angular velocity is another source of chaos. The generation of chaos when varying some parameters of the electromechanical system is interesting as its chaotic motion can improve the efficiency of various engineering activities such as sieving or sifting processes which need disorder to enhance the dispersion of particles.

These complex behaviours can find applications in engineering, e.g. sieves in which chaotic motion could enhance the dispersion of particles and avoid stagnation and formation of aggregates. The case of chaotic vibration sieve is interesting because sieving or sifting processes need disorder to enhance the dispersion of particles. The device can also give some idea on how to optimize the operation of home appliances such as those used for mixing various food components (flour, eggs, spices, vegetables, fruits, and so on).

This work has opened interesting perspectives for future investigations:

- Full automatization of the sieving process so that it could automatically and completely take place for any kind of product to sieve.
- Full automatization of the mixing process so that it could automatically and completely take place for any product to mix.
- Design, model, study and carry out a sieve with many levels
- The more important for us will be the experimental set-up of the chaotic sieve and chaotic mixer device using on one hand the bistable potential, the delay induced by the mechatronic delay generator and on the other hand the hysteretic iron-core inductor.



ANNEX
**Derivation of the
magnetic potential energy**



Annex- Derivation of the magnetic potential energy

Let us note E_{mag} as the potential magnetic energy. To derive this magnetic potential energy, let us consider Figure A1.

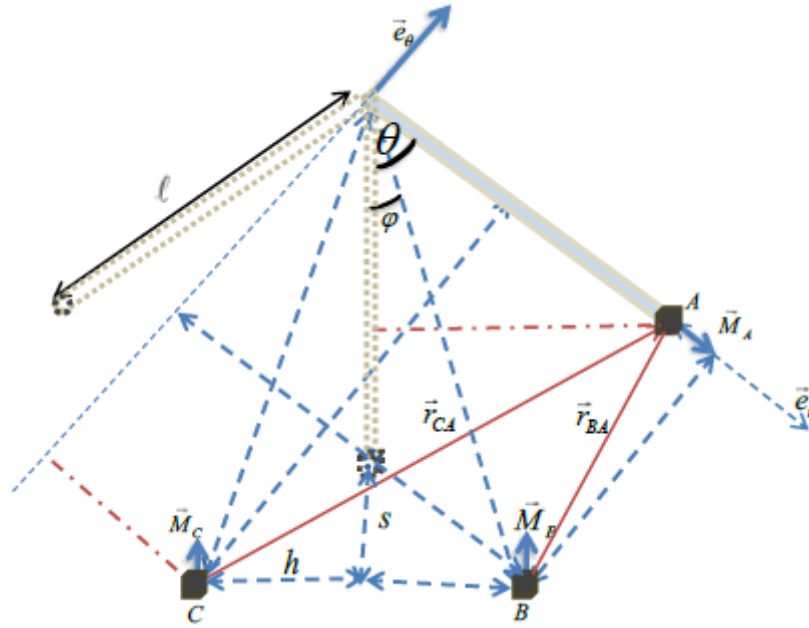


Fig.A1: Schematic structure for the derivation of the magnetic potential energy.

energy.

The magnets A, B, C are identical. The potential energy of the magnet A in the field generated by the magnets B and C is given as [26]:

$$E_{mag} = -(\vec{B}_{BA} + \vec{B}_{CA}) \cdot \vec{M}_A = \frac{\mu_0 M_A^2 \cos \theta}{2\pi} \left(\frac{1}{r_{BA}^3} + \frac{1}{r_{CA}^3} \right) \quad (A1)$$

Where \vec{B}_{BA} and \vec{B}_{CA} are respectively the magnetic field creates on magnet A by magnet B and magnet C . The distance between B and A is given by equation (A2) and the distance between C give A and A is given by equation (A3):

$$\begin{aligned}\vec{r}_{BA} &= -\overline{OB} + \overline{OA} = -\sqrt{h^2 + (s + \ell)^2} \sin\left(\frac{\pi}{2} - \theta + \varphi\right) \vec{e}_r + (\sqrt{h^2 + (s + \ell)^2}) \cos\left(\frac{\pi}{2} - \theta + \varphi\right) \vec{e}_\theta + \ell \vec{e}_r \\ \Rightarrow r_{BA}^3 &= \left[p_1 - q_1 \sin\left(\frac{\pi}{2} - \theta + \varphi\right) \right]^{\frac{3}{2}}\end{aligned}\quad (\text{A2})$$

$$\begin{aligned}\vec{r}_{CA} &= -\overline{OC} + \overline{OA} = -\sqrt{h^2 + (s + \ell)^2} \sin\left(\frac{\pi}{2} - \theta - \varphi\right) \vec{e}_r + (\sqrt{h^2 + (s + \ell)^2}) \cos\left(\frac{\pi}{2} - \theta - \varphi\right) \vec{e}_\theta + \ell \vec{e}_r \\ \Rightarrow r_{CA}^3 &= \left[q_1 - p_1 \sin\left(\frac{\pi}{2} - \theta - \varphi\right) \right]^{\frac{3}{2}}\end{aligned}\quad (\text{A3})$$

where:

$$q_1 = \ell^2 + h^2 + (s + \ell)^2; p_1 = 2\ell\sqrt{h^2 + (s + \ell)^2}; \varphi = \arctan\left(\frac{h}{s + \ell}\right)\quad (\text{A4})$$

Replacing (A2), (A3), and (A4) into (A1), one obtains:

$$E_{mag} = \frac{\mu_0 M_A^2 \cos \theta}{2\pi} \left[\frac{1}{\left[q_1 - p_1 \sin\left(\frac{\pi}{2} - \theta - \varphi\right) \right]^{\frac{3}{2}}} + \frac{1}{\left[q_1 - p_1 \sin\left(\frac{\pi}{2} - \theta + \varphi\right) \right]^{\frac{3}{2}}} \right]\quad (\text{A5})$$

The interaction force between the magnets can be obtained by taking the gradient of (A5)

$$\vec{f}_{mag} = -\overline{\text{grad}}(E_{mag}) = -\frac{1}{\ell} \frac{d}{d\theta} (E_{mag}) \vec{e}_\theta$$

$$\begin{aligned} &= \frac{\mu_0 M_A^2}{2\pi\ell} \left[\left(\frac{1}{\left[q_1 + p_1 \sin\left(\theta - \frac{\pi}{2} + \varphi\right) \right]^{\frac{3}{2}}} + \frac{1}{\left[q_1 + p_1 \sin\left(\theta - \frac{\pi}{2} - \varphi\right) \right]^{\frac{3}{2}}} \right) \sin \theta \right. \\ &\quad \left. + \frac{3}{2} \left(\frac{p_1 \sin\left(\theta - \frac{\pi}{2} + \varphi\right)}{\left[q_1 + p_1 \sin\left(\theta - \frac{\pi}{2} + \varphi\right) \right]^{\frac{5}{2}}} + \frac{p_1 \sin\left(\theta - \frac{\pi}{2} - \varphi\right)}{\left[q_1 + p_1 \sin\left(\theta - \frac{\pi}{2} - \varphi\right) \right]^{\frac{5}{2}}} \right) \cos \theta \right] \vec{e}_\theta\end{aligned}\quad (\text{A6})$$

By taking into account the fact that the magnets are at the end (distance ℓ) of the rotating arm, the displacement between the magnetic force and the rotational axis (ℓ) give the moment of the magnetic force as:

$$\vec{F}_{mag} = \vec{0A}\Lambda\vec{f}_{mag} = \frac{\mu_0 M_A^2}{2\pi} \left[\begin{array}{l} \left(\frac{1}{\left[q_1 + p_1 \sin\left(\theta - \frac{\pi}{2} + \varphi\right)\right]^{\frac{3}{2}}} + \frac{1}{\left[q_1 + p_1 \sin\left(\theta - \frac{\pi}{2} - \varphi\right)\right]^{\frac{3}{2}}} \right) \sin \theta \\ + \frac{3}{2} \left(\frac{p_1 \cos\left(\theta - \frac{\pi}{2} + \varphi\right)}{\left[q_1 + p_1 \sin\left(\theta - \frac{\pi}{2} + \varphi\right)\right]^{\frac{5}{2}}} + \frac{p_1 \cos\left(\theta - \frac{\pi}{2} - \varphi\right)}{\left[q_1 + p_1 \sin\left(\theta - \frac{\pi}{2} - \varphi\right)\right]^{\frac{5}{2}}} \right) \cos \theta \end{array} \right] \vec{e}_r \Lambda \vec{e}_\theta$$

$$= \frac{\mu_0 M_A^2}{2\pi} \left[\begin{array}{l} \left(\left[q_1 + p_1 \sin\left(\theta - \frac{\pi}{2} + \varphi\right)\right]^{-\frac{3}{2}} + \left[q_1 + p_1 \sin\left(\theta - \frac{\pi}{2} - \varphi\right)\right]^{-\frac{3}{2}} \right) \sin \theta \\ + \frac{3}{2} \left(p_1 \left[q_1 + p_1 \sin\left(\theta - \frac{\pi}{2} + \varphi\right)\right]^{-\frac{5}{2}} \cos\left(\theta - \frac{\pi}{2} + \varphi\right) + p_1 \left[q_1 + p_1 \sin\left(\theta - \frac{\pi}{2} - \varphi\right)\right]^{-\frac{5}{2}} \cos\left(\theta - \frac{\pi}{2} - \varphi\right) \right) \cos \theta \end{array} \right] \vec{k}$$



BIBLIOGRAPHY

Bibliography

- [1] B. E. Demartini, H. E. Butterfield, J. Moehlis, K. L. Turner, “Chaos for a microelectromechanical oscillator governed by the nonlinear Mathieu equation”, *Journal of Microelectromechanical Systems*, **16**(6), 1314–1323, (2007).
- [2] J. L. P. Felix, J. M. Balthazar, “Comments on a nonlinear and non-ideal electromechanical damping vibration absorber, Sommerfeld effect and energy transfer”, *Nonlinear Dyn.*, **55**, 1–11, (2009).
- [3] C. A. K. Kwuimy, B. Nana, P. Woaf, “Experimental bifurcations and chaos in a modified self-sustained macro electromechanical system”, *J Sound Vib.*, **329**, 3137–3148, (2010).
- [4] R. R. Reynolds, L. N. Virgin, E. H. Dowell, “High dimensional chaos can lead to weak turbulence”, *Nonlinear Dyn.*, **4**, 531–546, (1993).
- [5] T. Miura, T. Kai, “Chaotic behaviours of a system of three disk dynamos”, *Phys. Lett. A* **101**, 450–454, (1984).
- [6] C. H. Lamarque, J.M. Malasoma, M. N. Ouarzazi, “Chaos in the convective flow of a fluid mixture in a porous medium”, *Nonlinear Dyn.*, **15**, 83–102, (1998).
- [7] D. Belato, H. I. Weber, J. M. Balthazar, D. T. Mook, “Chaotic vibrations of a non-ideal electromechanical system”, *Int J Solids Struct.*, **38**, 1699–706, (2001).
- [8] J. Jerrelind, A. Stensson, “Nonlinear dynamics of parts in engineering systems”, *Chaos Solitons Fract.*, **11**, 2413–28, (2000).
- [9] N. Nbandjo, P. Woaf, “Active control with delay of horseshoes chaos using piezoelectric absorber on a buckled beam under parametric excitation”, *Chaos, Solitons & Fractals*, **32**, 73–79, (2007).
- [10] R. Yamapi, J. B. Chabi Orou, P. Woaf, “Harmonic Oscillations, Stability and Chaos Control in a Nonlinear Electromechanical System”, *J. Sound. Vib.*, **259**, 1253–1264, (2003)
- [11] Y. Chembo Kouomou, P. Woaf, “Triple Resonant States and Chaos Control in an Electromechanical Transducer with Two Outputs”, *J Sound Vib.* **270**, 75–92, (2004)
- [12] B.R. Andrievsky, A.L. Fradkov, P. Yu Guzenko, “Control of Nonlinear oscillations of Mechanical Systems by Speed-Gradient Method Autom Remote”, *Control _Engl. Transl.* **57**, 456–467, (1996).

- [13] D.O. Tcheutchoua Fossi, P. Wofo, “Generation of complex phenomena in a simple electromechanical system using the feedback control”, *Commun Nonlinear Sci Numer Simulat*, **18**, 209-218, (2013)
- [14] Z. M. Ge, J. W. Cheng, “Chaos synchronization and parameter identification of three time scales brushless DC motor system”, *Chaos, Solitons and Fractals*, **24**, 597-616, (2005)
- [15] J. Feng, J. Liu, “Chaotic dynamics of the vibro-impact system under bounded perturbation”, *Chaos Solitons Fractals*, **73**, 10-16, (2015).
- [16] C. Diyi, S. Peng, M. Xiaoyi, “Control and synchronization of chaos in an induction motor system”, *Int. J. Innovative Computing, Information and Control*, **8**, 7237–7248, (2012)
- [17] J. B. Mogo, P. Wofo, “Dynamics of a nonlinear electromechanical device with a pendulum arm”, *J. Comput. Nonl. Dyn*, **2**, 274-278, (2007).
- [18] L. Zhe, “Chaotic vibration sieve”, *Mech. Mach. Theory*, **30**, 608–613, (1995).
- [19] D. O. Tcheutchoua Fossi, P. Wofo, “Dynamics of an electromechanical system with angular and ferroresonant non linearities”, *J. Sound and Vibration*, **133**, 1–7, (2011).
- [20] J. M. Ottino, F. J. Muzzio, M. Tjahjadi, “Chaos, symmetry, and self-similarity: exploiting order and disorder in mixing process”, *Science*, **257**, 754–760, (1992).
- [21] C. A. Kitio Kwuimy, P. Wofo, “Experimental realization and simulation of a self-sustained macro electromechanical system”, *Mech Res Commun*, **37**, 106–110 (2010)
- [22] R. Tsapla Fotsa, P. Wofo, “Chaos in a new bistable rotating electromechanical system”, *Chaos, Solitons and Fractals*, **93**, 48-57, (2016)
- [23] J. J. Thomsen, D. M Tcherniak, “Chelomei's pendulum explained”, *Proc R Soc London A* **457**, 1889-1913 (2001)
- [24] J. Kennedy, J.A. Yorke, “The forced pendulum and the wada property”, In West T editor. *Continuum theory and dynamical systems*. New York Marcel Dekker Inc (1994)
- [25] K. T. Chau, S. Ye, Y. Gao, “Application to chaotic-motions motors to industrial mixing processes”, *IEEE*, **1AS**, 1874–1880 (2004).
- [26] G. A. Fusun, B. Hüseyi, L.P.F. Jorge, M.B. José, M. L. R. Reyolando, “A nonlinear electromechanical pendulum arm with a nonlinear energy sink control (nes) approach”, *Journal of Theoretical and Applied Mechanics*, **54**(3), 975-986 (2016)
- [27] H. A. Rafael, A.N. Hélio, M. L. R. Reyolando, J. M. B. Brasil, M. B. Átila, M. T. Angelo, “Statements on nonlinear dynamics behavior of a pendulum, excited by a crank-shaft-slider mechanism”, *Meccanica* **51**(6), 1301-1320, (2016)

- [28] M. T. Angelo, P. Vinicius, M.B. Atila, “Chaos control and sensitivity analysis of a double pendulum arm excited by an RLC circuit based nonlinear shaker”, *Journal of Vibration and Control*, **22**(17), 3621-3637, (2015)
- [29] Z. Wang, K. T. Chau, “Anti-control of chaos of a permanent magnet DC motor system for vibratory compactors”, *Chaos Solitons Fract*, **36**, 694–708, (2008)
- [30] Zheng Ming Ge, C. Jui Wen, C. Yen Shen, “Chaos anticontrol and synchronization of three time scales brushless DC motor system”, *Chaos Solitons Fract*, **22**, 1165–1182, (2004)
- [31] R. Yamapi, P. Wofo, “Nonlinear electromechanical devices: dynamics and synchronization Sapri RC”, *Mechanical vibrations, measurement, effects and control Nova Publishers* (2008)
- [32] W. Jean-Baptiste, “Nano computers and Swarm Intelligence”, London: *ISTE John Wiley & Sons*, ISBN 1848210094, (2008).
- [33] R. Ghodssi, P. Lin, “MEMS Materials and Processes Handbook”, *Berlin: Springer*, **1**, 925-1044, (2011).
- [34] P. Lin, R. Maboudian, C. Carraro, T. Fan-Gang, W. Pen-Cheng, Y. Lan, “Surface Treatment and Planarization”, *MEMS Materials and Processes Handbook*, **1**, 925-1044, (2011).
- [35] C. Acar, M. Andrei Shkel, “*MEMS Vibratory Gyroscopes*” *Structural Approaches to Improve Robustness*, ISBN, (2008).
- [36] Peter Clarke, “Smart MEMS microphones market emerges”, *EE Times Europe*. May 31, 2016. Retrieved June 1, 2016.
- [37] Louizos, L. Alexandros, Athanasopoulos, G. P. Varty, Kevin, "Microelectromechanical Systems and Nanotechnology. A Platform for the Next Stent Technological Era", *Vasc Endovascular Surg.*, **46**, 605–609, (2012).
- [38] H. Arman, K. Sang-Gook, "Ultra-wide bandwidth piezoelectric energy harvesting", *Applied Physics Letters*, **99**, doi:10.1063/1.3629551, (2011).
- [39] H. Arman, "Three-dimensional micro electromechanical system piezoelectric ultrasound transducer", *Applied Physics Letters*, **101**, doi:10.1063/1.4772469, (2012).
- [40] H. Arman "Monolithic ultrasonic integrated circuits based on micromachined semi-ellipsoidal piezoelectric domes", *Applied Physics Letters*, **103**, doi:10.1063/1.4831988, (2013).
- [41] M. Di Ventra, S. Evoy, R. H. James, Jr, “Introduction to Nanoscale Science and Technology”, *Nanostructure Science and Technology Berlin*, (2004).
- [42] M. Di Ventra, S. Evoy, R. H. James, Jr, “Introduction to Nanoscale Science and Technology”, *Nanostructure Science and Technology Berlin*, (2012).

- [43] M. Despont, J. Brugger, U. Drechsler, U. Dürig, W. Häberle, M. Lutwyche, H. Rothuizen, R. Stutz, R. Widmer, "VLSI-NEMS chip for parallel AFM data storage", *Sensors and Actuators A Physical*, **80**, 100–107, (2000).
- [44] B. Nana, S. B. Yamgou, I. Kemajou, R. Tchitnga, P. Wofo, " Dynamics of a RLC series circuit with hysteretic iron-core inductor ", *Chaos, Solitons and Fractals*, **106**, 184–192, (2018).
- [45] W. Jean-Baptiste, "Nano computers and Swarm Intelligence", London: *ISTE John Wiley & Sons*, ISBN 1848210094, (2008).
- [46] R. Ghodssi, P. Lin, "MEMS Materials and Processes Handbook", *Berlin: Springer*, **1**, 925-1044, (2011).
- [47] P. Lin, R. Maboudian, C. Carraro, T. Fan-Gang, W. Pen-Cheng, Y. Lan, "Surface Treatment and Planarization", *MEMS Materials and Processes Handbook*, **1**, 925-1044, (2011).
- [48] C. Acar, M. Andrei Shkel, "MEMS Vibratory Gyroscopes" *Structural Approaches to Improve Robustness*, ISBN, (2008).
- [49] Peter Clarke, EE Times Europe. "Smart MEMS microphones market emerges." May 31, 2016. Retrieved June 1, 2016.
- [50] Louizos, L. Alexandros, Athanasopoulos, G. P. Varty, Kevin "Microelectromechanical Systems and Nanotechnology. A Platform for the Next Stent Technological Era", *Vasc Endovascular Surg.*, **46**, 605–609, (2012).
- [51] H. Arman, K. Sang-Gook, "Ultra-wide bandwidth piezoelectric energy harvesting", *Applied Physics Letters*, **99**, doi:10.1063/1.3629551, (2011).
- [52] H. Arman, "Three-dimensional micro electromechanical system piezoelectric ultrasound transducer", *Applied Physics Letters*, **101**, doi:10.1063/1.4772469, (2012).
- [53] H. Arman "Monolithic ultrasonic integrated circuits based on micromachined semi-ellipsoidal piezoelectric domes", *Applied Physics Letters*, **103**, doi:10.1063/1.4831988, (2013).
- [54] M. Di Ventra, S. Evoy, R. H. James, Jr, "Introduction to Nanoscale Science and Technology ", *Nanostructure Science and Technology Berlin*, (2004).
- [55] M. Di Ventra, S. Evoy, R. H. James, Jr, "Introduction to Nanoscale Science and Technology ", *Nanostructure Science and Technology Berlin*, (2012).
- [56] M. Despont, J. Brugger, U. Drechsler, U. Dürig, W. Häberle, M. Lutwyche, H. Rothuizen, R. Stutz, R. Widmer, "VLSI-NEMS chip for parallel AFM data storage", *Sensors and Actuators A Physical*, **80**, 100–107, (2000).
- [57] S. Haan, "NEMS-emerging products and applications of nano-electromechanical systems", *Nanotechnology Perceptions*, **2**, 267–275, (2006).

- [58] Wikipedia. Hurricane sandy.[http://en.wikipedia.org/wiki/Hurricane sandy](http://en.wikipedia.org/wiki/Hurricane_sandy), Retrieved -11-24, (2012).
- [59] D. Marc, T. Zhi, N. R. Aluru, "Static and Dynamic Analysis of Carbon Nanotube-Based Switches", *Journal of Engineering Materials and Technology*, **126**, doi:10.1115/1.1751180, (2004).
- [60] K. Changhong, E. D. Horacio, "Numerical Analysis of Nanotube-Based NEMS Devices— Part I: Electrostatic Charge Distribution on Multiwalled Nanotubes", *Journal of Applied Mechanics*, **72**, doi:10.1115/1.1985434, (2005).
- [61] K. Changhong, E. D. Horacio, P. Nicola, "Numerical Analysis of Nanotube Based NEMS Devices — Part II: Role of Finite Kinematics, Stretching and Charge Concentrations", *Journal of Applied Mechanics*, **72**, doi:10.1115/1.1985435, (2005).
- [64] J. C. Garcia, J. F. Justo, "Twisted ultrathin silicon nanowires: A possible torsion electromechanical nanodevice", *Europhys. Lett*, **108**, doi:10.1209/0295-5075/108/36006, (2014).
- [63] A. Kis, A. Zettl, "Nanomechanics of carbon nanotubes", *Philosophical Transactions of the Royal Society A*, **366**, 1591–1611, (2008).
- [64] Ge ZM, J. M. Cheng, Y. S. Chen, "Chaos anticontrol and synchronization of three time scales brushless DC motor system", *Chaos, Solitons and Fractals*, **22**, 1165–1182, (2004).
- [65] C. A. Kitio Kwuimy, G. Litak, C. Nataraj. "Enhancing energy harvesting system using materials with fractional order stiffness", Proceedings of the ASME, *Dynamic Systems and Control Conference*, DSCC2013-4109, (2013).
- [66] J. C. Chedjou, P. Woafu, and S. Domngang. "Shilnikov chaos and dynamics of self-sustained electromechanical transducer"; *Journal of Vibration and Acoustics*, **123**, 170–174, (2001).
- [67] R. Yamapi, J. B. Chabi Orou, and P. Woafu, "Effects of discontinuity of elasticity and damping on the dynamics of an electromechanical transducer", *Journal of Vibration and Acoustics*, **127**, 588–593, (2005).
- [68] R. Yamapi, J. B. Chabi Orou, and P. Woafu, "Harmonic oscillations, stability and chaos control in a non-linear electromechanical system", *Journal of Sound and Vibration*, **259**, 1253–1264, (2003).
- [69] R. Yamapi, J. B. Chabi Orou, and P. Woafu, "Harmonic dynamics and transition to chaos in a nonlinear electromechanical system with parametric coupling", *Physica Scripta*, **67**, 269–275, (2003).

- [70] Tian X and Xu R, “Global dynamics of a predator-prey system with holling type ii functional response”, *Nonlinear Analysis: Modelling and Control*, **16**, 242–253, (2011).
- [71] S. Hsu, T. Hwang, “Hopf bifurcation analysis for predator-prey system of holling and leslie typ”, *Taiwanese Journal of Mathematics*, **3**, 35–53, (1999).
- [72] J. Cai, M. Lin, Z. Yuan, “Secure communication using practical synchronization between two different chaotic systems with uncertainties”, *Mathematical and Computational Applications*, **15**, 166–175, (2010).
- [73] E. E. Mand, M. M. El-Dessoky, “Adaptive feedback control for the projective synchronization of the lü dynamical system and its application to secure communication”, *Chinese Journal of Physics*, **48**, 863–872, (2010).
- [74] John Chan, Andrei Vladimirescu, Xiao-Chun Gao, Peter Liebmann, and John Valainis, “Nonlinear Transformer Model for Circuit Simulation”, *IEEE transactions on computer-aided Design*, **10**, 476–482, (1991)
- [75] D. J. D. Earn, P. Rohani, B. T. Grenfell, “Persistence, chaos and synchrony in ecology and epidemiology”, *Proc Royal. Society. London. B.*, **265**, 7–10, (1998).
- [76] H. Baek, “A holling-type ii food chain system with biological and chemical controls”, *Commun. Korean Math. Soc*, **24**, 215–226, (2009).
- [77] R. Yamapi and P. Woafu, “Nonlinear Electromechanical Devices: Dynamics and Synchronization, in Mechanical Vibrations: Measurement, Effects and Control”, Eds. R. C. Sapri, Nova Publishers, (2008).
- [78] J. C. Chedjou, "Etude de la dynamique régulière et chaotique du système couplé oscillateur de Van der Pol-oscillateur de Duffing", Thèse de Doctorat de 3eme cycle, Laboratoire d'électronique, Université de Yaoundé I, Cameroun, 1999.
- [79] Y. Chembo Kouomou, P. Woafu, “Stability and chaos control in electrostatic transducers”, *Physica Scripta*, **62**, 255-260, (2000).
- [80] R. Yamapi, “Dynamics of an Electromechanical Damping device with Magnetic Coupling”, *Nonlinear Science and Numerical Simulations* **11**, 907–921, (2006).
- [81] H. Zhang, D. Chen, B. Xu, F. Wang, “Nonlinear modelling and dynamic analysis of hydro-turbine governing system in the process of load rejection transient”, *Energy Conversion and Management*, **90**, 128-137, (2015).
- [82] D. Chen, C. Ding, X. Ma, P. Yuan, D. Ba “Nonlinear dynamical analysis of hydro-turbine governing system with a surge tank”, *Applied Mathematical Modelling*, **37**, 7611–7623, (2013).

- [83] D. Belato, H. I. Weber, J.M. Balthazar, D. T. Mook, “Chaotic vibrations of a non-ideal electromechanical system”, *Int. J. Solids Struct*; **38**, 1699–706, (2001).
- [84] K. Fallahi, H. Leung “A chaos secure communication scheme based on multiplication modulation”, *nonlinear science and numerical simulation*, **15**, 368–383, (2010).
- [85] Baggio, Rodolfo, ” Symptoms of Complexity in a Tourism System”, *Tourism Analysis*, **13**, 1–20, (2008).
- [86] Y. Tsividis, “White Paper on Certain Aspects of CAS Education”, prepared for the meetings of the IEEE CAS president’s advisory council, April 4, June 6, and September 27, 1997, and disseminated to past and present IEEE officers.
- [87] B. Nana, P. Wofo, S. Domngang. “Chaotic synchronization with experimental application to secure communications”, *Commun Nonlinear Science Numerical Simulation*, **14**, 2266-2276, (2009).
- [88] R. Yamapi and P. Wofo. “Nonlinear Electromechanical Devices: Dynamics and Synchronization, in Mechanical Vibrations: Measurement, Effects and Control”, *Eds. R. C. Sapri, Nova Publishers*, (2008).
- [89] C. A. Kitio Kwuimy and P.Wofo. “Dynamics of a self-sustained electromechanical system with flexible arm and cubic coupling”, *Nonlinear Science and Numerical Simulation*, **12**, 1504-1517, (2007). “Dynamics, chaos and synchronization of self-sustained electromechanical systems with clamped-free flexible arm”, *Nonlinear Dynamics*, **53**, 201–213, (2008). “Experimental bifurcations and chaos in a modified self-sustained macro electromechanical system”, *Journal of Sound and Vibration*, **329**, 3137-3148, (2010).
- [90] J. B. Mogo, " Modelling and dynamics of pendulum Arms of electromechanical robots", Doctorat thesis, Laboratory of Modelling and Simulation in Engineering and Biological Physics, University of Yaoundé I, Cameroun, (2010).
- [91] R. A. Walsh, “Electromechanical design handbook”, *Mc-GRAW-Hill, New York*, (2000).
- [92] C. Hayashi, “Nonlinear Oscillations in physical systems”, *Mc-Graw-Hill, New York*, (1964).
- [93] H. John, Andrei Vladimirescu, Xiao-Chun Gao, Peter Liebmann, and John Valainis, “Nonlinear Transformer Model for Circuit Simulation”, *IEEE transactions on computer-aided design*, **10**, 476–482, (1991)
- [94] Ge. Zheng-Ming, C. Jui-Wen, C.Yen-Sheng, “Chaos anticontrol and synchronization of three time scales brushless DC motor system”, *Chaos Solitons Fract*, **22**, 1165–1182, (2004).

- [95] A. Argyris, D. Syvridis, L. Larger, V. Annovazzi-Lodi, P. Colet, I. Fischer, J.C. R. Mirasso, L. Pesquera, K. L. Shore, “Chaos-based communications at high bit rates using commercial fibre-optic links”, *Nature Letter*, **43**, 443-446, (2005).
- [96] S. H. Crandall, D. C. Karnopp, E. F. Krutz, and D. C. Pridmore-Brown, “Dynamics of Mechanical and Electromechanical Systems”, *McGraw-Hill, New York*, 1968.
- [97] D. O. Tcheutchoua Fossi, " Sieving Devices based on Nonlinear Dynamics of Electromechanical Systems with Rotating Electric Actuator: Theory and Experiment", Doctorate thesis in Physics, Option: Mechanics, University of Yaoundé I, Cameroun, 2011.
- [98] A. Notué Kadjie, P. Wofo, “Effects of springs on a pendulum electromechanical energy harvester”, *Theor. Appl. Mech. Lett*, **4**: 2-7, (2014).
- [99] M. Hasler, T. Schimming, “Chaos communication over noisy channels”, *Int. J. Bifurc. Chaos*, **10**, 719–732, (2000).
- [100] Hayashi C, “Nonlinear Oscillations in physical systems”, Mc-Graw-hill New York, (1964).
- [101] A. Nayfeh, D.T. Mook, “Nonlinear oscillations. Wiley-Inter-science”, New York,(1979).
- [102] J. Guckenheimer, P. J. Holmes, “Non-Linear Oscillations, Dynamical Systems and Bifurcations of Vector Fields”, *Springer, New York* (1983).
- [103] Jezequel, “Active Control in Mechanical Engineering”, *Editions Hermes*, 1995
- [104] W. H. Press, S. A. Teukolsky, W. T. Vetterling, and B. P. Flannery, “Numerical Recipes: The Art of Scientific Computing”, *Cambridge University Press* ISBN 0521880688, August (2007).
- [105] A. Bellen and M. Zennaro, “Numerical Methods for delay differential equations”, *Oxford University Press* (2003).
- [106] P. Wofo. Cours de méthodes numériques. Master 1, Université de Yaoundé 1, 2011.
- [107] T. Erneux, “applied delay diffequations”. Springer New York, (2009)
- [108] G. Chen, D. Lai, “Feedback anticontrol of discrete chaos”, *Int. J. Bifurcat. Chaos*, **8**,1585–1590, (1998)
- [109] Y. Gao, T. K. Chau, “Chaotification of permanent-magnet synchronous motor drives using time-delay feedback”, *Proceedings Industrial Electronics Conference*, **1**, 762-766, (2002)

- [110] J. Guckenheimer, P. J., “Holmes Non-Linear Oscillations, Dynamical Systems and Bifurcations of Vector Fields”, *Springer, New York*, (1983)
- [111] M. Lakshmanan, D. V. Senthilkumar, “Dynamics of nonlinear time-delay systems”, *Springer-Verlag Heidelberg, New York*, (2010)
- [112] M. Chen, J. Kurths, “Synchronization of time-delayed systems”, *Physical Review E*, **76**, 1-5, (2007).
- [113] Y. Zhai, I. Z. Kiss, J. L. Hudson, “Control of complex dynamics with time-delayed feedback in populations of chemical oscillators: Desynchronization and clustering”, *Ind. Eng. Chem. Res.*, **47**, 3502-3514, (2008).
- [114] Y. Bouteraa; A. B. Mansour, J. Ghommam, G. Poisson, “Cooperative control and synchronization with time delays of multi-robot systems”, *Journal of Engineering and Computer Innovations*, **2**, 28–39, (2011)
- [115] J. C. Sprott, “A simple chaotic delay differential equation”, *Physics Letters A*, **366**, 397-402, (2007).
- [116] P. Louodop; H. Fotsin; S. Bowong, T. S. A. Kemmogne, “Adaptive time-delay synchronization of chaotic systems with uncertainties using a nonlinear feedback coupling”, *Journal of Vibration and Control*, DOI: 10.1177/1077546312467811, (2012).
- [117] Qing-Chang Zhong, “Robust Control of Time-delay Systems”, *Springer-Verlag, London*, (2006)
- [118] M. Faithcan, Atay, “Complex time-delay systems: Theory and applications”, *Springer-Verlag Heidelberg*, (2010).
- [119] Wu M; He Y and She J. Stability analysis and robust control of time-delay systems. Science Press Beijing and Springer-Verlag, China, second edition.
- [120] D. V. Senthilkumar, J. Kurths, Lakshmanan, “Stability of synchronization in coupled time-delay systems using krasovskii-lyapunov theory”, *Physical Review E*, **79**, 1-4, (2009)
- [121] Z. Sun, X. Yang, “Parameters identification and synchronization of chaotic delayed systems containing uncertainties and time-varying delay”, *Mathematical Problems in Engineering*, **1**, doi:10.1155/2010/105309, (2010).
- [122] S. Q. Zheng Bi, G. Cai “Adaptive projective synchronization in complex networks with timevarying coupling delay”, *Physics Letters A*, **373**:1553-1559, (2009).
- [123] X. Gao, S. Zhong, F. Gao, “Exponential synchronization of neural networks with time-varying delays”, *Nonlinear Analysis*, **71**:2003-2011, (2009)

- [124] M. Y. Bashir Nouri, “Modelling and control of mobile robot”, *First International Conference on Modelling, Simulation and Applied Optimization*, **5**, 1-6, (2005)
- [125] Bergé P, Pomeau Y, Vidal C (1988) L’ordre dans le chaos : vers une approche déterministe dans la turbulence. Hermann
- [126] Ranada AF (1986) *Methods and applications of Nonlinear Dynamics*. Actif Series 7

List of publications

- 1- **R. Tsapla Fotsa, P. Wofo** , “ Chaos in a new bistable rotating electromechanical system”, *Chaos, Solitons and Fractals*, **93**, 48-57, (2016).